Analysis of *MYCN* and *MAX* alterations in Wilms Tumor

Analyse von *MYCN*- und *MAX*-Veränderungen im Wilms Tumor

Doctoral thesis for a doctoral degree
at the Graduate School of Life Sciences,
Julius-Maximilians-Universität Würzburg,
Section Biomedicine

submitted by

Ovidio Manuel Jiménez Martín

from:

Seville

Würzburg 2021

Submitted on:

Members of the Doctorate Committee:

Chairperson: **Prof. Dr. Alexander Buchberger**

Primary Supervisor: **Prof. Dr. Manfred Gessler**

Supervisor (Second): **Prof. Dr. Martin Eilers**

Supervisor (Third): **Prof. Dr. Stefan Gaubatz**

Date of Public Defence:

Date of Receipt of Certificates:

Index

1. Summary

1.1. Summary (English)

Wilms tumor (WT) is the most common renal tumor in childhood. Among others, *MYCN* copy number gain and *MYCN* P44L and *MAX* R60Q mutations have been identified in WT. The proto-oncogene *MYCN* encodes a transcription factor that requires dimerization with MAX to activate transcription of numerous target genes. *MYCN* gain has been associated with adverse prognosis. The *MYCN* P44L and *MAX* R60Q mutations, located in either the transactivating or basic helix-loop-helix domain, respectively, are predicted to be damaging by different pathogenicity prediction tools. These mutations have been reported in several other cancers and remain to be functionally characterized.

In order to further describe these events in WT, we screened both mutations in a large cohort of unselected WT patients, to check for an association of the mutation status with certain histological or clinical features. *MYCN* P44L and *MAX* R60Q revealed frequencies of 3 % and 0.9 % and also were significantly associated to higher risk of relapse and metastasis, respectively. Furthermore, to get a better understanding of the *MAX* mutational landscape in WT, over 100 WT cases were analyzed by Sanger sequencing to identify other eventual *MAX* alterations in its coding sequence. *R60Q* remained the only *MAX* CDS alteration described in WT to date.

To analyze the potential functional consequences of these mutations, we used a doxycycline-inducible system to overexpress each mutant in HEK293 cells. This biochemical characterization identified a reduced transcriptional activation potential for *MAX* R60Q, while the *MYCN* P44L mutation did not change activation potential or protein stability. The protein interactome of N-MYC-P44L was likewise not altered as shown by mass spectrometric analyses of purified N-MYC complexes. However, we could identify a number of novel N-MYC partner proteins, several of these known for their oncogenic potential. Their correlated expression in WT samples suggested a role in WT oncogenesis and they expand the range of potential biomarkers for WT stratification and targeting, especially for high-risk WT.

1.2. Zusammenfassung (Deutsch)

Der Wilms Tumor (WT) ist der im Kindesalter am häufigsten auftretende Nierentumor. Neben anderen genetischen Veränderungen, wurden *MYCN*-Kopienzahlgewinn und der *MYCN* P44L- und *MAX* R60Q-Mutationen in WT identifiziert. Das Proto-Onkogen *MYCN* kodiert einen Transkriptionsfaktor, der eine Dimerisierung mit MAX erfordert, um die Transkription zahlreicher Zielgene zu aktivieren. Der *MYCN*-Gewinn wurde mit einer negativen Prognose assoziiert. Die *MYCN* P44L- und *MAX* R60Q-Mutationen, die sich entweder in der transaktivierenden oder in der basischen Helix-Loop-Helix-Domäne befinden, wurden durch verschiedene pathogene Vorhersage-Werkzeuge als schädigend prognostiziert. Über diese Mutationen wird bei mehreren anderen Krebsformen berichtet, doch sie wurden noch nicht umfassend biochemisch charakterisiert.

Um diese Vorgänge in WT weitergehend zu charakterisieren, untersuchten wir beide Mutationen in einer großen Gruppe zufällig ausgewählter WT-Patienten mit dem Ziel, einen Zusammenhang zwischen dem Mutationsstatus und gewissen histologischen und klinischen Eigenschaften zu überprüfen. *MYCN* P44L und *MAX* R60Q ergaben eine Frequenz von 3 % bzw. 0,9 % in WT und wurden jeweils mit einem signifikant höheren Rückfall- und Metastasierungsrisiko assoziiert. Um ein besseres Verständnis der *MAX*-Mutationsszenarien in WT zu erlangen, wurden darüber hinaus mehr als einhundert WT-Fälle durch Sanger-Sequenzierung analysiert, mit dem Ziel, andere mögliche Veränderungen in der *MAX*-Kodierungssequenz zu identifizieren. R60Q blieb dabei die einzige bis heute beschriebene Veränderung der MAX-Kodierungssequenz in WT.

Um die potentiellen funktionalen Folgen dieser Mutationen zu untersuchen, nutzten wir ein Doxycyclin-induziertes System, um eine Überexprimierung jedes Mutanten in HEK293-Zellen zu erzielen. Diese biochemische Charakterisierung identifizierte ein reduziertes Transkriptionsaktivierungspotential für *MAX* R60Q, während die *MYCN* P44L-Mutation das Aktivierungspotential oder die Proteinstabilität nicht veränderte. Das N-MYC Interaktom wurde während der Massenspektrometrie-Analyse von gereinigten N-MYC-Komplexen ebenfalls nicht verändert. Jedoch konnten wir eine Anzahl von neuartigen N-MYC Partnerproteinen bestimmen, von denen einige für ihr

onkogenes Potenzial bekannt sind. Deren korrelierte Expression in WT-Proben deuteten auf eine Rolle bei der WT Onkogenese hin und erweitern die Auswahl potentieller Biomarker für die Stratifizierung von WTs und Gentargeting, insbesondere bei Hochrisiko-WTs.

2. Introduction

2.1. The Wilms tumor

Wilms tumor (WT), also known as nephroblastoma, is the most common pediatric renal tumor. It was first described in 1814 by Thomas F. Rance, but the tumor was named after the German surgeon Max Wilms (1867 - 1918). In his monography "The mixed tumors of the kidney" published in 1899, Wilms described the emergence of childhood renal tumors from cells of the mesodermal layer, in a similar process to the arising of the different tissues from undifferentiated precursor cells during the embryonic development.

2.1.1. Epidemiology

WT accounts for 6 % of tumors in patients under the age of 15, representing the second most common intraabdominal pediatric cancer and the fifth most common malignancy overall in childhood (Davidoff 2012). The incidence shows a great difference depending on the race: WT affects 10 cases per million in children of African descent, 6-9 cases per million in white children, and 3 cases per million in Asian populations (Breslow et al. 1993, Nakata et al. 2018). Almost 90 % of WT cases are sporadic and unilateral (Breslow et al. 1993), although 1-2 % of patients have a family history (Huff 1998). Familial cases are associated with a higher frequency of bilateral tumors, as well as a lower age at diagnosis (Matsunaga 1981). Bilateral cases are diagnosed at a mean age of 31 months, while unilateral cases at around 44 months (Horner et al. 2009).

2.1.2. Symptoms and diagnosis

A WT presents itself most of times as asymptotic and painless, so a first suspected diagnosis is in most cases due to a painless swelling of the upper abdomen (60 %) or by chance during a checkup (about 10 %). Symptoms and signs including abdominal pain, malaise and either microscopic or macroscopic hematuria are present in 20-30 % of cases (Davidoff 2012). 25 % of cases are diagnosed with hypertension, which may be due to increased renin activity. Other not so frequent symptoms include constipation, urinary tract infection or diarrhea (Gutjahr et al. 1990).

Due to the current lack of tumor-specific markers in blood or urine, a diagnosis is given using imaging techniques like ultrasound, magnetic resonance imaging and computed tomography. Only if the previous techniques do not give a definitive diagnosis, and if the patient age is under 6 months or over 16 years, a tumor biopsy can be recommended to avoid mistakes and provide a reliable diagnosis (Babyn et al. 1995).

In terms of differential diagnosis, the WT must be distinguished from other malignant tumors such as lymphoma of the kidney or renal cell carcinoma. Wilms tumors can occur together with other malformations or syndromes, most frequently urogenital anomalies, including both renal and genital malformations.

2.1.3. Histology and classification

WTs arise from embryonic undifferentiated tissues, whose precursors can be nephrogenic remnants with a high mitotic activity. A WT may consist of three different cell types: blastema, epithelia, and stroma. The blastema component consists of sheets of densely packed small cells with hyperchromatic nuclei and conspicuous mitotic activity; the epithelial part consists of primitive cuboidal cells forming tubular structures and rosettes; and the stromal component is composed mainly of fibroblast-like cells that reside between nodules of blastemal. If all three are present in the tumor, it is called a triphasic or mixed tumor, but if one of them predominates significantly (>65 %), the tumor is designated accordingly as epithelial, stromal or blastemal type. Another subtype, where the cell nuclei tend to be very large and distorted, is called anaplastic, and can be subclassified into diffuse or focal anaplasia, depending if the malignancy is spread throughout the tumor or just limited to certain parts of it.

The histological subtype of a WT is of prognostic significance. Depending on the histology, it is divided into three risk-groups: low, intermediate and high malignancy (Vujanic et al. 2002) **[Table 1]**. In addition, a distinction is made between tumors with primary resection or preoperative chemotherapy (see section 2.1.4), because the response of the tumor to the chemotherapy may give rise to new histological subtypes, like regressive (with >65 % necrosis) or completely necrotic.

Table 1. WT classification based on histological subtypes (adapted from Vujanic et al. 2002).

Risk Group	Pre-operative Chemotherapy	Primary Operation
Low Malignancy	Mesoblastic nephroma Cystic partially differentiated Completely necrotic	Mesoblastic nephroma Cystic partially differentiated
Middle Malignancy	Epithelial predominant Stromal predominant Mixed type Regressive type Focal anaplasia	Epithelial predominant Stromal predominant Blastemal predominant Mixed type Regressive type Focal anaplasia
High Malignancy	Blastemal type Diffuse anaplasia	Diffuse anaplasia

In addition, a staging based on the local spread of the tumor, lymph node involvement and the metastasis status is available (Vujanic et al. 2018).

2.1.4. Therapy

Two therapeutic approaches can basically be distinguished. On one hand, the treatment in Europe works conform the protocol of the Societé Internationale d'Oncologie Pédiatrique - Renal Tumors Study Group (SIOP). In this protocol, a pre-operative chemotherapy is performed to reduce the volume of the tumor before its surgical removal, therefore reducing the risk of an intra-operative tumor rupture (Metzger and Dome 2005, van den Heuvel-Eibrink et al. 2017). The therapy scheme is dependent of the tumor histology and stage, but chemotherapy is usually carried out with vincristine and actinomycin D. After the operation, further chemotherapy and/or radiotherapy will be required depending of the stage of the WT (Furtwängler 2008).

On the other hand, most children in North America undergo the National Wilms Tumor Study / Children´s Oncology Group (NWTS/COG) protocol. A primary tumor resection followed by chemotherapy is performed, and radiotherapy is only added in case of a high-risk WT (Metzger and Dome 2005). This protocol is also performed in Europe for patients younger than 6 months and older than 16 years, because the incidence of other renal tumors in these age ranges is higher and the use of inappropriate cytotoxic drugs should be avoided.

The different treatment protocols can influence the contribution of the different WT cell components. 9.5 % of tumors treated with preoperative chemotherapy are classified as blastemal, but for primarily resected tumors they represent a 35 % (Weirich et al. 2001). In patients treated with preoperative chemotherapy, this blastemal contribution is of prognostic significance, because this apparently chemotherapy-resistant remaining viable blastema is associated with poor prognosis and reduced relapse-free survival, dropping from 86.7 % to 58.4 % (Weirich et al. 2004).

2.1.5. Prognosis and late sequelae

Thanks to the medical progress and the acquired knowledge on WT treatment, the prognosis for this disease is satisfactory, with a current survival rate of 90 % (Davidoff 2012). However, the survival rate depends on the histological type and stage of the tumor (Varan 2008). Relapses occur in 15 % of WT cases, usually within two years after the primary diagnosis (Brok et al. 2018, Spreafico et al. 2009), where mostly lungs/pleura, tumor bed and liver are involved (Varan 2008). Overall survival depends on initial treatment, histology and relapse site (Furtwangler et al. 2011, Green et al. 2007, Ha et al. 2013, Malogolowkin et al. 2008). Up to 70 % of relapses are detected with current surveillance imaging (Brok et al. 2018), and the treatment includes surgical, radio- and chemotherapeutic measures (Furtwängler 2008). Regarding molecular biomarkers, copy number gain of chromosome 1q consistently predicts poorer event-free survival and a reduction in overall survival among NWTS/COG patients (Chagtai et al. 2016, Gratias et al. 2016, Segers et al. 2013), but additional biomarkers for risk stratification are urgently needed (Treger et al. 2019).

If the WT occurs as a part of a congenital malformation syndrome **[Table 2]**, the risk of renal failure twenty years after diagnosis is at approximately 1 %. Patients with WAGR (Wilms tumor, Aniridia, Genitourinary anomalies, mental Retardation) syndrome have an increased risk of 40 %, while in patients with Denys-Drash syndrome it goes up to 70 % (Lange et al. 2011).

Table 2. WT predisposition syndromes (adapted from Treger et al. 2019).

Risk of WT	Syndrome	Genetics
High (>20 %)	WAGR syndrome	*WT1* deletion
	Denys-Drash syndrome	*WT1* missense mutation
	Perlman syndrome	*DIS3L2* mutation
	Fanconi anaemia	Biallelic *BRCA2* or *PALB2* mutation
	Mosaic variegated aneuploidy	Biallelic *BUB1B* or *TRIP13* mutation
Moderate (5-20 %)	Beckwith-Wiedemann syndrome	Uniparental disomy or H19 epimutation
	Simpson-Golabi-Behmel syndrome	GPC3 mutation
Low (<5 %)	Bloom syndrome	Biallelic *BLM* mutation
	DICER1 syndrome	*DICER1* mutation
	Li-Fraumeni syndrome	*TP53* mutation
	Isolated hemihypertrophy	Variable
	Hyperparathyroidism-jaw tumor syndrome	*CDC73* mutation
	Mulibrey nanism syndrome	*TRIM37* mutation
	PIK3CA-related segmental overgrowth	*PIK3CA* mutation

2.1.6. Wilms Tumor genetics

The genetic causes of WT are very different, including gene mutations and chromosomal aberrations during fetal nephrogenesis. Until recently, knowledge of the genetic underpinnings of Wilms tumor was largely limited to abnormalities of 11p15 methylation, activating mutations in the Wnt pathway involving *CTNNB1* and *WTX*, and *WT1* aberrations (Gadd et al. 2012), this last being frequently associated to urogenital developmental malformations and WT-associated syndromes **[Table 2]**. However, mutations in *WT1*, *WTX*, and *CTNNB1* are present in only one third of tumors (Ruteshouser, Robinson and Huff 2008), which motivated in the last years the search of potential oncogenic driver genes in the remaining tumors.

A better genetic understanding of WT was provided by two studies, which identified novel recurrent mutations involving miRNA processing genes *DROSHA, DGCR8*, and *DICER1*, as well as *MYCN, SMARCA4* and *ARID1A* (Rakheja et al. 2014, Torrezan et al. 2014). Shortly after, another study analyzed a large cohort of high-risk blastemal-type WTs and provided a broader genetic landscape overview (Wegert et al. 2015). Recurrent mutations were observed in the renal developmental genes *SIX1* and *SIX2* (18.1 %), as well *DROSHA/DGCR8* (18.2 %), *DICER1, DIS3L2, MYCN* and *TP53*, the latter being

associated with poor outcome, among other genes. These findings were validated by a parallel study performed in favorable histology WTs (Walz et al. 2015). Loss of imprinting of IGF2 was also observed in around 69% of WTs (Scott et al., 2012). The results of a later study, which used a larger cohort of WT patients with primary resection (Gadd et al. 2017), not only verified several genes previously reported as recurrently mutated in WT, but even provided new recurrent candidates, broadening the spectrum of somatic oncogenes in WT **[Table 3]**.

Table 3. Summary of somatic oncogenes with copy number variation or point mutations in WT, with a prevalence >1 % (adapted from Treger et al. 2019).

Gene (locus)	Prevalence (%)	*Gene* (locus)	Prevalence (%)
TP53 (17p13)	27-46	*NF1* (17q11)	2.9
miRNAPGs*	15-18	*BCOR* (Xp11)	2.6
WTX (Xq11)	15-20	*NONO* (Xq13)	2
WT1 (11p13)	10-20	*ARID1A* (1p36)	1.8
CTNNB1 (3p22)	15	*MAP3K4* (6q26)	1.7
MYCN (2p24)	13	*MAX* (14q23)	1.7
SIX1 (14q23)	7-18	*ASXL1* (20q11)	1.7
SIX2 (2p21)		*BRD7* (16q12)	1.5
SMARCA4 (19p13)	4.5	*FGFR1* (8p11)	1.4
MLLT1 (19p13)	4	*HDAC4* (2q37)	1.2
BCORL1 (Xq26)	3.8	*CHD4* (12p13)	1.2
COL6A3 (2q37)	3.2	*ACTB* (7p22)	1.1

*miRNAPGs, microRNA processing genes: DROSHA (5p13), DICER1 (14q32), DGCR8 (22q11), XPO5 (6q21), DIS3L2 (2q37) and TARBP2 (12q13).

2.1.7. *in vitro* and *in vivo* systems for Wilms tumor

Although the multimodal therapy (surgery, radiation and chemotherapy) has brought considerable improvement in survival in the last decades, there is still an urgent need for overcoming the side effects and long-term sequelae of chemotherapy, especially in high-risk WT (Bhakta et al. 2017, Sadak, Ritchey and Dome 2013). Functional analysis of tumor driver candidates and preclinical drug testing would require the establishment of appropriate cell lines and preclinical animal models, where the main challenge is the heterogeneity of the WT regarding its genetic background and histological appearance.

A few WT cell lines are currently available, mostly from rare anaplastic tumors with *TP53* mutations (Alami, Williams and Yeger 2003, Faussillon et al. 2008), and primary cultures of stromal and epithelial WT have been established and partly characterized (Royer-Pokora et al. 2010, Wegert et al. 2012). 3D spheroid cultures from epithelial, stromal and high-risk blastemal WT have been recently presented as promising tools for drug testing and *in vitro* modeling (Wegert et al. 2020). As for WT *in vivo* models, transplantation of xenografts from human tumors into mice recapitulating triphasic WT characteristics has been reported (Garvin et al. 1987, Houghton et al. 2007, Pode-Shakked et al. 2013), a method unfortunately expensive and laborious. Mouse lines have been established expressing cre-recombinase under the *Six2*/*Cited1* or *Wt1* promotors, which are nephron progenitor and intermediate mesoderm specific, allowing a tissue-specific expression of the gene of interest. Using these Cre mouse lines, recapitulation of kidney triphasic tumors has been limited to combined *Wt1* ablation and deregulation of imprinted *Igf2* (Hu et al. 2011) or rare *Lin28* overexpression (Urbach et al. 2014).

2.2. The transcription factors N-MYC and MAX

2.2.1. The *MYC* oncogene family

The MYC family is a small group of basic-helix-loop-helix-leucine zipper transcription factors, which has been extensively studied in the last four decades due to its broad involvement in many cancers. The name of this family originates from a viral oncogene discovered in the late 1970s, termed *v-myc*, responsible of causing myelocytomatosis in chickens (Sheiness and Bishop 1979). C-MYC, also referred to as MYC and encoded by the *MYC* gene, was shortly after identified as its cellular homologue (Vennstrom et al. 1982). Its coding sequence is highly conserved in vertebrates through evolution, and it is also expressed in *Drosophila melanogaster* (Gallant et al. 1996).

Two other family members, N-MYC (encoded by *MYCN*) and L-MYC (encoded by *MYCL*), were identified in human neuroblastoma and human small cell lung cancer (SCLC) respectively (Kohl et al. 1983, Nau et al. 1985). The discovery of these two homologues in different tumor types draw attention to the different expression patterns among the family members. As proven years later with murine development studies, *Mycn* and

Mycl expression took only place in early stages of embryogenesis and was tissue-specific: *Mycn* expression was located in the central nervous system and the kidneys, while *Mycl* was highly expressed in the kidneys, lungs and some parts of the brain and neural tube, although *Mycl* expression was even dispensable during embryonic development (Hatton et al. 1996, Mugrauer and Ekblom 1991, Schmid, Schulz and Hameister 1989, Zimmerman et al. 1986). *Myc* expression, on the other hand, was more generalized and even persisted until the postnatal stage P21 (Zimmerman et al. 1986). The expression of *MYCN* becomes redundant after birth with *MYC* (Malynn et al. 2000), and it is only observed to be overexpressed in stem cells and some types of tumors (Huang and Weiss 2013).

Besides their different expression patterns, MYC family members have very similar protein structures and functions **[Figure 1]**. All of them include at the C-terminus the basic helix-loop-helix (bHLH) and leucine-zipper (LZ) protein domains, which are involved in the dimerization of MYC proteins with other partners and in DNA binding (Phillips 1994). MYC proteins require the formation of a dimer to bind to DNA, but their homodimers are quite unstable due to major steric and electrostatic clashes between the amino acid residues involved in dimerization (Soucek et al. 1998). Therefore, MYC relies on heterodimers like MYC/MAX for binding DNA (see section 2.2.2). Additionally, MYC proteins contain five relatively short stretches of amino acids, six in the case of N-MYC and C-MYC, termed MYC-boxes (MB), where the sequence conservation is the highest. They are numbered 0, I, II, IIIa, IIIb and IV, and only MBIIIa is not present in L-MYC. These boxes have been shown to interact with different types of effector proteins, allowing MYC proteins to perform different functions, like activating or repressing the transcription, controlling the transcriptional machinery, and regulating its own protein turnover via post-translational modifications (Conacci-Sorrell, McFerrin and Eisenman 2014, Tu et al. 2015). The binding of these effectors to the different boxes has helped to elucidate some of the functional roles of the MBs **[Figure 2]** (Baluapuri, Wolf and Eilers 2020). Within the protein structure of the MYC proteins there are additional functional elements **[Figure 1]**: the transactivation domain (TAD), comprising the MB0-II at the N-terminus, involved in the recruitment of cofactors for transcriptional regulation and MYC stability (Kato et al. 1990, Lee et al. 1996); a D-element and a PEST sequence (rich

in amino acids proline, glutamic acid, serine and threonine) in the central region, both implicated in MYC degradation (see section 2.2.4); and a nuclear localization signal (NLS), a sequence that 'tags' the protein for import into the cell nucleus, were MYC proteins execute their functions (Dang and Lee 1988).
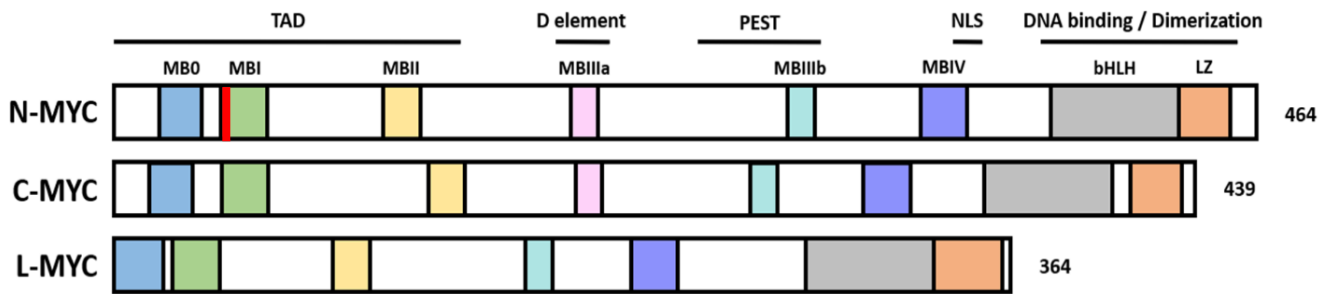
Figure 1. Protein structure of the human MYC protein family.
Schematic representation of the human MYC proteins. The corresponding MYC-boxes (MB), have been highlighted in different colors and are labeled only for N-MYC. On top of the MBs other functional elements are indicated: transactivation domain (TAD), D element, PEST sequence and nuclear localization signal (NLS). The basic helix-loop-helix (bHLH) and leucine zipper (LZ) domains, located in the C-terminus, are involved in dimerization with other proteins and DNA-binding. The right numbers refer to the amino acid length of the protein. The red mark indicates the position of the N-MYC-P44L mutation, one of the subjects of this study.

The MYC family integrates signals from several upstream pathways and consequently direct different gene expression programs. This makes MYC proteins key regulators of many cellular functions, such as DNA repair, metabolism, cell cycle, signal transduction, transcription, translation, protein biosynthesis and cell adhesion (Carabet et al. 2018, Chen, Liu and Qing 2018). The expression of MYC proteins is tightly controlled by multiple mechanisms, like negative autoregulation, miRNAs, translation regulation, and protein stability and degradation (Facchini et al. 1997, Gabay, Li and Felsher 2014, Kalkat et al. 2018). However, their deregulated expression has major consequences in cancer development and its quick and unlimited progression. In tumors, MYC proteins induces cell proliferation and growth, regulates the metabolism for a faster energetic consume, promotes angiogenesis and metastasis, inhibits apoptosis induction signals and induces mutations and genome instability (Tansey 2014) **[Figure 3]**.
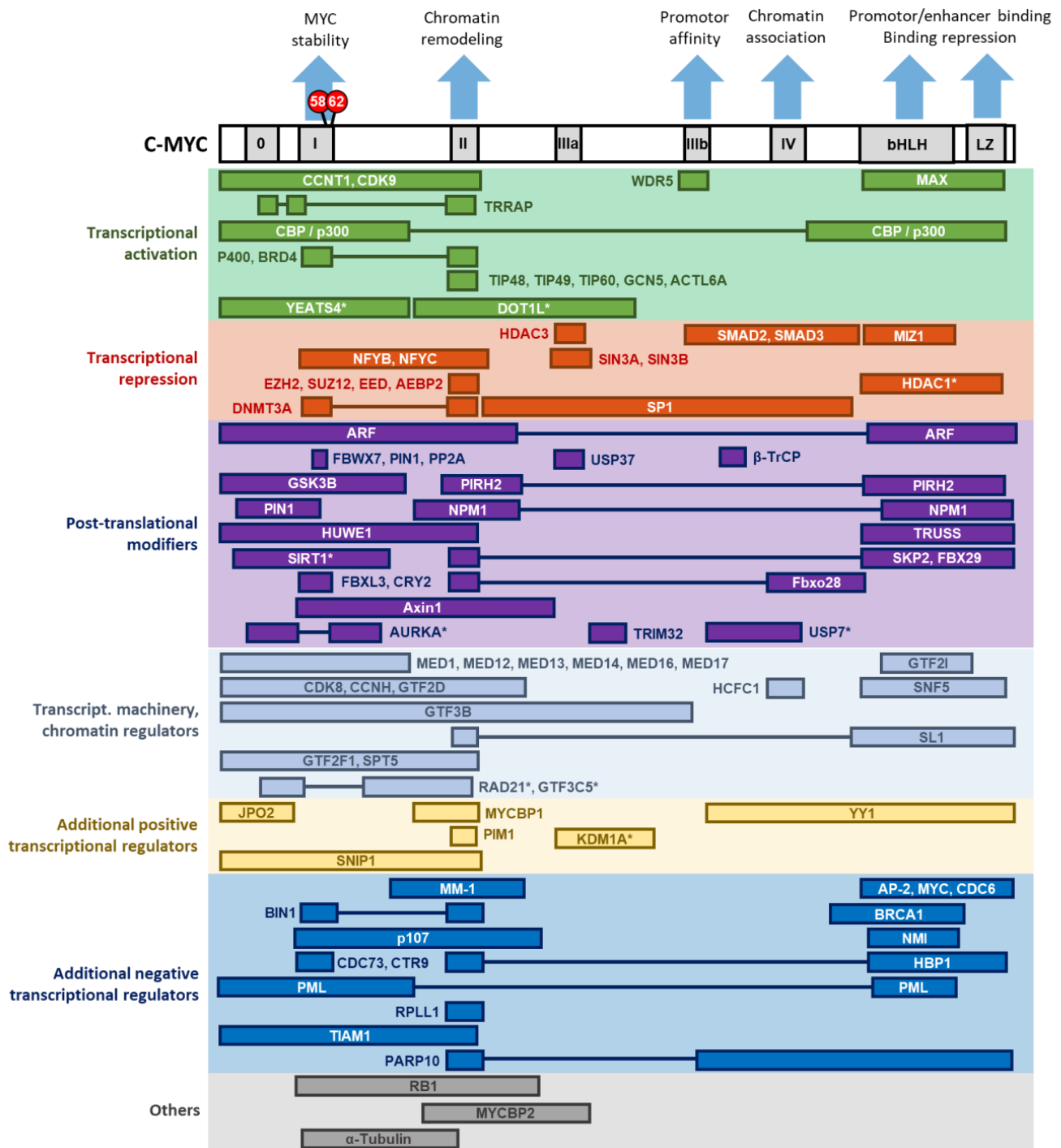
Figure 2. MYC protein domains and interacting proteins.

Overview of C-MYC protein domains and their canonical functions, as well as a list of MYC interactors and the C-MYC regions where they bind. The interactors have been grouped according to their known function. The protein domains correspond to the MYC-boxes I to IV (labelled I to IV), the basic helix-loop-helix domain (bHLH) and the leucine zipper domain (LZ). Phosphorylation sites involved in proteasomal degradation of MYC proteins are identified in red circles (indicating the amino acid position). Those interactors with an asterisk indicate that the binding has been only proved with N-MYC.

13
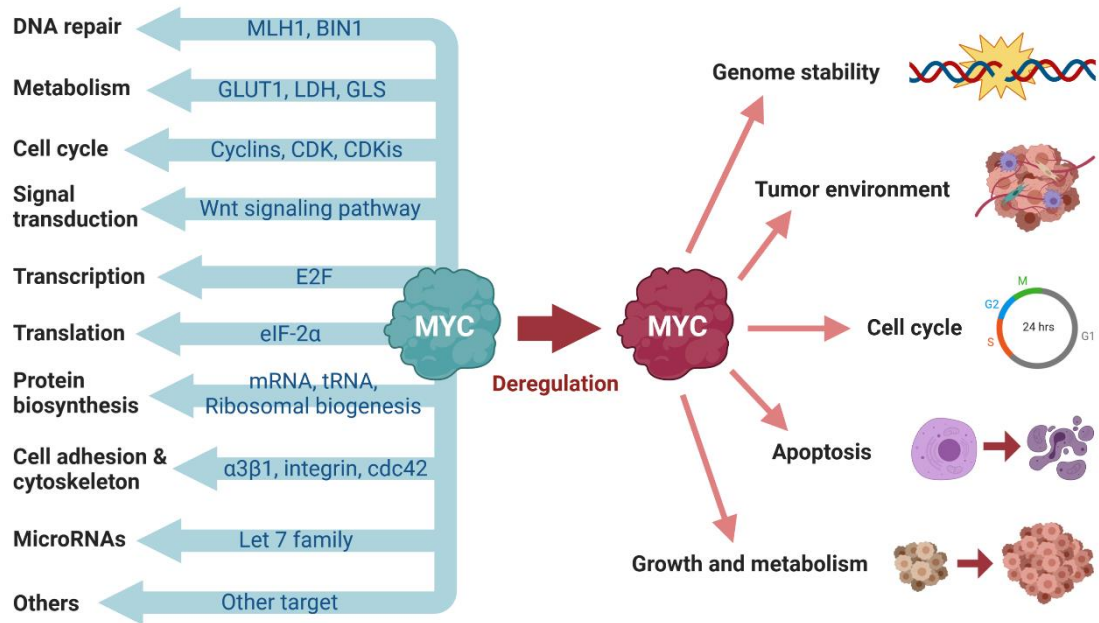
Figure 3. Biological functions of MYC proteins.
MYC regulates many protein-coding or non-coding genes involved in different cellular functions (left). But when deregulated and expressed in high levels, MYC is involved in several tumor-relevant processes (right). Adapted from (Chen et al. 2018) and (Tansey 2014).

Although L-MYC is mostly known for its amplification and expression in SCLC, C-MYC deregulated expression is estimated to contribute to at least 75% of all human cancers (Carabet et al. 2018). N-MYC is overexpressed in a large set of human malignancies too, WT included, like medulloblastoma, neuroblastoma, astrocytoma, retinoblastoma, gliobastoma multiforme, neuroendocrine prostate cancer, rhabdomyosarcoma, SCLC, hematologic malignancies, castration-resistant prostate cancer and pancreatic tumors (Rickman, Schulte and Eilers 2018).

2.2.2. The MAX protein

MYC-associated protein X (MAX) was the first MYC interactor to be identified (Blackwood and Eisenman 1991). Like MYC proteins, MAX is a nuclear basic-helix-loop-helix-leucine zipper transcription factor which can form dimers and bind to DNA **[Figure 4]**, but in contrast to them, MAX can also homodimerize (Carroll et al. 2018). The MYC/MAX and MAX/MAX dimers recognize Enhancer box (E-box) DNA elements with the sequence CANNTG and present the highest affinity for the palindromic sequence CACGTG, called the canonical MYC E-box (Carabet et al. 2018). MYC proteins are not the

only dimerization partners of MAX: while the MYC/MAX dimers are involved in transcriptional activation (see section 2.2.3.1), MAX also binds members of the MAX dimerization protein I (MXD1) protein family, the MAX-binding protein (MNT) and the MAX gene-associated protein (MGA) to repress transcriptional activation. This concedes MAX a central role in controlling the MYC/MAX/MXD1 axis, one of the better-known cellular networks whose deregulation contributes to the creation of many human cancers (Cascon and Robledo 2012, Grandori et al. 2000). Additionally, MAX homodimers are unable to transactivate gene expression, but they can indirectly induce transcriptional repression by competing with the MYC/MAX dimers for binding E-boxes (Kato, Wechsler and Dang 1992).
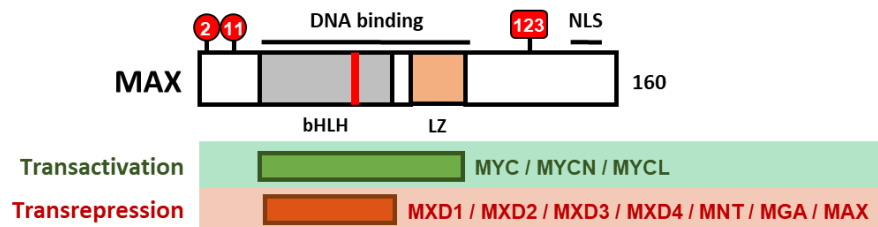
Figure 4. MAX protein structure and interacting proteins.
Schematic representation of the MAX protein. The basic helix-loop-helix domain (bHLH) is located in the N-terminus, and together with the leucine zipper domain (LZ) it mediates DNA-binding. These domains are also responsible for binding with different interactors, with which MAX is able to carry its transactivating or transrepressing functions. The nuclear localization signal (NLS) is located in the C-terminus. Major sites of phosphorylation are identified in red (indicating the amino acid position), while the number on the right refer to amino acids of the protein. The red mark indicates the position of the MAX-R60Q mutation.

The tumorigenic role of MAX, besides its well-characterized role as MYC dimerization partner, has been particularly studied in hereditary pheochromocytoma (PCC) and paraganglioma: 1.12 % of patients present germline loss-of-function *MAX* mutations, most of them within the bHLH-LZ domain, presumably destroying the ability of MAX to form dimers and bind DNA (Burnichon et al. 2012, Comino-Mendez et al. 2011, Comino-Mendez et al. 2015). The involvement of MAX in PCC is further supported by the lack of functional MAX in the rat PCC tumor cell line PC12, due to a C-terminal mutation preventing dimer formation (Hopewell and Ziff 1995). Additionally, 4.3 % cases of endometrial cancer harbored mutations in *MAX* and were associated with reduced

recurrence-free survival (Walker et al. 2018), and non-functional MAX proteins due to intragenic homozygous deletions were identified in 6 % of SCLC patients (Romero et al. 2014). MAX expression also seems to correlate with clinical outcome in neuroblastoma (Cascon and Robledo 2012, Ferrucci et al. 2018, Liu et al. 2014). Altogether, these observations point *MAX* as an important component of cancer development, acting as a classic tumor suppressor gene. However, considering the diversity of MYC proteins regarding their functionality and interaction partners, and due to the subjects of this study, we will further focus on the transcriptional regulation mediated by MYC, its interactome and the protein stability of N-MYC.

2.2.3. Transcriptional regulation by MYC

MYC proteins play an important role regulating the transcription of nuclear, nucleolar and mitochondrial DNA by different types of RNA polymerases. This MYC-mediated regulation has been better characterized for the transcription by RNA polymerase II (POL II), which is responsible for the synthesis of protein encoding mRNAs. In a similar situation to the knowledge available for MYC interactors, the transcriptional regulation by MYC proteins is best studied for C-MYC, but many findings could be reproduced and extended to N-MYC (Dang 2012).

2.2.3.1. MYC-mediated transactivation

MYC can induce transactivation by recruiting cofactors which either are adaptor molecules or perform different enzymatic activities, such as modifying the chromatin structure or modulating the actual process of transcription (Adhikary and Eilers 2005). These cofactors can be histone acetyltransferases (HATs) or chromatin-remodeling ATPases, and some of them can even be part of well characterized complexes involved in chromatin remodeling, such as the Nua4 histone acetyltransferase complex, the STAGA complex, the nucleosome remodeling factor (NURF) complex, and the SWI/SNF complex (McMahon et al. 1998, Wood, McMahon and Cole 2000, Richart et al. 2016, Liu et al. 2008, Cheng et al. 1999). Other recruited cofactors include histone kinases (Zippo et al. 2007), histone methyltransferase (HMT) (Wong et al. 2017) and histone demethylases (HDM) (Amente et al. 2010, Amente et al. 2015, Yang et al. 2015) **[Figure 2] [Figure 5]**. However, it is important to note that histone methylation and

demethylation can be associated with either activation or repression of transcription, depending on which effector protein is being recruited (Cloos et al. 2008), unlike histone acetylation which is directly associated with active promoters. MYC is also able to recruit topoisomerases involved in relieving DNA tension (Buchel et al. 2017).
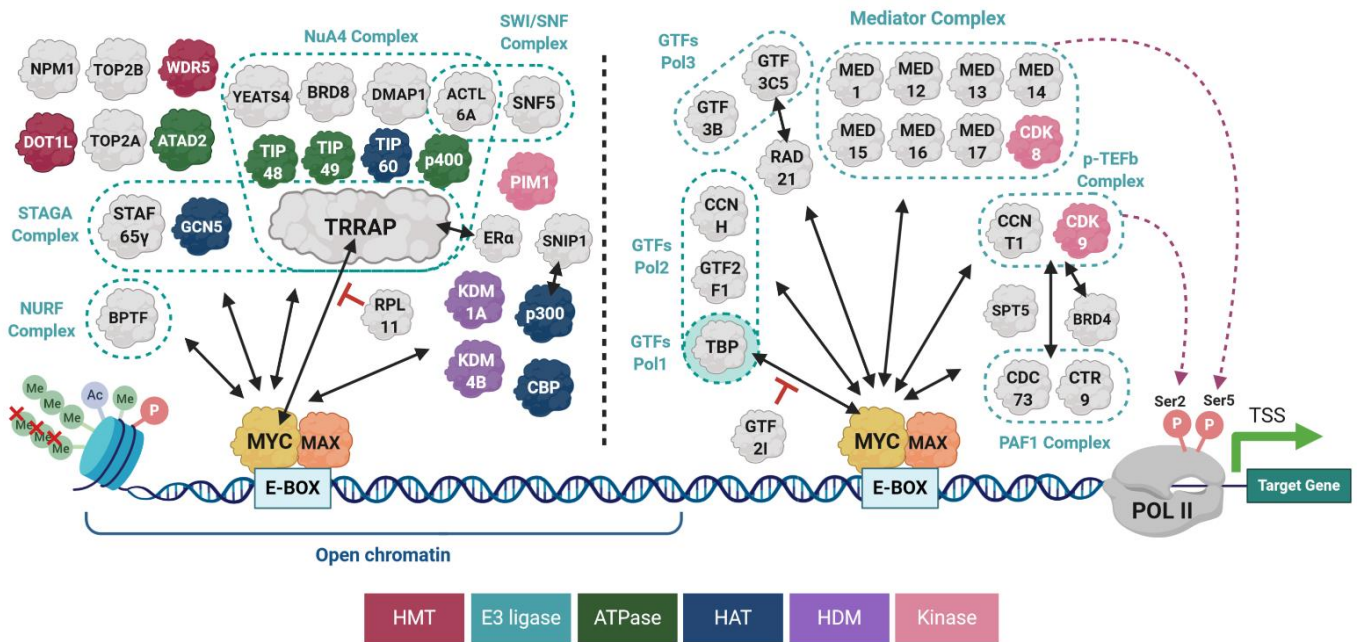
Figure 5. MYC-mediated transactivation.
Scheme illustrating C-MYC direct interactors and the MYC-mediated mechanisms of transcriptional activation in which they are involved. MYC heterodimerizes with MAX to bind to DNA elements, like E-boxes, and recruit a myriad of coactivators, involved in different processes like chromatin remodeling (left) or the actual process of transcription (right). Those interactors belonging to relevant protein families or complexes are grouped in dashed boxes, and if their molecular function is known, they are colored according to the legend indicated in the bottom.

This open chromatin structure will allow transcription to take place through different stages: the transcriptional pre-initiation and initiation, the promoter clearance, the POL II pause release, the transcriptional elongation, and finally the termination of transcription (Kouzine, Levens and Baranello 2014, Shandilya and Roberts 2012). MYC plays a major role in some of these steps, by recruiting some required effectors **[Figure 2] [Figure 5]**. During the pre-initiation step, MYC is involved in the recruitment of general transcription factors (GTFs), which will form the pre-initiation complex and help the POL II, and even other RNA polymerases like POL I and III, to correctly position themselves

on the promoter and start the transcription (Orphanides, Lagrange and Reinberg 1996). At the promoter clearance step, MYC contributes by recruiting several members of the Mediator complex, which phosphorylates the S5 residues of the POL II. This way, POL II can escape from the promoter and elongate the transcript (Eberhardy and Farnham 2001, Liu et al. 2003, Liu et al. 2008). However, before starting the elongation, POL II gets stuck near the promoter and needs to be reinitiated: this pause release is achieved by the p-TEFb complex and other associated proteins like BRD4, which bind MYC and mediate the POL II phosphorylation at S2 residues to induce its restart (Eberhardy and Farnham 2001, Kouzine et al. 2014, Liu et al. 2008, Poole and van Riggelen 2017). p-TEFb can also be recruited by the PAF1 complex (via its component CDC73), forming a complex with C-MYC and TRRAP to in parallel promote histone acetylation (Jaenicke et al. 2016). At the elongation step, MYC has been reported to bind SPT5 and hand it over to POL II in a CDK7-dependent manner, to increase POL II processivity and productive transcription (Baluapuri et al. 2019). Only for N-MYC, recruitment of BRCA1 via USP11 has been observed to prevent MYCN-dependent accumulation of stalled RNAPII and enhance transcriptional activation by MYCN too (Herold et al. 2019), although other studies report BRCA1 and NMI, members of the BRCA1 complex and direct interactors of C-MYC, as inhibitors of the transcriptional activation (Bao and Zervos 1996, Li, Lee and Avraham 2002, Wang et al. 1998).

2.2.3.2. *MYC-mediated transrepression*

MYC does not only regulate the activation of the transcription but also its repression, being both mechanisms of equal importance for MYC-driven tumor initiation and maintenance (van de Wetering et al. 2002, Walz et al. 2014). There are different ways MYC mediates transrepression. For example, MYC represses several non-canonical target genes by interacting with other transcription factors, like SP1 (Gartel et al. 2001), NFY (Izumi et al. 2001), YY1 (Shrivastava et al. 1996), FOXO3 (Chandramohan et al. 2008) and MIZ-1 (Peukert et al. 1997, Walz et al. 2014). The interaction of MIZ-1 with C-MYC has been very well characterized **[Figure 6]**, although it associates only weakly with N-MYC (Rickman et al. 2018). MIZ-1 recognizes INR sequences at core promoters to activate the transcription of genes and recruit co-activators like p300/CBP or NPMI, but

when MIZ-1 binds C-MYC, this recruitment is interfered (Staller et al. 2001). In addition, MYC recruits other co-repressors involved in chromatin remodeling to MIZ-1 location, repressing even more the transcription (Wanzel, Herold and Eilers 2003, Wu et al. 2003). Although there are evidences of C-MYC interacting with both MIZ-1 and MAX to form a ternary repressive complex, some studies suggest that MIZ-1 and MAX compete to engage C-MYC, repressing or activating transcription respectively (Bedard et al. 2017). MIZ-1 is stabilized by the ligase HUWE1, since inhibition of HUWE1 leads to the selective repression of MYC-activated target genes (Adhikary et al. 2005, Peter et al. 2014). Another transrepression mechanism consists in hindering the binding of MYC to DNA or even to MAX, and consequently interfering with its transactivating functions **[Figure 6]**.
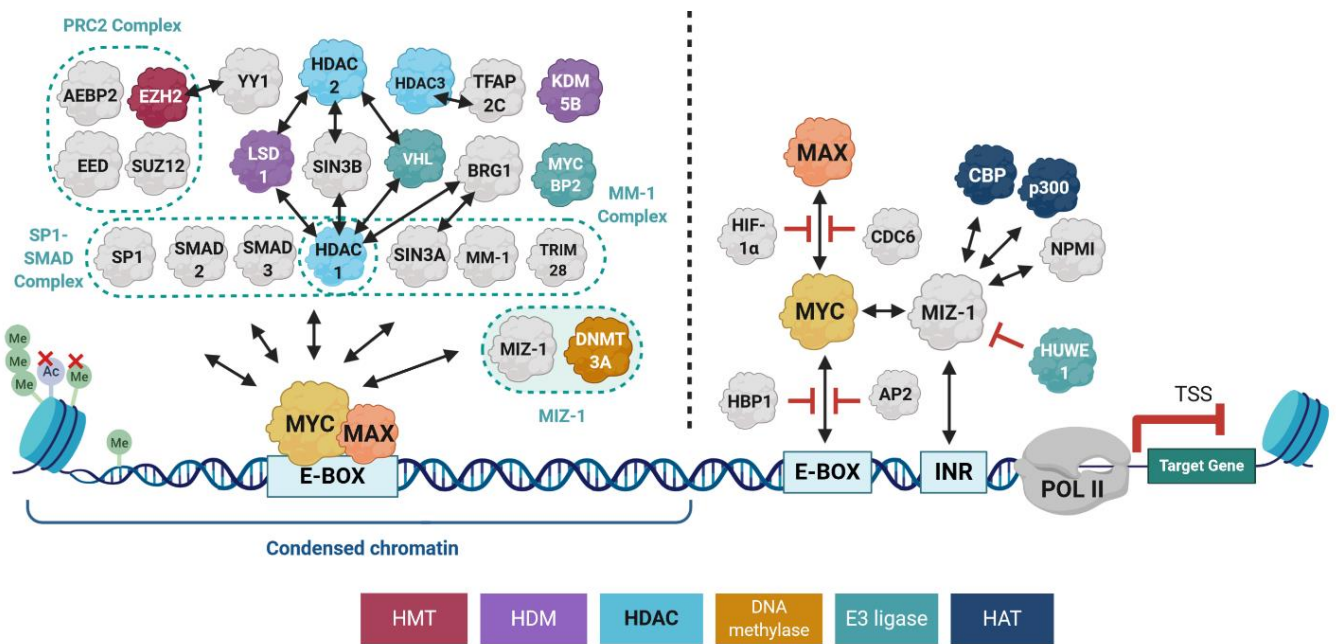
Figure 6. MYC-mediated transrepression.
Scheme illustrating C-MYC direct interactors and the MYC-mediated mechanisms of transcriptional repression in which they are involved. Some of these mechanisms involve recruiting cofactors necessary for chromatin remodeling (left). C-MYC transcriptional repression can be also achieved by interfering with the MYC-MAX dimerization (required for the transactivating functions of MYC), directly impeding the binding of MYC to E-boxes, or by dimerization of C-MYC with MIZ1, which not only a MAX competitor, but also has its own transcriptional activation functions inhibited by C-MYC. Interactors belonging to relevant protein families or complexes are grouped in dashed boxes, and if their molecular function is known, they are colored according to the legend indicated in the bottom of the figure.

MYC can also induce transrepression by recruiting co-repressors involved in chromatin remodeling, which can undo the open chromatin modifications required for transactivation **[Figure 2] [Figure 6]**. These cofactors include histone deacetylases (HDACs), which oppose the role of HATs in transactivation (Kurland and Tansey 2008, Liu et al. 2007, Marshall et al. 2010, Zhang et al. 2012); DNA methylases, which increases the DNA methylation of promoter regions or nearby CpG islands (Brenner et al. 2005); and the already mentioned double-edged HDMs (Amente et al. 2010, Amente et al. 2015, Wong et al. 2012). Some of these proteins have been reported to interact together, what could lead to synergistic effects (Humphrey et al. 2008, Shi et al. 2005), or are even components of larger well-characterized complexes involved in transrepression, such as the SP1-SMAD complex (Feng et al. 2002, Gartel et al. 2001) or the MM-1 complex (Fladvad et al. 2005, Satou et al. 2001). Some E3 ligases interacting with C-MYC like MYCBP2 or VHL have been speculated to be associated with chromosomal condensation too (Hwang et al. 2012, Sakamuro and Prendergast 1999). Last but not least, MYC has been observed to regulate the expression and recruitment of the Polycomb Repressive Complex 2 (PRC2) protein, involved in transcriptional silencing via chromatin modifications (Fagnocchi et al. 2016, Poole and van Riggelen 2017, Rao et al. 2015).

2.2.4. N-MYC proteasomal degradation

MYC proteins need to be tightly regulated, due to their role in several cellular processes. Although C-MYC regulation has been well characterized, much less is known for N-MYC, mainly due to the assumption that both proteins are redundant (Malynn et al. 2000), but there are indeed some differences regarding their regulatory mechanisms. There are several possibilities for regulating N-MYC, like targeting its transcription (Matsushima and Bogenmann 1993, Strieder and Lutz 2003) or its resulting mRNA (Shams et al. 2020), or via different types of post-translational modifications at the protein level. These modifications include phosphorylation, acetylation and ubiquitinylation, and they have multiple implications such as protein stability. Considering the aims of our study, we will only focus on the protein stability of N-MYC via phosphorylation and ubiquitinylation.

N-MYC is a relatively unstable protein, with a short half-life of around 30 min (Cohn et al. 1990). The control of N-MYC expression and stability via degradation is crucial to prevent high N-MYC levels which can develop into transformation and tumor development (see section 2.2.1) **[Figure 3]**. Its degradation takes place through the ubiquitin-system or using an ubiquitin-independent mechanism. The second one is mediated by the D-element and the PEST sequence in the central part of the protein **[Figure 1]**, which act as signal peptides for protein degradation (Gregory and Hann 2000, Herbst et al. 2004). Different E3 ligases have been reported to target N-MYC for degradation: the E3 ligase complexes SCF^{Fbw7} and DCX^{TRUSS}, with their respective substrate-specific adaptors FBXW7 and TRUSS, as well as HUWE1 and TRIM32 (Choi et al. 2010, Farrell and Sears 2014, Izumi and Kaneko 2014, Sjostrom et al. 2005, Zhao et al. 2008). The SCF^{Fbw7}-mediated degradation is the best characterized and is triggered by phosphorylation of two conserved residues at MBI, T58 and S62. Some studies suggest including S64 in this phospho-degron, but further functional studies would be required (Baluapuri et al. 2020, Rickman et al. 2018). This degron not only plays a major role in MYC protein stability, but also in the MYC-mediated regulation of apoptosis and transformation (Chang et al. 2000).

Phosphorylation of the N-MYC phospho-degron and the consequent proteasomal degradation goes through several steps **[Figure 7]**. N-MYC is initially phosphorylated at S62 by CDK1/CyclinB, becoming stable and competent to enter in the nucleus, where it will execute its transcriptional functions. Phosphorylation of S62 will allow then GSK3β, which is negatively regulated by the PI3K signaling pathway, to phosphorylate T58, generating a doubly phosphorylated and transcriptionally active N-MYC (Gregory, Qi and Hann 2003). The PI3K signaling pathway promotes metabolism, proliferation, cell survival, growth and angiogenesis in response to extracellular signals, connecting these biological processes with MYC degradation (Cohen and Frame 2001, Parisi et al. 2011). Phosphorylation of T58 makes MYCN also unstable, because it becomes susceptible of being recognized by its substrate-specific E3 ligases. These ligases mediate poly-ubiquitination of N-MYC, which acts as a mark for proteasomal degradation (Otto et al. 2009, Popov et al. 2010). There are some enzymes which can contribute to N-MYC stabilization: the deubiquitinating enzymes (DUBs) USP7 and USP28, which can revert

the poly-ubiquitinylation of the E3 ligases (Popov et al. 2007, Tavana et al. 2016); EYA phosphatases, which can dephosphorylate T58 and therefore prevent E3 ligases-dependent turnover (Herold et al. 2019, Xu et al. 2014); or Aurora A kinase, which can bind to and stabilize poly-ubiquitinated and/or phosphorylated N-MYC, but not C-MYC (Otto et al. 2009), remaining able to dimer with MAX and activate transcription (Richards et al. 2016).
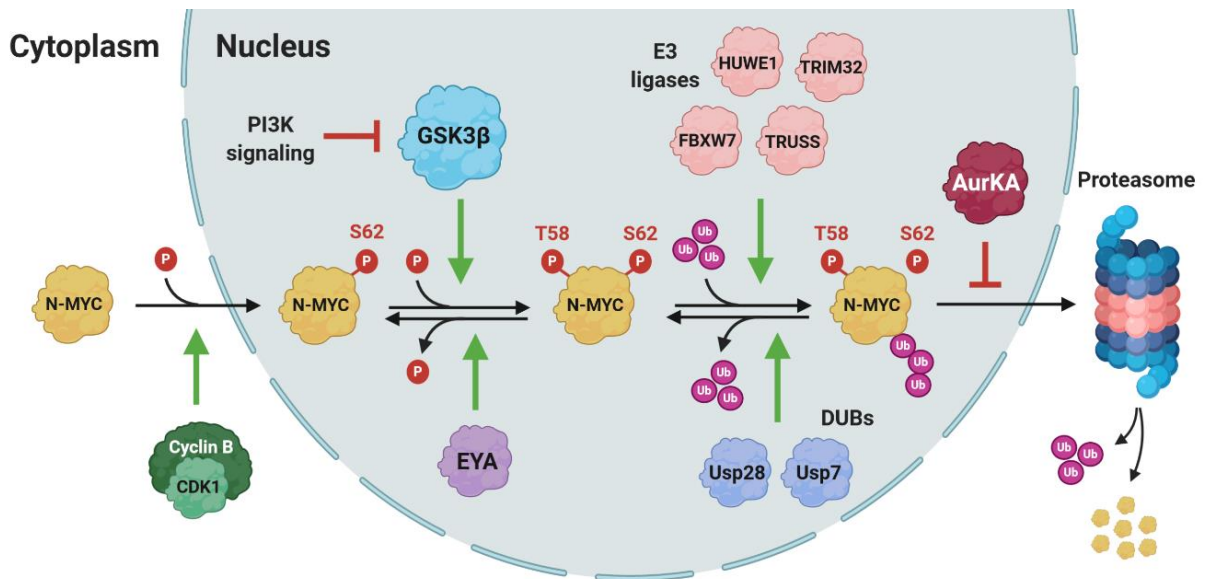
Figure 7. N-MYC proteasomal degradation.
Overview of the pS62/pT58 N-MYC degradation pathway and the proteins involved in N-MYC stabilization. N-MYC phosphorylation of S62 by CDK1/Cyclin B allows its transportation into the nucleus and primes the T58 phosphorylation by GSK3β, which can be reversed by EYA phosphatases. Double-phosphorylated N-MYC is susceptible of being poly-ubiquitinated by E3 ligases, marking the protein for proteasomal degradation. This degradation can be prevented by removing the poly-ubiquitin tag with the help of deubiquitinating enzymes (DUBs), or by the stabilization of poly-ubiquitinated/phosphorylated N-MYC via Aurora kinase A (AurKA).

2.2.5. *MYCN* and *MAX* in WT

The role of these two transcription factors in renal development is only known for N-MYC, which acts regulating the proliferation of the NPCs (Laurenti, Wilson and Trumpp 2009, Mugrauer, Alt and Ekblom 1988). This fact, together with the results of recent studies aiming to unveil the genetic background of WT (see section 2.1.6), has

underlined the potential of dysregulated *MYCN* events in WT tumorigenesis. *MYCN* alterations represent 18.5 % of cases treated with preoperative chemotherapy (Wegert et al. 2015), and two alterations are predominantly observed in WT: *MYCN* copy number gain, and the somatic variant *MYCN* P44L.

MYCN copy number gain has been reported in several studies for WT (Gadd et al. 2017, McQuaid and O'Meara 1990, Norris et al. 1988, Perotti et al. 2012, Schaub et al. 2007, Wegert et al. 2015, Williams et al. 2010, Williams et al. 2011, Williams et al. 2015), mostly with low copy amplification. Reports from SIOP studies have observed this event in 12-16 % of overall analyzed WT cases, and when they are limited to high-risk blastemal or diffuse anaplastic cohort, it represented 8.6 % and 30.4 % respectively (Wegert et al. 2015, Williams et al. 2015). Putting aside the results obtained from the blastemal cohort, these frequencies were similar to the results obtained within a NWTS/COG study (Gadd et al. 2017). Therefore, gain of *MYCN* correlates with anaplasia, and according to results derived from additional SIOP studies, it is correlated with poorer relapse-free and overall survival too (Williams et al. 2015). *MYCN* amplification is also associated with poor outcome in other pediatric cancers such as medulloblastoma, neuroblastoma and rhabdomyosarcoma (Beltran 2014).

N-MYC was considered an "undruggable" target, but with the recent development of small molecule inhibitors indirectly interfering with N-MYC functions (Carabet et al. 2018), the establishment of *MYCN*-driven *in vivo* tumor models recapitulating human disease types has become essential. Two murine models of MYCN-driven neuroblastoma have been developed, closely resembling human neuroblastomas in terms of tumor localization and histology, genomic aberrations and gene expression: TH-MYCN (Weiss et al. 1997) and LSL-MYCN;Dbh-iCre (Althoff et al. 2015). Using the same LSL-MYCN mouse strain and aiming for a tissue-specific *MYCN* upregulation, similar findings were achieved in a mouse model of neuroendocrine prostate cancer (Dardenne et al. 2016). Therefore, this mouse strain is a promising tool to achieve an *in vivo MYCN*-driven WT model, combined with mouse lines expressing Cre-recombinase under the nephron progenitor cells-specific Six2/Cited1 promoters (see section 2.1.7).

A few studies have identified several *MYCN* somatic variants in WT (Gadd et al. 2017, Wegert et al. 2015, Williams et al. 2015), but the one observed with far more frequency is *MYCN* P44L. This missense mutation (c.131 C>T) has been spotted at low frequencies in several other tumor types **[Table 4]**, and it is predicted as pathogenic and activating according to different functional prediction tools, such as PolyPhen-2, SIFT and FATHMM (Adzhubei, Jordan and Sunyaev 2013, Kumar, Henikoff and Ng 2009, Shihab et al. 2013). *MYCN* P44L affects the MBI **[Figure 1]**, which is involved in protein stability and recruiting of transcriptional co-factors **[Figure 2]**. In one study, wild-type and P44L mutant N-MYC were overexpressed in HEK293T cells, followed by a Western blot analysis of the T58 and S62 residues phosphorylation levels. The observed increase of phosphorylation in the mutant protein at these positions suggested that the mutation could affect the biological activity of N-MYC, but further evidences to validate these theories are required (Kato et al. 2019). The *MYCN* P44L mutation frequency in WT obtained from SIOP studies of no more than 270 patients was 3 %, representing around 5 % of cases with high-risk histology (Wegert et al. 2015, Williams et al. 2015). A larger NWTS/COG study with 651 patients observed this mutation in 22 patients, with a similar incidence as its European counterpart (Gadd et al. 2017). Despite the recurrence of *MYCN* P44L in different tumor types, as well as its potential as an oncogenic driver and biomolecular marker of clinicopathological relevance, a complete functional characterization of this mutation has not been presented yet.

Furthermore, a few N-MYC interactors have been identified mutated in WT, such as: FBXW7, involved in N-MYC protein stability (see section 2.2.4); NONO, implicated in transcriptional upregulation of *MYCN* mRNA and protein expression; and the already in detail described MAX (Gadd et al. 2017, Liu et al. 2014, Wegert et al. 2015, Williams et al. 2015). Also, a functional link between N-MYC, EYA1 and SIX2 has been identified driving expansion and maintenance of the multipotent progenitor cells during nephrogenesis (Xu et al. 2014), being SIX2 recurrently mutated in high-risk blastemal WT too (Wegert et al. 2015). All these events represent additional mechanisms of *MYCN* regulation to be explored in WT. Among these mutations, the *MAX* R60Q missense mutation (c.179 G>A) has been also observed in several tumors at low frequencies

[Table 4], and it is the most common *MAX* mutation reported in the COSMIC database (Tate et al. 2019).

Table 4. Summary of cancers with *MYCN* P44L and/or *MAX* R60Q mutations.
Sorted by number of entries in COSMIC database. Those cancers where both *MYCN* P44L and *MAX* R60Q were identified are highlighted in bold.

MYCN P44L	*MAX* R60Q
Wilms Tumor	**Wilms Tumor**
Endometrioid carcinoma	**Endometrioid carcinoma**
Neuroblastoma	**Pancreatic ductal adenocarcinoma**
T-lineage acute lymphoblastic leukemia	Acute myeloid leukemia
Astrocytoma	**Astrocytoma**
Basal cell carcinoma	Caecum adenocarcinoma
Oligodendroglioma	Sigmoid colon adenocarcinoma
Pancreatic ductal adenocarcinoma	Transverse colon adenocarcinoma
Mesonephric carcinoma	Paraganglioma
Papillary thyroid cancer	Pheochromocytoma
Neoplastic cyst of the pancreas	Germ cell tumor (mixed)
Medulloblastoma	Duodenum adenocarcinoma
Sebaceous carcinoma	Lung adenocarcinoma
Sinonasal adenocarcinoma	Oligoastrocytoma
Pancreas cancer	**Medulloblastoma**
Melanoma	Squamous cell carcinoma
	Gastric cancer

Also of interest is that, although several germline and somatic *MAX* variants have been reported in different types of cancers (Burnichon et al. 2012, Comino-Mendez et al. 2011, Walker et al. 2018), no other mutations besides R60Q have been reported for WT until now: only one of 58 high-risk blastemal WT cases was identified in a SIOP study (Wegert et al. 2015), and 11 among 651 WT in a NWTS/COG study (Gadd et al. 2017). The R60Q mutation is located in the bHLH domain of MAX **[Figure 4]**, and functional prediction tools classify it as pathogenic and activating, presumably interfering in the protein dimerization and DNA-binding features. Some studies have been performed to biochemically characterize this mutant (Comino-Mendez et al. 2015, Dela Cruz et al. 2016, Wang et al. 2017), but further functional studies to analyze the potential of *MAX* R60Q are required.

3. Aims of the thesis

The objectives of this project can be summarized in the following points:

1) Determination of *MYCN* P44L and *MAX* R60Q mutations in WT and analysis of possible associations to specific histological WT subtypes or clinical features.

2) Screening of alternative *MAX* coding sequence variants in WT, in addition to the already reported *MAX* R60Q mutation.

3) Functional characterization of the N-MYC-P44L and MAX-R60Q mutants. For MAX-R60Q, this characterization will focus on its eventual consequences on protein dimerization, binding to DNA and cell proliferation. For N-MYC-P44L, we will also cover the possible impact of the mutation on binding to other interactors, as well as its effect on N-MYC stability and phosphorylation.

4. Materials

4.1. Chemicals and disposables

All used disposables were either purchased from Sarstedt or Eppendorf. Chemicals that
are not listed separately were either purchased from ROTH, Sigma-Aldrich or Applichem.
If not listed here, all enzymes used for cloning were purchased from NEB.

Table 5. Used chemicals.

Chemicals	Company
Anti-Flag-M2-Affinity Gel	Sigma-Aldrich
Anti-HA Magentic Beads	Thermo Fisher
Aprotinin	Sigma-Aldrich
Benzonase nuclease purity > 99%	VWR/Novagen
Beta-mercaptoethanol	Sigma-Aldrich
Cycloheximide	Roth
Dulbecco's Modified Eagle Medium (DMEM)	Sigma-Aldrich
Dimethyl sulfoxide (DMSO)	Roth
DNase I	Thermo Fisher
Doxycycline (DOX)	Applichem
Ethylene glycol (EG)	Roth
Exonuclease I	Thermo Fisher
Fetal calf serum (FCS)	Sigma-Aldrich
His-taq polymerase	self-made
His-Pfu polymerase	self-made
Leupeptin	Sigma-Aldrich
MG-132	Biomol
NuPAGE LDS Sample buffer	Thermo Fisher
Penicillin/Streptomycin 100x	PAA
Pepstatin	Sigma-Aldrich
peqGOLD TriFast	Peqlab
Phenylmethylsulfonyl fluoride (PMSF)	Applichem
Phosphatase Inhibitor Cocktails II and III	Sigma-Aldrich
Puromycin	Sigma-Aldrich
10x RT Random primer	Applied Biosystems
Shrimp Alkaline Phosphatase (rSAP)	NEB
SybrGreen	Sigma-Aldrich
Thiazolyl Blue Tetrazolium Bromide (MTT)	Sigma-Aldrich

4.2. Buffers and solutions

Table 6. Used buffers.

Standard buffers	
PBS	150 mM NaCl, 2.7 mM KCl, 8 mM Na_2HPO_4, 1.8 mM KH_2PO_4
TE	10 mM Tris pH 8.0, 1 mM EDTA
TBST	140 mM NaCl, 2.7 mM KCl, 25 mM Tris-HCl pH 7.5, 0.1 % Tween-20
DNA buffers	
DNA loading dye 10x	50 % glycerol, 15 % ficoll, 10 mM EDTA pH 8.0
PCR buffer 10x	200 mM Tris pH 8.8, 100 mM $(NH_4)_2SO_4$, 100 mM KCl, 20 mM $MgSO_4$, 1 % TritonX-100, 1 % BSA-acetylated
SB 20x	200 mM NaOH pH 8.0 with boric acid
TAE 50x	50 mM EDTA, 2 M Tris acetate pH 8
Protein buffers	
Blotting buffer	25 mM Tris pH 8.3, 150 mM glycine, 10 % Methanol
Co-IP lysis buffer	20 mM HEPES pH 7.9, 180 mM NaCl, 1.5 mM MgCl2, 10 % glycerol, 0.2 % Nonidet P40. *Fresh before use: 1 µg/ ml Aprotinin, Leupeptin and Pepstatin, 50 µg/ml PMSF, and phosphatase inhibitors II and III at 1:10000 dilution.*
Detection buffer	100 mM Tris pH 8.0, 250 mM luminol, 90 mM p-coumaric acid, 0.01% H_2O_2
Protein loading buffer x4	200 mM Tris pH 6.8, 8 % SDS, 0.4 % Bromophenol blue, 40 % glycerol, 400 mM DTT
RIPA buffer	50 mM Tris pH 8.0, 1 % Nonidet P40, 0.5 % Sodium deoxycholate, 0.1 % SDS, 150 mM NaCl, 1 mM EDTA. Fresh before use: 1 µg/ml Aprotinin, Leupeptin and Pepstatin, 50 µg/ml PMSF, and phosphatase inhibitors II and III at 1:10000
SDS running buffer	25 mM Tris pH 8.3, 192 mM glycine, 1% SDS
Silver staining	
Solution 1	127 mM trichloroacetic acid, 0,04% formaldehyde, 50 % (v/v) acetone
Solution 2	50 % (v/v) acetone
Solution 3	0,67 mM $Na_2O_3S_2 \cdot 5H_2O$
Solution 4	26mM Silver nitrate, 1 % formaldehyde
Solution 5	190 mM Na_2CO_3, 0,04 % formaldehyde, 0,168 mM $Na_2O_3S_2 \cdot 5H_2O$
Luciferase assay buffers	
Assay buffer	25 mM glycyl-glycine pH 7.8, 15 mM magnesium sulphate, 15 mM potassium phosphate, 4 mM EGTA, 1 mM DTT, 1 mM ATP, 1 µg/µl Luciferin
Cell lysis buffer	25 mM glycyl-glycine pH 7.8, 15 mM magnesium sulphate, 15 mM potassium phosphate, 4 mM EGTA, 1 mM DTT and 2 % TritonX-100

4.3. Plasmids

After cloning or receipt, all constructs were verified by Sanger sequencing.

Table 7. Used plasmids.

Name	Description
pSB-ETiE	Sleeping Beauty vector (Izsvak and Ivics 2004) containing a doxycycline dependent transactivator (TA), for inducing the bicistronic expression of a GOI and GFP upon addition of doxycycline. The construct allowed selection through puromycin and identification of transfected and induced cells through green fluorescence. In this work it was used as backbone vector for the N-MYC and MAX plasmids (see below), and as an "empty vector" for transfecting equal plasmid amounts.
pCMV(CAT)T7-SB100x	Transposase vector used for stable transfection of the Sleeping Beauty vector (see above).
pSB-ETiE-HA-MYCN-WT and -P44L	pSB-ETiE with CDS of human N-terminal HA-tagged wild-type or P44L mutant N-MYC **[Figure 8]**.
pSB-ETiE-FLAG-MAX2-WT and -R60Q	pSB-ETiE with CDS of human N-terminal FLAG-tagged wild-type or R60Q-mutant MAX **[Figure 8]**.
pGL3-6XEBOX-prom	Firefly luciferase reporter vector, containing six E-box sites (cloned from pGL2-6XEBOX vector (Perini et al. 2005)) upstream of the SV40 promoter **[Figure 8]**.
pcDNA3.1-FLAG-BMP2K	pcDNA3.1-CMV vector with CDS of human N-terminal FLAG-tagged wild-type BMP2K.
pCDH-FLAG-DAB2-201	pCDH-CMV vector with CDS of human N-terminal FLAG-tagged wild-type DAB2.
p3FL-YEATS2-FLAG	p3xFlag-CMV-7.1 vector with CDS of human N-terminal FLAG-tagged wild-type YEATS2. Provided by Xiaolu Wang (Mi et al. 2017)
p3FL-PEG10-RF1/2	p3xFlag-CMV-7.1 vector with CDS of human N-terminal FLAG-tagged wild-type PEG10.
p3FL-TROVE2	p3xFlag-CMV-7.1 vector with CDS of human N-terminal FLAG-tagged wild-type TROVE2.
pcS2p-FLAG-hTLE1	pCS2P-CMV vector with CDS of human N-terminal FLAG-tagged wild-type TLE1.
pcDNA3.1-FLAG-MCRS1	pcDNA3.1-CMV vector with CDS of human N-terminal FLAG-tagged wild-type MCRS1.
pcDNA3.1-FLAG-FOXK1	pcDNA3.1-CMV vector with CDS of human N-terminal FLAG-tagged wild-type FOXK1.
pcDNA3.1-FLAG-DVL2	pcDNA3.1-CMV vector with CDS of human N-terminal FLAG-tagged wild-type DVL2.
pcDNA3.1-FLAG-CBLL1	pcDNA3.1-CMV vector with CDS of human N-terminal FLAG-tagged wild-type CBLL1.
pfRFP-FOXK1-1 pfRFP-FOXK1-2 pfRFP-FOXK1-3 pfRFP-FOXK1-4 pfRFP-FOXK1-5 (F)	pFlag-RFP vectors with CDS of human FOXK1 deletion mutants: each plasmid codes for the aminoacids 1-64 (1), 66-222 (2), 222-464 (3), 464-734 (4) or the full CDS (5 or F) of the wild-type FOXK1.
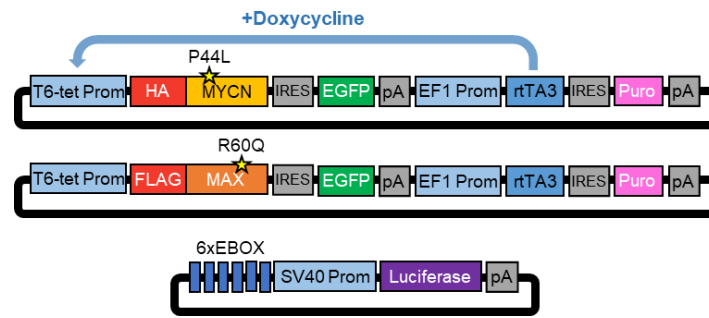
Figure 8. Plasmid constructs used for *MYCN* and *MAX* mutants biocharacterization.
From top to bottom: vectors for doxycycline-inducible expression of HA-N-MYC (wild-type or P44L mutant) and FLAG-MAX (wild-type or R60Q mutant); and firefly luciferase reporter vector. Tet-responsive promoter (T6-tet Prom), internal ribosome entry site (IRES), polyadenylation signal (pA), EF1 promoter (EF1 Prom), reverse tetracycline-regulated transactivator gene (rtTA3) and puromycin-resistance gene (Puro). Upon addition of doxycycline, the rtTA protein binds to it and only then they can bind the tet-responsive promoter and induce the expression of downstream genes.

4.4. Antibodies

Table 8. Used antibodies.

Primary Antibodies			
Name	**Species**	**#**	**Company**
α-c-Myc/N-Myc (D3N8F)	rabbit	#13987	Cell Signaling
α-c-Myc [Y69]	rabbit	ab32072	Abcam
α-Flag-M2	mouse	F3165	Sigma-Aldrich
α-GFP	goat	ABIN100085	antibodies-online
α-HA	mouse	H9658	Sigma-Aldrich
α-MAX (C-17)	rabbit	sc-197	Santa Cruz
α-MYC-pS62	rabbit	Gift from AG Eilers (Uni Würzburg)	
α-MYC-pT58	rabbit	ab28842	Abcam
α-Vinculin	mouse	V9131	Sigma-Aldrich
Secondary Antibodies			
Name	**Species**	**#**	**Company**
α-goat-POD	rabbit	A5420	Sigma-Aldrich
α-mouse-HRP	goat	AP124P	Sigma-Aldrich
α-rabbit-HRP	goat	#7074	Cell Signaling

4.5. Cell lines

Table 9.Used cell lines.

Cell line	Description
HEK293T	Human embryonic kidney cell line with constitutive expression of SV40 large T antigen. Used for transient and stable transfection of plasmids.
U2OS	Human osteosarcoma cell line. Used for transient transfection of plasmids.

4.6. Bacterial strains

E. coli DH5α competent cells were used for transformation of plasmid DNA.

4.7. Equipment

Table 10. Used equipment.

Equipment	Company
Avanti J-26 XP ultracentrifuge	Beckman Coulter
Bioruptor Standard sonifier	Diagenode
Concentrator 5301	Eppendorf
EASY-nLC 1000	Thermo Fisher
JA-25.50 fixed angle rotor	Beckman Coulter
Mastercycler ep realplex	Eppendorf
NanoDrop ND-1000 Spectrophotometer	PeqLab
Orbitrap Fusion	Thermo Fisher
PicoView Ion Source	New Objective
Tristar LB941 Multimode Microplate Reader	Berthold
Ultrasonifier W-250 D	Heinemann

4.8. Kits

Table 11. Used kits.

Name	Company
Cycle pure kit	Omega Bio-Tek
Gel extraction kit	Omega Bio-Tek
Plasmid midi and mini kits	Omega Bio-Tek
RevertAid Reverse Transcriptase	Thermo Fisher

4.9. Software

Table 12. Used equipment.

Software	Company
Andromeda	Cox et al., 2011
EndNote X9	Clarivate Analytics
Mastercycler ep realplex 2.2	Eppendorf
MaxQuant v.1.6.2.2	Cox et al., 2008
MikroWin (2000) v. 4.41	Mikrotek Laborsysteme GmbH
MS Office Professional Plus 2016	Microsoft
NanoDrop ND-1000 3.3	Coleman Technologies Inc.
PEKAS Studio X	Bioinformatics Solution Inc.
Prism 8	GraphPad Software Inc.
Snapgene 5.0.6	GSL Biotech LLC
SPSS Statistics v.25	IBM

4.10. Online programs and databases

Table 13. Used online programs and databases

Program/database	Publication/Website
BioGRID 3.5	Oughtred et al., 2019
	https://thebiogrid.org/
BioRender	https://www.biorender.com/
COSMIC	https://cancer.sanger.ac.uk/cosmic
Ensembl (release 98)	Hunt et al., 2018
	http://www.ensembl.org/
GeneCards	Stelzer et al., 2016
	https://www.genecards.org/
NetPhos 2.0	http://www.cbs.dtu.dk/services/NetPhos-2.0/
PhosphoMotif Finder	http://www.hprd.org/PhosphoMotif_finder
PhosphoSitePlus	https://www.phosphosite.org
PRIDE	Perez-Riverol et al., 2019
	https://www.ebi.ac.uk/pride/
PubMed	https://www.ncbi.nlm.nih.gov/pubmed/
R2 Genomics Analysis and Visualization Platform	http://r2.amc.nl/
Spotfire	TIBCO Software Inc.
	http://spotfire.tibco.com
UniProtKB	The UniProt Consortium, 2019
	https://www.uniprot.org/uniprot/
WebSNAPER	http://pga.mgh.harvard.edu/cgi-bin/snap3/websnaper3.cgi

5. Methods

5.1. Patient material

WTs and other pediatric renal tumors were obtained from the German SIOP93-01/GPOH and SIOP2001/GPOH studies, including control tissues. Clinical data was available for all samples through the WT study data centers. All subjects or their parents provided written consent for tumor banking and future research use according to German regulations (*Ethikkommission der Ärztekammer des Saarlandes*, 136/01). Sample names were coded and pseudonymized for central processing. DNA and RNA were isolated from the snap frozen tumor tissue by Barbara Ziegler (AG Gessler, EBCh, Würzburg), using standard procedures or kits like QIAgen Allprep mini kit. Isolated DNA was diluted to 50 ng/µl in TE buffer and used as DNA template for further PCR analysis. Only DNA was isolated from control tissues, i.e. blood or non-tumoral kidney.

5.2. Allele-specific PCR

DNA isolated from WT and other pediatric renal tumor patients was used to perform *MYCN* P44L and *MAX* R60Q allele-specific PCRs (ASPs), as well as a *XIST* PCR to verify sample integrity **[Table 14] [Table 15] [Supplement 10.1]**. All oligonucleotides were designed using the WebSNAPER software. Tumor samples with known alterations were used as control. SB agarose gel electrophoresis was used to verify PCR products. Potential variants were verified by Sanger sequencing (see section 5.3). Only for confirmed patients with *MYCN* P44L and *MAX* R60Q mutations, additional ASPs for other recurrent somatic mutations in high-risk blastemal WT were performed: *SIX1* Q177R, *SIX2* Q177R, *DROSHA* E1147K and *DGCR8* E518K.

Table 14. Program for *XIST* PCR, ASPs and sequencing PCRs.

94°C	5 min	Initial denaturation	
94°C	20 sec	Denaturation	
*	20 sec	Annealing	35 cycles
72°C	20 sec **	Elongation	
72°C	5 min	Final elongation	
16°C	∞	End	

* See section 10.1 for each oligonucleotide combination corresponding annealing temperature.
** For MAX CDS sequencing PCR, use 35 sec.

Table 15. Reactions for different types of PCR.

	XIST PCR and ASPs	Sequencing PCR potential variants	Sequencing PCR *MAX* CDS
10X PCR buffer	2.5 µl	3 µl	3 µl
dNTPs 100 mM	0.25 µl	0.3 µl	0.3 µl
His-Taq 15 U/µl	0.4 µl	0.48 µl	0.1 µl
Oligonucleotide #1 10 pmol	0.8 µl	1 µl	0.5 µl
Oligonucleotide #2 10 pmol	0.8 µl	1 µl	0.5 µl
EG (if required) *	(1.5 µl)	(2.7 µl)	
DNA template	1 µl	1 µl	1 µl
H$_2$O	to 25 µl	to 30 µl	to 30 µl

* See section 10.1 to see in which oligonucleotide combinations EG or DMSO is required.

5.3. Sanger sequencing

DNA or cDNA samples were used for a sequencing PCR **[Table 14] [Table 15] [Supplement 10.1]**, and PCR products were verified by SB agarose gel electrophoresis. The sequencing was performed by a commercial provider (Eurofins Genomics Germany GmbH, Ebersberg). Prior to their shipment together with their sequencing oligonucleotide, PCR products were treated with an Exonuclease I - Shrimp Alkaline Phosphatase (Exo/SAP) clean up, to remove residual oligonucleotides and to dephosphorylate remaining dNTPs.

For the identification of *MAX* CDS variants in WT, oligonucleotides annealing to the 5'- and 3'-UTR of the CDS were used for the sequencing PCR, and an internal reverse oligonucleotide binding to the 3'-UTR of the *MAX* CDS was shipped as the sequencing oligonucleotide **[Supplement 10.1]**.

Data analysis was performed using SnapGene (GSL Biotech LLC).

5.4. Digestion-based screening of MAX-R60Q

5 µl of the *MAX* R60Q sequencing PCR reaction for each patient (see section 5.3) were used for a restriction digestion, performed overnight at 25 °C with 5 U of ApaI per reaction. The following day, the PCR products and their digestions were analyzed in parallel using SB agarose gel electrophoresis. For validating the allele frequency of analyzed patients, the digestion was performed using 5 µl of a PCR reaction, using pSB-

ETiE-FLAG-MAX-WT/R60Q plasmids mixed in different ratios (1:1, 1:3 and 3:1) as DNA templates **[Supplement 10.1]**.

5.5. Patients data analysis

All statistical analyses were performed with SPSS (IBM) using the two-tailed Fisher's exact test or the Mann-Whitney-U test for continuous variables. A significant association was confirmed when the resulting p-value (p) was ≤ 0.05.

5.6. Cloning

All cloning was done using standard molecular methods. Cloned constructs were always verified by Sanger sequencing.

For generating new expression vectors, the GOI was amplified based on existing expression vectors or using cDNA from HEK293 cells of from tumor material of WT patients. By using specifically designed oligonucleotides **[Supplement 10.1]**, new restriction sites, tag-encoding sequences and the *MYCN* P44L and *MAX* R60Q single-base mutations were added to the coding sequence (CDS) of the GOI, which were later inserted into different expression vectors.

The CDS of human *MYCN* and *MAX* (long isoform, NM002382) were cloned from the pcDNA3-MYCN and pBJ3-Max2 plasmids (M. Eilers, Dept. of Molec. Biochemistry, Uni Würzburg). The PEG10 expression vector was produced by cloning the *PEG10* CDS from the pcDNA3.1-PEG10-RF1/2-HisA vector, provided by Fan Zhang (Akamatsu et al. 2015), into a p3xFlag-CMV-7.1 vector. The pGL3-6XEBOX-prom luciferase reporter vector was generated by inserting six E-box sites (CACGTG), cloned from the pGL2-6EXBOX vector (G. Perini, Dept. of Pharmacy and Biotechnology, University of Bologna), upstream of the SV40 promoter of the pGL3-Promoter vector (Promega). The FOXK1 deletion mutants were generated by Anja Winkler (Develop. Biochem., Uni Würzburg) by cloning the corresponding section of the wild-type *FOXK1* CDS from the pCDNA3.1-FLAG-FOXK1.

A combination of His-*Taq* and His-*Pfu* DNA polymerases was used for all cloning PCRs, except for *FOXK1* and *BMP2K*, which CDS was amplified using the Q5 High-Fidelity DNA Polymerase (NEB), following manufacturer´s recommendations.

5.7. Cell culture and transfection

HEK293 and U2OS cells were cultured at 37 °C in 5 % CO_2 in D10 medium: DMEM containing 10 % FCS and penicillin/streptomycin (100 U/ml / 100 µg/ml). For passaging of all lines, cells were washed with PBS, detached with 0.25 % Trypsin / 1 mM EDTA, and finally plated in a 1:3 to 1:10 ratio. For seeding, trypsinized cells were resuspended in D10 medium and cell density was determined using a Neubauer chamber before plating.

Stable and transient transfections of HEK293 and U2OS cells were performed using polyethylenimine (PEI) **[Table 16]**. As an example, for transfection in a 10 cm-dish, 5 x 10^6 cells were seeded, and 8 µg plasmid DNA and 16 µg PEI (from a 1 µg/µl stock solution) were separately diluted in 250 µl serum-free DMEM. After 5 minutes incubation at RT, DNA and PEI were mixed together, followed by another 15 min incubation at RT, and then the mix was added to the cells. The medium was changed after 6 to 12 h, including doxycycline if induction was required. For the stable transfection of the doxycycline-inducible vectors pSB-ETiE-HA-MYCN (wild-type or P44L mutant) and pSB-ETiE-FLAG-MAX (wild-type or R60Q mutant), the transposase vector pCMV(CAT)T7-SB100x was co-transfected, followed by puromycin selection. For transient transfections, induction of these vectors was performed with 500 ng/mL doxycycline. For stably transfected clones, a doxycycline titration was carried out among all clones, to determine the optimal doxycycline concentration and protein expression level, as well for ensuring a similar protein expression level among different clones **[Table 17]**. For all transfected cells induction was carried for 48 hours. Expression vector transfection and/or induction was verified by realtime RT-PCR and/or Western blot analysis.

Table 16. **Conditions for PEI transfection.**

Culture plate or dish	100 cm	6-well	24-well
Cells seeded	5 x 10^6	5 x 10^5	10^5
DNA	8 µg	3 µg	0.5 µg
DMEM to DNA	to 250 µl	to 100 µl	to 20 µl
PEI (1 µg/µl)	16 µg	6 µg	1 µg
DMEM to PEI	to 250 µl	to 100 µl	to 20 µl

Table 17. Doxycycline concentrations used for *MYCN/MAX* inductions.

Stably transfected HEK293 cells		
Cell line	**Clon**	**DOX (ng/ml)**
HEK293 pSB-ETiE-HA-MYCN-WT	#1	30
	#2	20
	#3	10
HEK293 pSB-ETiE-HA-MYCN-P44L	#1	150
	#2	20
	#3	15
HEK293 pSB-ETiE-FLAG-MAX-WT	#1	50
	#2	40
	#3	8
HEK293 pSB-ETiE-FLAG-MAX-R60Q	#1	80
	#2	8
	#3	20
Transiently transfected HEK293 or U2OS cells		
Transfected vector		**DOX (ng/ml)**
pSB-ETiE-HA-MYCN-WT		
pSB-ETiE-HA-MYCN-P44L		500
pSB-ETiE-FLAG-MAX-WT		
pSB-ETiE-FLAG-MAX-R60Q		

5.8. Luciferase assay

10^5 HEK293 or U2OS cells were plated on 24-well-plates and transiently transfected in triplicates, with a total of 500 ng per well: 100 ng of pGL3-6XEBOX-prom and the rest with corresponding amounts of pSB-ETiE-HA-MYCN or pSB-ETiE-FLAG-MAX plasmids, alone or in combination, ensuring the same protein expression level. After 48 hours of induction, cells were washed twice with PBS and incubated with orbital rotation for 15 min in 150 µl cell lysis buffer. The suspension was transferred in tubes and centrifuged for 10 min at 4 °C at maximum speed. 50 µl of the supernatants were transferred to a black 96-well-microtiter plate. A Berthold Tristar multimode reader was used to inject 100 µl assay buffer into the sample supernatants, and measure luminescence for 5 sec. Protein expression was confirmed using an extra replicate in parallel, harvesting the whole cell lysate in 30 µl 1x protein loading buffer, followed by Western blot analysis.

5.9. Protein stability assay

To assess the stability of the P44L mutant N-MYC, cycloheximide (Roth) and MG-132 (Biomol) were used. Cycloheximide is an inhibitor of the eukaryotic *de novo* protein synthesis, by interfering with the translocation step in protein synthesis and therefore blocking translational elongation (Schneider-Poetsch et al., 2010). MG-132, on the other hand, is a potent and selective proteasomal inhibitor, which consequently leads to an accumulation of poly-ubiquitinated proteins (Gaczynska et al., 2005).

5×10^5 cells of stably transfected HEK293 pSB-ETiE-HA-MYCN-WT and -P44L were seeded in 6-well-plates and induced with doxycycline for 48 hours. Culture media was then replaced, and cells were treated with 100 µM cycloheximide and/or 20 µM MG-132 inhibitor for 0, 15, 30, 45, 60 and 90 min. Following these incubation times, cells were washed with PBS and whole cell lysates were assayed by Western blot.

5.10. MTT assay

The MTT assay is one of the most versatile and recurrent assays used for determination of cell viability. It is based on conversion of the soluble yellow dye MTT (3-(4,5-dimethylthiazol-2-yl)-2,5-diphenyltetrazolium bromide) to an insoluble purple formazan by mitochondrial reductases of living cells.

Three biological replicates of stably transfected HEK293 pSB-EtiE-HA-MYCN-WT/P44L and pSB-ETiE-FLAG-MAX-WT/R60Q cells were used. 2000 cells were cultivated in 96-well-plates in 50 µl D10 medium, and doxycycline induction was started 12 hours later by adding 50 µl fresh medium with the required doxycycline concentration. Cells were cultured at 37 °C for up to four days, and cell proliferation was analyzed in intervals of 24 hours. For each biological replicate and treatment, technical triplicates were performed. For analyzing protein expression, cells were seeded and induced in 6-well-plates in parallel, with the same cell density and doxycycline concentration as used for the 96-well format, for later Western blot analysis.

Cell viability was tested by adding to each well 20 µl of 5 mg/ml MTT (Sigma) diluted in PBS, prewarmed and sterile filtered, and incubating for 2 hours. Afterwards, the medium

was removed and the 96-well-plates were frozen at 20 °C. When plates of all time points were collected, 150 µl DMSO was added to each well to solubilize the produced formazan, and then the plates were covered with tinfoil and incubated for 1 hour at RT with shaking in an orbital motion. Finally, a Berthold Tristar multimode reader was used to read absorbance at 540nm with a reference filter at 690nm.

5.11. RNA isolation

Cells were resuspended in peqGOLD TriFast (Peqlab), and RNA is isolated according to manufacturer´s protocol. Sample RNA concentration was obtained by absorbance measurement using a Nanodrop spectrometer, before being stored at -80 °C.

5.12. cDNA synthesis

1 µg RNA was treated with DNase I (Thermo Fisher), to get rid of contaminant DNA, following manufacturer´s recommendations. Afterwards, DNA-free RNA was reverse transcribed using the RevertAid Reverse Transcriptase kit (Thermo Fisher) with oligo(dT)-oligonucleotides or RT random oligonucleotides (Applied Biosystems), according to manufacturer´s recommendations.

5.13. Real-time PCR

cDNA samples were diluted 1:5 for the realtime PCR reaction, containing SybrGreen (Sigma-Aldrich; 1:2000 in H_2O / 0.5 % DMSO) for quantification, and the annealing temperature was set to 60 °C **[Table 18] [Supplement 10.1]**. Melting curve analysis and SB agarose gel electrophoresis were used for verification of the PCR products, and the housekeeping gene *HPRT* for expression level normalization. All measurements were done as technical duplicates.

For the analysis of gene expression in WT samples, three reference cDNAs were used on each PCR plate to ensure the comparability of values between plates.

Table 18. PCR reaction and program for real-time PCR.

H2O	To 25 µl	95 °C	3 min	**Initial denaturation**	
10X PCR buffer	2.5 µl	95 °C	15 sec	**Denaturation**	
dNTPs 100 mM	0.25 µl	60 °C	10 sec	**Annealing**	40 cycles
SybrGreen	0.75 µl	72 °C	20 sec	**Elongation**	
His-Taq 15 U/µl	0.1 µl	55-60 °C	10 min	**Melting curve** (+ 4 °C/min)	
5' oligonucleotide 10 pmol	0.5 µl	16 °C	∞	**End**	
3' oligonucleotide 10 pmol	0.5 µl				
EG/Betain *(if required)*	1.5 µl				
DNA template	5 µl				

* See section 10.1 to see in which oligonucleotide combinations EG or Betain is required.

5.14. Whole cell lysates

For quick verification of protein expression after induction, cells were washed with ice cold 1x PBS and harvested by centrifugation (300 g, 3 min, 4 °C). The cell pellet was resuspended in adequate volume of 1x protein loading buffer (100 µl for a well from a 6-well plate). Optionally, for pellets difficult to resuspend, benzonase could be used to reduce the viscosity caused by nucleic acids: benzonase would be previously diluted 1:1000 in the 1x protein loading buffer, and then incubated with the cell pellet for 15 min at RT with a rotating mixer. The lysates were then incubated at 95 °C for 10 min and centrifuged at maximal speed for 1 min at RT. Samples could be used immediately for Western blot analysis or stored at -80 °C.

5.15. Co-immunoprecipitation (Co-IP)

10-12 million transfected and induced HEK293 cells, expressing HA or FLAG tagged proteins, were washed twice with ice cold PBS supplemented freshly with protease and phosphatase inhibitors (50 µg/ml PMSF; 1 µg/ml aprotinin, leupeptin and pepstatin; phosphatase inhibitors at 1:10000 dilution) and harvested by centrifugation (300 g, 20 min, 4 °C). Cell pellets containing the intact nuclei were resuspended in Co-IP lysis buffer containing fresh inhibitors and homogenized 15 times using 27G needles, to lysate the nuclei at physiological salt concentration. The chromatin was sheared by sonicating four times 10 sec with 45 sec pausing using a Bioruptor sonifier (intensity H). Benzonase (100 U/ml; Novagen) was then added and the sample was incubated for 40 min at 4 °C. Unsolubilized material was pelleted by centrifugation (18,000 rpm, 30 min, 4 °C). The

soluble protein fraction was used in IP with 20 ml of HA-coupled magnetic beads (Pierce Thermo Fisher Scientific) or FLAG-coupled agarose beads (Sigma), with additional 15 U benzonase per reaction. Both beads were incubated at 4 °C with rotation, the HA-beads for 3 hours, and the FLAG-beads overnight. HA-beads were washed 3 times at 4 °C in Co-IP lysis buffer containing 0.1 % Triton X-100 and then twice in buffer without Triton X-100. FLAG-beads were washed 6 times at 4 °C in Co-IP lysis buffer. Beads were resuspended in 30 μl 1x Protein loading buffer, incubated at 95 °C for 5-10 min, centrifuged at maximum speed for 1 min, and finally stored at -20 °C or used for Western blot analysis.

5.16. Western blot analysis

Protein samples were separated using a 12 % SDS-polyacrylamide gel, which was run for 1-2 hours in SDS running buffer at 45 mA per gel. Following separation, proteins were transferred to a nitrocellulose membrane using a wet blotting chamber, filled up with blotting buffer and run at 100 V for 75 min at 4 °C.

The membrane was washed in PBS or TBST (depending of the primary antibody to be used) and blocked in 5 % milk powder in PBS or TSBT for 1 hour at RT. Afterwards, it was incubated overnight at 4 °C with the primary antibody diluted in blocking solution. The following day, the membrane was washed three times 10 min in PBS or TBST at RT and incubated with the second antibody in blocking solution. After washing the membrane three times 10 min in PBS or TBST at RT, proteins were detected by incubation in detection buffer for 1 min and following imaging.

5.17. Silver staining

The silver staining of proteins is a highly sensitive technique, used for detecting proteins which are separated by SDS-polyacrylamide gel electrophoresis, based on the selective reduction of silver into metallic silver at the initiation site in close proximity of protein molecules (Kumar 2018). The use of gloves during this protocol is strongly recommended, since silver nitrate reacts with skin proteins and it can lead to staining artifacts. Protein samples were separated in a 12 % SDS-polyacrylamide gel in SDS running buffer for 1-2 hours at 45 mA per gel. After protein separation, the gel was

thoroughly rinsed with deionized water and transferred to a staining tray with the minimum liquid possible. All subsequent incubations and washes were performed with continuous gentle agitation on a platform shaker.

The gel was first incubated in 60 ml solution 1 for 5 min, followed by three washings with deionized water for 5 sec each, another 5 min washing, and again three washings for 5 sec. Afterwards, it was incubated for 5 min in 60 ml solution 2 and then for 1 min in 60 ml solution 3. The gel was washed three times with deionized water for 5 sec, before being incubated for 8 min in 60 ml solution 4. After rinsing the gel 5 times for 5 sec, it was developed by adding 60 ml solution 5 for a few sec. The development was stopped with glacial acetic acid, once the bands were clearly visible. The gel was then washed once with deionized water, and kept in 30 % methanol.

5.18. Mass spectrometry (MS)

Mass spectrometry (MS) is an analytical technique used to identify and quantify the compounds in a mixture, by measuring the mass-to-charge ratio of ions. It can be used for determining the proteins present in a cell sample, and even for analyzing post-translational modifications within these proteins. After purification of N-MYC complexes and assessment of their quality, the sample preparation for MS and subsequent analysis was performed in the group of Andreas Schlosser (Rudolf Virchow Center, University of Würzburg), for later proteomics analysis of the output data in our lab.

5.18.1. Purification of N-MYC complexes and sample preparation for quantitative MS

Untransfected HEK293 cells or expressing a HA-tagged version of the wild-type or P44L mutant N-MYC under doxycycline induction for 48 hours were used as a source for the purification. 200 million cells were washed twice with ice cold PBS supplemented freshly with phosphatase and protease inhibitors (see section 5.15), and then harvested by centrifugation (300 g, 20 min, 4 °C). The following steps are practically equal to the ones performed in section 5.15, but adapted for a larger input of cells: for homogenization, cell pellets were dounced 15 times; the chromatin was sheared by sonicating four times 10 sec with 45 sec pausing (20 % output); the soluble protein fraction was immunoprecipitated with 80 µl HA-coupled magnetic beads (Pierce Thermo Fisher

Scientific) and an additional 150 U benzonase; and for the elution of HA-N-MYC complexes, 100µl 1x NuPAGE® LDS Sample Buffer (Thermo Fisher Scientific) was used. The quality of the elutions was assessed by Western blot analysis and silver staining of SDS-acrylamide gels.

Protein precipitation of wild-type and mutant HA-N-MYC was performed overnight at -20 °C with fourfold volume of acetone. Pellets were washed three times with acetone at -20 °C. Precipitated proteins were dissolved in NuPAGE® LDS sample buffer (Life Technologies), reduced with 50 mM DTT at 70 °C for 10 minutes and alkylated with 120 mM Iodoacetamide at room temperature for 20 min. Separation was performed on NuPAGE® Novex® 4-12 % Bis-Tris gels (Life Technologies) with MOPS buffer according to manufacturer's instructions. Gels were washed three times for 5 min with water and stained for 45 min with Simply Blue™ Safe Stain (Life Technologies). After washing with water for 2 h, each gel lane was cut into 15 slices. The excised gel bands were destained with 30 % acetonitrile in 0.1 M NH4HCO3 (pH 8), shrunk with 100 % acetonitrile, and dried in a vacuum concentrator (Concentrator 5301, Eppendorf, Germany). Digests were performed with 0.1 µg trypsin per gel band overnight at 37 °C in 0.1 M NH4HCO3 (pH 8). After removing the supernatant, peptides were extracted from the gel slices with 5 % formic acid, and extracted peptides were pooled with the supernatant.

NanoLC-MS/MS analyses were performed on an Orbitrap Fusion (Thermo Scientific) equipped with a PicoView Ion Source (New Objective) and coupled to an EASY-nLC 1000 (Thermo Scientific). Peptides were loaded on capillary columns (PicoFrit, 30 cm x 150 µm ID, New Objective) self-packed with ReproSil-Pur 120 C18-AQ, 1.9 µm (Dr. Maisch) and separated with a 30-minute linear gradient from 3 % to 30 % acetonitrile and 0.1 % formic acid and a flow rate of 500 nl/min.

Both MS and MS/MS scans were acquired in the Orbitrap analyzer with a resolution of 60,000 for MS scans and 15,000 for MS/MS scans. HCD fragmentation with 35 % normalized collision energy was applied. A Top Speed data-dependent MS/MS method with a fixed cycle time of 3 sec was used. Dynamic exclusion was applied with a repeat count of 1 and an exclusion duration of 30 sec; singly charged precursors were excluded from selection. Minimum signal threshold for precursor selection was set to 50,000.

Predictive AGC was used with an AGC target value of 2e5 for MS scans and 5e4 for MS/MS scans. EASY-IC was used for internal calibration.

5.18.2. N-MYC purification and sample preparation for phosphorylation assay

The protocol used for the phosphorylation assay was essentially the same used for the purification of N-MYC complexes (see section 5.18.1), but some adjustments were performed, due to the larger input required by this assay for the later MS analysis. Since we aimed to get samples richer in our protein of interest, without interactors interfering, we replaced the Co-IP lysis buffer with RIPA buffer during the purification protocol. Also, after protein separation with the NuPAGE® Novex® 4-12 % Bis-Tris gels, only the gel area corresponding to the N-MYC protein size was excised and further prepared for MS analysis. The area of excision was verified by loading a small portion of the eluates in parallel lanes, which were separately used for Western Blot analysis in our laboratory, to confirm the location of the N-MYC protein in the same gel. Additionally, for the enzymatic digestion of the samples, trypsin was replaced by chymotrypsin. Chymotrypsin preferentially cleaves peptide amide bonds of large hydrophobic amino acid, like tyrosine, tryptophan, and phenylalanine, while trypsin cleaves peptide chains mainly at the carboxyl side of the amino acids lysine or arginine. This different digestion pattern allowed us to obtain peptide fragments of different sizes and nature from the N-terminal N-MYC, which were better detected and analyzed compared to the ones obtained from the digestion with trypsin.

5.18.3. MS data analysis

Raw MS data files were analyzed with MaxQuant version 1.6.2.2 (Cox and Mann 2008). Database search was performed with Andromeda, which is integrated in the utilized version of MaxQuant. The search was performed against the UniProt Human database. Additionally, a database containing common contaminants was used. The search was performed with tryptic cleavage specificity with 3 allowed miscleavages. Protein identification was under control of the false-discovery rate (1 % FDR on protein and peptide level). In addition to MaxQuant default settings, the search was performed against following variable modifications: Protein N-terminal acetylation, Gln to pyro-Glu formation (N-term. Gln) and oxidation (Met). Carbamidomethyl (Cys) was set as fixed

modification. For protein quantitation, the LFQ intensities were used (Cox et al. 2014). Proteins with less than two identified razor/unique peptides were dismissed. Further data analysis was performed using R scripts developed in-house. Missing LFQ intensities in the control samples were imputed with values close to the baseline. Data imputation was performed with values from a standard normal distribution with a mean of the 5 % quantile of the combined log10-transformed LFQ intensities and a standard deviation of 0.1. For the identification of significantly co-immunoprecipitated proteins, boxplot outliers were identified in intensity bins of at least 300 proteins. Log2 transformed protein ratios of Co-IP versus control (Log2FC) with values outside a 1.5x (potential) or 3x (extreme) interquartile range (IQR), respectively, were considered as significantly co-immunoprecipitated.

Data analysis for phosphorylation site identification of wild type and P44L HA-N-MYC was performed with PEKAS Studio X (Bioinformatics Solution Inc., Canada). Database searching was performed against a custom database containing the protein sequence of HA-MYCN with the following parameters: parent mass tolerance: 8 ppm, fragment mass tolerance: 0.02 Da, enzyme: chymotrypsin, variable modifications: oxidation (M), pyro-glutamate (N-term. Q), Protein N-term acetylation, phosphorylation (STY). Results were filtered to 1% PSM-FDR by target-decoy approach, and MS/MS spectra of phosphopeptides were validated manually.

5.18.4. Data availability

The mass spectrometry proteomics data for the analysis of wild-type and mutant N-MYC complexes have been deposited to the ProteomeXchange Consortium via the PRIDE (Perez-Riverol et al., 2019) partner repository with the dataset identifier PXD025996.

6. Results

6.1. *MYCN* P44L and *MAX* R60Q mutation screenings in WT

In order to determine the presence of *MYCN* P44L (c.131 C>T) and *MAX* R60Q (c.179 G>A) mutations in WT, as well as to analyze possible associations to specific histological WT subtypes or clinical features, both mutations were screened in a cohort of unselected WT cases, which had been treated according to the SIOP protocol. Whenever RNA from tumors and DNA from control tissues were available, Sanger sequencing was also used to respectively test the expression of mutant alleles on corresponding cDNA fragments, and to confirm the somatic or germinal origin of the mutation. The clinical data corresponding to the tumor samples included patient sex and age, tumor histological type, and presence of familial WT or syndromes predisposed by WT, including hemihypertrophy and the WAGR, Perlman, Beckwith-Wiedemann and Denys-Drash syndromes. Follow-up examinations were also tracked, to account eventual cases of metastasis, relapse or death. Those patients which did not present signs of metastasis or relapse in follow-up examinations two years after being diagnosed with WT were accounted as metastasis- or relapse-free. For metastasis, we made a distinction between cases where metastasis was reported within two years after WT diagnosis ("late metastasis"), or including those patients which also presented metastasis at diagnosis time ("all metastasis").

The *MYCN* P44L mutation was detected in 24 of 810 WT patients (3 %) **[Table 19]**. All cases presented somatic and heterozygous mutations with an allele frequency between 10 and 50 %, except for one case where the wild-type allele was lost **[Supplement 10.2]**. Regarding preferential histology, the mutation was detected in practically all histological types with exception of completely necrotic and focal and diffuse anaplasia, which were part of the histotypes with least representation in our cohort of patients **[Table 19].** *MYCN* P44L was most enriched among the epithelial, regressive and pre-chemotherapy blastemal types, and the post-operative persistent blastemal type, classified as a high-risk malignancy subtype. However, no significant correlation was found between these histotypes and the mutation status.

A significant correlation (p = 0.020) was found between *MYCN* P44L status and relapse: 5 of 53 cases harboring the mutation (9.4 %) suffered a relapse within the 2 following years after being diagnosed for the first time, compared to 18 of 681 non-mutated cases (2.6 %) **[Table 19] [Supplement 10.3]**. *MYCN* P44L presented no significant age or sex bias among the patients, neither was it associated with a predisposition to urogenital malformations or WT-associated syndromes. Mutations were also more frequent in cases with metastasis or fatal outcome, but this trend did not reach statistical significance.

Table 19. *MYCN* P44L and *MAX* R60Q mutation frequency in histological and clinical WT subgroups.
825 (*MYCN* P44L) and 797 (*MAX* R60Q) tumors from 810 and 782 cases respectively were analyzed, 15 of them being bilateral WT. Gray shading indicate significant difference (p < 0.05). See also sections 10.2 and 10.3.

			MYCN P44L	(%)	*MAX* R60Q	(%)
Clinical data		Late Metastasis	4/83	4.8	2/75	2.7
		All Metastasis	7/194	3.6	4/187	2.1
		Relapse	5/53	9.4	2/49	4.1
		Death	3/44	6.8	1/40	2.5
Histology	Low-risk	Compl. Necrotic	0/31	-	0/30	-
	Intermediate-risk	Epithelial	3/81	3.7	0/80	-
		Stromal	1/80	1.3	0/77	-
		Mixed	6/231	2.6	2/225	0.9
		Regressive	9/267	3.4	4/255	1.6
		Focal Anaplastic	0/15	-	0/15	-
		Blastemal primary OP	1/25	4.0	0/24	-
	High-risk	Blastemal	4/61	6.6	1/57	1.8
		Diffuse Anaplastic	0/34	-	0/34	-
Total cases			**24/810**	**3.0**	**7/782**	**0.9**

On the other hand, the *MAX* R60Q mutation was identified in 7 of 782 cases (0.9 %) **[Table 19]** as somatic mutations, and allele frequencies only reached 5 – 30% in sequence chromatographs **[Supplement 10.2]**. Due to this unexpectedly low allelic fraction, we performed a parallel *MAX* R60Q screening based on restriction digests, where the results of the ASP-based screening could be reproduced (data not shown). This analysis took advantage of the restriction site for ApaI (CCCGGG) located in the

bases corresponding the amino acid positions R60 and A61: amplification of the wild-type *MAX* allele via PCR followed by ApaI digestion resulted in two fragments of 177 and 68 bp. However, when the R60Q mutation is present, the replacement of G by A disrupts the palindrome recognized by ApaI (CCCAGG), and the PCR product harboring the R60Q mutation preserved its total size, 245 bp **[Figure 9]**.

Figure 9. Rationale for *MAX* R60Q digestion analysis.
Rationale for the *MAX* R60Q screening by ApaI restriction digestion. On the left, SB agarose gel electrophoresis representing a patient with *MAX* R60Q mutant and wild-type alleles (het), and a patient with both wild-type *MAX* alleles (wt). On the right side, representation of the cleavage recognition site for ApaI in the wild-type (wt) and mutant (mut) allele, and the resulting digest products from the PCR product containing the *MAX* R60Q mutation.

The digestion-based screening also allowed us to validate the mutation allele frequency observed after Sanger sequencing, so we could discern potential artifacts generated during sequencing. Pre-defined wild-type and mutant MAX plasmid concentrations were used as PCR templates and digested with ApaI. The band intensity of the digestion products, as well as the sequences obtained for each plasmid mixtures, were used as a reference to analyze the digestion product and Sanger sequences obtained for each *MAX* R60Q positive case **[Figure 10]**.
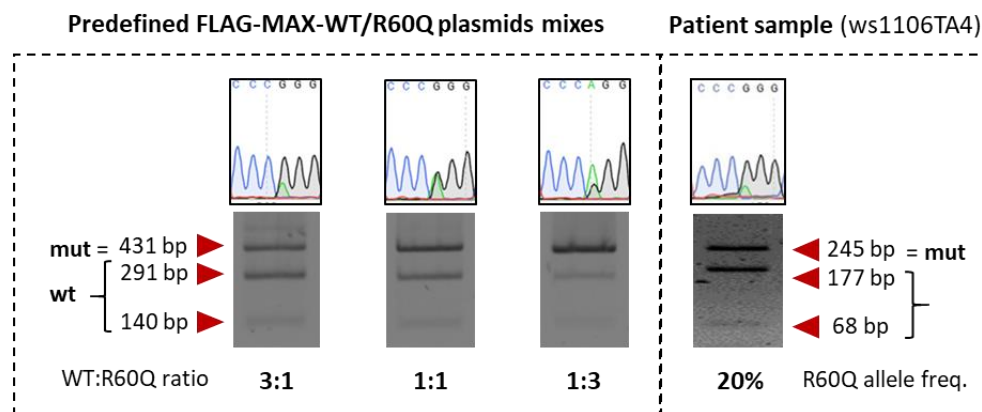

Figure 10. Procedure for validation of *MAX* R60Q allele frequency in variant cases.
Overview of the workflow used for validating the allele frequency of the positive *MAX* R60Q patients (e.g. ws1106TA4), observed after direct sequencing.

48

In four tumors with multiple biopsies, percentages ranged from 0% to 20% mutant allele per each case [Supplement 10.2], while complete allele loss (LOH) for markers on chromosome 11p or 16q assured high tumor cell content even for *MAX* wild-type specimens (performed by Jenny Wegert and Barbara Ziegler, Developmental Biochemistry, University of Würzburg; data not shown). This indicates that the *MAX* R60Q mutation must be present in just a fraction of tumor cells, occurring as a late event.

The *MAX* R60Q mutation was observed in tumors with regressive (n=4), mixed (n=2) and blastemal histology (n=1). We identified a significant correlation between *MAX* R60Q status and metastasis, as 2.1 % of cases harboring the mutation presented metastasis at WT diagnosis time or within two years after diagnosis, compared to 0.4 % of the non-mutated cases [Table 19] [Supplement 10.3]. The mutation also had a higher incidence in relapsing cases (4.1 % vs. 0.6 %).

All samples harboring *MYCN* P44L and *MAX* R60Q mutations were analyzed for additional recurrent genomic alterations in WT, including the *SIX1* Q177R, *SIX2* Q177R, *DROSHA* E1147K and *DGCR8* E518K point mutations, and *p53*, *CTNNB1* and *WT1* alterations [Supplement 10.2]. There was a significant co-occurrence of *MYCN* P44L and *DROSHA* E1147K, although it did not reach statistical significance (p = 0.0869) [Table 20].

Table 20. Overlap of WT patients with the MYCN P44L and DROSHA E1147K mutations.
p-value (two-tailed Fisher's exact test) = 0.0869.

	DROSHA WT	*DROSHA* E1147K
MYCN WT	524	25
MYCN P44L	19	3

In addition, both *MYCN* P44L and *MAX* R60Q mutations were screened in other available pediatric renal tumors: 35 clear cell sarcomas of the kidney, 29 mesoblastic nephromas, 15 rhabdoid tumors of the kidney, 9 cystic partially differentiated nephroblastoma, and 7 renal cell carcinomas. However, we did not identify these alterations in other pediatric kidney tumors except for WT.

6.2. Lack of other *MAX* coding sequence variants in WT

Aiming to identify *MAX* CDS variants in WT in addition to the already reported R60Q, we used Sanger sequencing to analyze the *MAX* exons of a cohort of 101 unselected WT patients. Except for 12 aa of exon 1 and the alternatively spliced exon 2, exons 3–5 were sequenced, covering the vast majority of the CDS (aa 22-160).

Among the analyzed patients, only the silent N125N mutation (c. 375 C>T) was observed in two cases **[Figure 11]**. These results led us to the conclusion that the missense mutation R60Q is so far the only functional alteration observed within *MAX* CDS in WT.
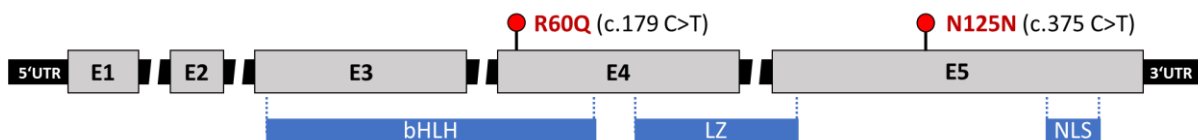
Figure 11. *MAX* CDS variants in WT.
Schematic representation of *MAX* CDS and its different exons (UniProt ID: P61244-1), with the identified mutations in WT highlighted in red. The CDS regions corresponding to relevant protein domains have been highlighted in blue in the bottom: basic helix-loop-helix (bHLH), leucine zipper (LZ) and nuclear localization signal (NLS).

6.3. N-MYC-P44L and MAX-R60Q functional characterization

6.3.1. Impact of *MYCN* P44L and *MAX* R60Q on E-box sequences binding and N-MYC-MAX dimerization

To functionally characterize both mutations, we used a luciferase reporter construct containing 6 canonical E-boxes upstream of the promoter sequence, to test the transactivating capacity of the N-MYC and MAX mutants binding E-box sequences and subsequently driving transcription **[Figure 5]**. Transient transfection of the reporter vector in HEK293 cells already lead to luciferase expression, due to the binding of endogenously expressed proteins which also recognize and bind to E-boxes, like C-MYC **[Figure 12A,** upper section**]**. Cotransfection with wild-type or P44L mutant N-MYC constructs led to a comparable 40 % increase in luciferase expression, and a 4-fold increase in transactivation was observed when the reporter vector was cotransfected

together with the wild-type MAX construct. In a parallel test, we could confirm that the transactivation was further enhanced with stronger wild-type MAX expression, and higher expression of only wild-type N-MYC led to a decrease in transcription **[Figure 12B]**. The reason for these observations could be the high endogenous expression in HEK293 cells of C-MYC **[Figure 12C]**, which can also form heterodimers with MAX: by increasing the concentration of available intracellular MAX, more C-MYC-MAX dimers are generated and consequently bind to E-boxes to activate transcription. On the other hand, in this system where MAX is acting as the limiting reagent in the MYC-MAX dimerization process, increasing the intracellular concentration of N-MYC would not only not increase transactivation: it could even inhibit it by shifting the balance to other dimers involved in transrepression, or it could simply interfere with the regular binding of transactivating dimers to the E-boxes.

Interestingly, when the wild-type MAX construct was replaced by the R60Q mutant vector, a considerable decrease in luciferase expression was observed **[Figure 12A**, upper section**]**. The protein expression in all these scenarios was validated in parallel by Western blot **[Figure 12A**, lower section**]**. Comparable results were obtained in U2OS cells **[Figure 12D]**, indicating that this is a general phenomenon. These observations led to the conclusion that the MAX-R60Q mutation, located in the bHLH domain involved in dimerization, has a negative impact in the binding of N-MYC-MAX dimers to E-boxes and consequently results in a decreased transactivation of downstream genes.

We used co-immunoprecipitation (co-IP) experiments to test the formation of N-MYC-MAX heterodimers, in presence of the N-MYC-P44L and MAX-R60Q mutations, using transient cotransfections in HEK293 cells **[Figure 12E]**. We did not detect differences in binding of mutant compared to wild-type dimers under these conditions, which may be too subtle to be detected by this assay and consistent with (partly) retained transactivation capacity in the mutants.
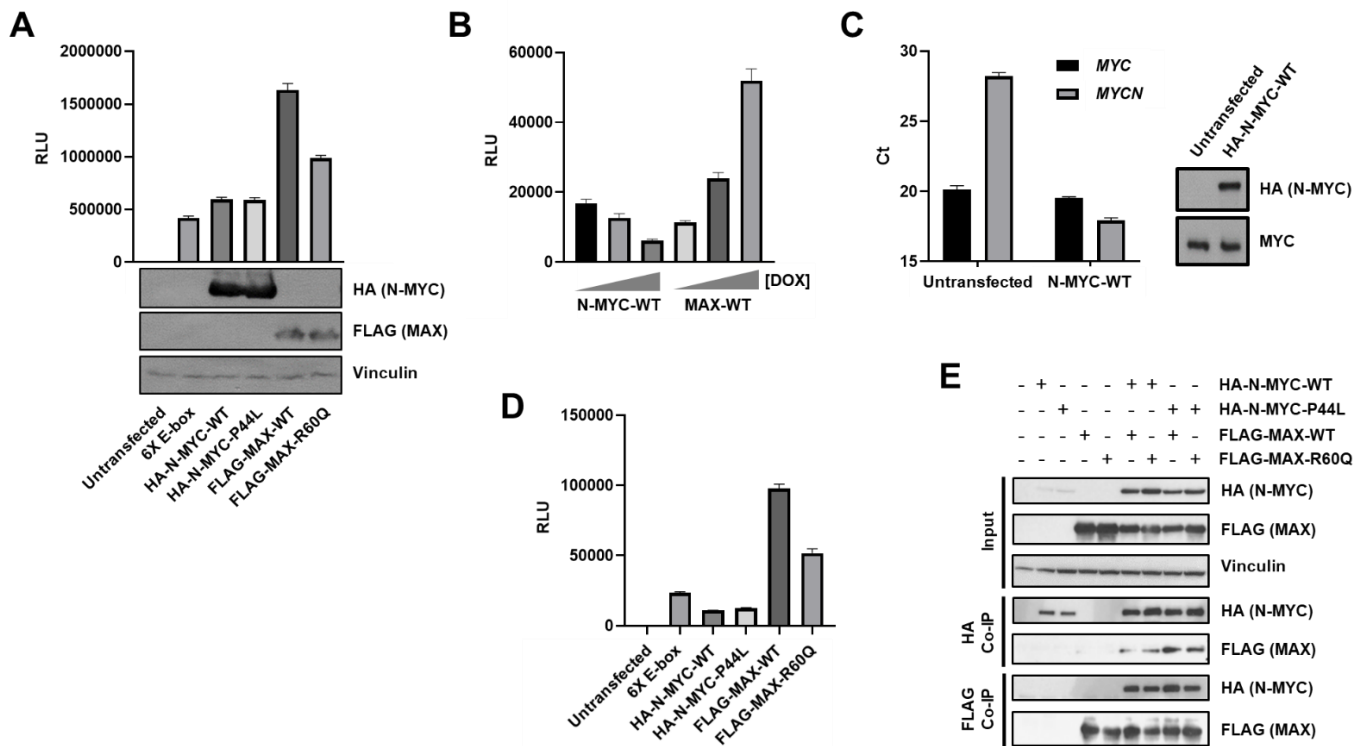
Figure 12. Impact of MAX R60Q on E-box binding and N-MYC-MAX dimerization.
(A) Luciferase activity (RLU) in HEK293 cells, transiently transfected with a reporter construct containing 6 E-boxes (6X E-box), and the wild-type or mutant HA-N-MYC or FLAG-MAX expression vectors or empty vector control. In the lower panel, corresponding Western blots confirming protein expression with Vinculin as control. **(B)** Luciferase activity (RLU) in HEK293 cells transiently transfected with the same luciferase reporter construct as in (A) and the wild-type HA-N-MYC or FLAG-MAX expression vectors, followed by induction with increasing doxycycline concentrations leading to different concentrations of HA-N-MYC and FLAG-MAX proteins. **(C)** On the left side, realtime PCR results showing the *MYC* and *MYCN* expression in untransfected HEK293 cells, and the same cells after transient transfection with the wild-type HA-N-MYC expression vector. To the right, Western blots of both scenarios showing C-MYC and HA-N-MYC protein expression. **(D)** Luciferase activity (RLU) in U2OS cells, using the same set-up as in (A). **(E)** Immunoblots of co-IP experiments. Wild-type and mutant HA-N-MYC and FLAG-MAX were overexpressed by transient transfection in HEK293 cells. Lysates from input control and the corresponding immunoprecipitates were tested by Western blot.

6.3.2. Impact of *MYCN* P44L on binding to protein interactors

The P44L mutation is located in the TAD of the N-MYC protein, a domain involved in the recruitment of cofactors so N-MYC can regulate transcription and its own protein turnover. Therefore, we decided to perform a MS analysis of wild-type and P44L mutant N-MYC complexes and evaluate if the presence of the mutation affected the recruitment of any of the many cofactors reported to bind the MBI of MYC **[Figure 2]**.

Wild-type and P44L mutant HA-N-MYC were induced in stably transfected HEK293 pSB-ETiE-HA-MYCN-WT/P44L cells in biological duplicates, and untransfected HEK293 cells were used as empty controls. The overexpression was performed by doxycycline induction for 48 hours, and to ensure the formation of physiological N-MYC complexes. To avoid generating binding artifacts, cells were previously titrated with doxycycline, to determine the concentration required for an equal and minimal expression of wild-type and P44L mutant HA-N-MYC. The N-MYC complexes were subsequently purified by IP under native conditions. Before proceeding with the preparations for the MS analysis, we assessed the quality of our IP elutions by Western blot and silver staining. The Western analysis of a 1/20 fraction of our elutions confirmed the overexpression and purification of HA-N-MYC **[Figure 13A**, lower panel**]**. At the same time, to get evidence of the presence of other proteins being co-purified with our wild-type and mutant N-MYC, another 1/20 fraction of each elution was loaded in an acrylamide gel, so all enriched proteins could be separated by SDS-PAGE and consequently detected by silver staining **[Figure 13A**, upper panel**]**.

HA-N-MYC-associated proteins were analyzed by label-free quantification MS (LFQ-MS), resulting in the identification of approx. 2900 different proteins within our four biological replicates, two of the wild-type and two of the mutant HA-N-MYC. Those proteins which in at least one of the four replicates were significantly co-immunoprecipitated and had a positive value for its Log2FC, were included in our list of potential candidates for proteomic analysis. We decided to focus on those interactors which enrichment (log2FC) in HA-N-MYC-expressing cells compared to control cells was positive, since we should not expect enrichment of HA-N-MYC interactors in untransfected HEK293 cells compared to HA-N-MYC expressing cells, resulting in 140 interactors **[Figure 13B]**. GeneCards was consulted for annotation of the cellular location (nuclear or cytoplasmic) of the potential interactors, and the BioGRID and Pubmed databases were used for literature mining on already known C-MYC and N-MYC interactors.
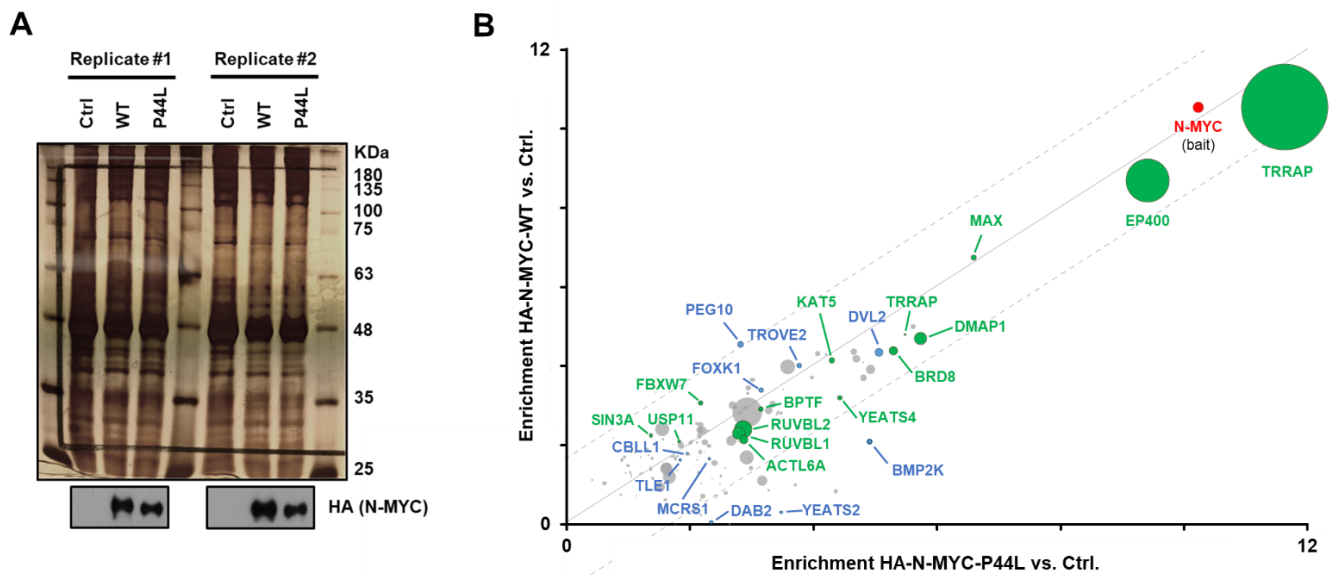
Figure 13. MS analysis of native wild-type and P44L mutant N-MYC complexes.
(A) Immunoprecipitates of HA-N-MYC from untransfected HEK293 control cells (Ctrl) or stably transfected HEK293 pSB-ETiE-HA-MYCN-WT or -P44L (WT and P44L) cells, separated by SDS-PAGE and visualized by silver staining. At the bottom, corresponding immunoblots confirming the comparable expression of wild-type and P44L mutant N-MYC. **(B)** Summary of the proteins enriched in the wild-type and P44L mutant N-MYC complexes. The x axis displays the enrichment (log2 fold-change) of proteins in wild-type HA-N-MYC-expressing cells compared to control cells, while the y axis displays the enrichment in HA-N-MYC-P44L-expressing cells, both calculated from the mean of biological duplicates. Previously characterized N-MYC interactors are depicted in green, novel interactors that were tested via immunoprecipitation in blue, and the bait (HA-N-MYC) in red. The size of the dots correlates with the number of identified razor and unique peptides of the corresponding protein. Dots located close to the solid diagonal line represent proteins equally enriched in both complexes, while dots beyond the dotted lines were more strongly enriched either in the wild-type or the mutant complexes.

Among the top 140 significantly enriched proteins identified across our four biological replicates, we could recognize several known N-MYC interactors, confirming that the N-MYC IP and the following MS analysis were performed successfully **[Table 21**, proteins marked in green]. These known partners included: its obligated dimerization partner MAX; several members of chromatin-remodeling complexes, like the Nua4, NURF, SWI/SNF and Sp1-SMAD complexes, required for the MYC-mediated regulation of transcriptional activation and repression **[Figure 5] [Figure 6]**; FBXW7, the substrate-specific adaptor of the E3 ligase complex SCF^{Fbw7}, involved in N-MYC proteasomal degradation **[Figure 7]**; and the ubiquitin-specific protease USP11, required for recruitment of BRCA1 and enhancement of transcriptional activation (see section

2.2.3.1). We decided then to perform a Gene Ontology (GO) enrichment analysis of the extreme outliers (values lying more than 3 times the interquartile range below the first quartile or above the third quartile), using a PANTHER Overrepresentation Test and allowing only to enrich for cellular location. The *Homo sapiens* reference list was used, as well as the False Discovery rate (FDR) correction method to account for multiple hypothesis testing. In line with the previous observations from the top 140 enriched proteins, the GO term analysis showed that the immunoprecipitates were significantly enriched for nuclear and chromatin-related proteins, as well as for components of complexes involved in remodeling of chromatin **[Table 22]**. The majority of proteins among our 140 were also found in two additional independent replicates for wild-type HA-N-MYC, which we performed in an independent experiment, also by overexpression in HEK293 cells, followed by purification and MS analysis (data not shown).

Table 21. Top 140 enriched protein in native wild-type and P44L mutant N-MYC complexes.
Characterized N-MYC interactors are depicted in green, novel interactors that were tested via immunoprecipitation in blue. Enrichment (log2 fold-change) and cellular location according to the GeneCards database (n=nucleus and c=cytosol) are indicated.

#	Gene	WT	P44L	Loc	#	Gene	WT	P44L	Loc	#	Gene	WT	P44L	Loc	#	Gene	WT	P44L	Loc
1	TRRAP	10,55	11,63	n	36	BPTF	2,91	3,14	n	71	ANKFY1	1,98	2,31	c	106	AGO1	1,22	2,5	n
2	MYCN	10,54	10,23	n	37	TTC28	2,88	3,28	c	72	ATP6V1C1	1,9	1,3	c	107	PSMC6	1,21	2,09	n
3	EP400	8,7	9,41	n	38	JAZF1	2,84	3,43	n	73	CHMP5	1,84	2,23	n	108	STRBP	1,19	1,05	n
4	MAX	6,75	6,59	n	39	NEFM	2,83	2,92	c	74	MTHFD1L	1,83	1,05	c	109	XPOT	1,16	1,39	n
5	GAS1	5,01	5,61	c	40	CEP72	2,82	2,81	c	75	ZNF48	1,83	2,17	n	110	DNAJB11	1,15	2,36	c
6	TRRAP	4,8	5,48	n	41	HIRA	2,81	3,47	n	76	ENDOD1	1,81	1,11	c	111	AP2A1	1,1	3,17	n
7	POTEE/F	4,79	4,09	c	42	VPS72	2,79	3,41	n	77	MCRS1	1,78	1,96	n	112	SHMT2	1,03	2,48	n
8	DMAP1	4,7	5,73	n	43	DSC1	2,68	-	c	78	EIF2B2	1,77	1,99	c	113	RNF2	1,03	2,18	n
9	PEG10	4,55	2,82	n	44	HK1	2,66	1,5	c	79	PDHB	1,75	1,95	n	114	AP2A2	1	3,71	c
10	BRD8	4,39	5,3	n	45	MAGEB2	2,59	-	c	80	WLS	1,75	1,33	c	115	CLTB	0,86	3,27	c
11	IRS2	4,37	4,65	n	46	CKAP2	2,56	1,99	c	81	DUSP11	1,73	1,8	n	116	DNAJC13	0,84	4,36	c
12	DVL2	4,35	5,06	n	47	RPF1	2,55	2,1	n	82	ZC3H18	1,72	1,74	n	117	INTS1	0,79	2,58	n
13	ATXN10	4,31	4,07	c	48	ZNF771	2,52	2,17	n	83	ERAL1	1,71	2,15	c	118	KHSRP	0,75	0,88	n
14	KLF4	4,3	4,2	n	49	ZNHIT6	2,51	3,36	n	84	ANKRD28	1,7	0,93	n	119	PRPF38A	0,72	1,13	n
15	EPC2	4,18	4,69	n	50	MBTD1	2,45	3,75	n	85	EPHA5	1,7	1,19	c	120	FBRS	0,71	2,44	c
16	KAT5	4,14	4,29	n	51	SRCAP	2,4	2,78	n	86	PIK3C2A	1,69	2,92	n	121	LSR	0,67	2,41	c
17	MGA	4,09	4,8	n	52	RUVBL2	2,4	2,86	n	87	CDK11B/A	1,66	2,97	n	122	PPP6R3	0,62	1,6	n
18	TROVE2	4,01	3,77	n	53	BUB3	2,37	2,26	n	88	CBLL1	1,66	2,31	n	123	PLOD2	0,62	2,17	c
19	EPPK1	3,97	3,58	n	54	PTPRG	2,36	2,29	c	89	FAM126A	1,65	-0,65	c	124	IFFO1	0,48	2,12	c
20	AP2B1	3,92	4,92	c	55	ACAT1	2,35	2,93	c	90	CTBP2	1,63	2,12	n	125	GNAZ	0,39	1,19	c
21	EHD4	3,71	3,97	n	56	EPB41L2	2,34	1,52	n	91	TLE1/4	1,62	1,84	n	126	DAB2	0,3	3,48	n
22	EPC1	3,71	4,81	n	57	SIN3A	2,25	1,36	n	92	CHD1	1,48	1	n	127	HIP1R	0,24	2,17	c
23	MDC1	3,66	3,01	n	58	AIMP1	2,21	3,54	c	93	MAK16	1,44	1,36	n	128	YEATS2	0,05	2,34	n
24	AKAP8L	3,45	2,94	n	59	ZNF444	2,19	2,16	n	94	GAP43	1,42	2,57	c	129	FOPNL	-	2,1	n
25	PYCR2	3,41	3,51	c	60	SNX33	2,18	0,76	c	95	VPRBP	1,42	2,98	n	130	HIP1	-	2,64	n
26	FOXK1	3,39	3,15	n	61	PRDM15	2,14	1,56	n	96	ADD2	1,35	1,79	c	131	EPN1	-	1,77	n
27	BCCIP	3,34	1,44	n	62	ACTL6A	2,14	2,87	n	97	BBS4	1,35	1,98	n	132	ATG13	-	8,51	c
28	WDR74	3,32	2,93	n	63	IQCB1	2,11	2,03	n	98	RBM26	1,32	1,02	n	133	CISD3	-	4,4	c
29	YEATS4	3,2	4,43	n	64	NUP43	2,1	2,78	n	99	MRPS9	1,3	1,22	n	134	CNTFR	-	1,88	-
30	FBXW7	3,06	2,17	n	65	BMP2K	2,09	4,91	n	100	CDC42EP1	1,29	0,96	c	135	TTC27	-	2,41	c
31	AKAP12	3,03	3,33	c	66	USP11	2,09	1,82	n	101	PSMB6	1,29	2,46	n	136	REPS1	-	2,82	c
32	ZC3HAV1	3,01	2,68	n	67	MYO10	2,07	2,24	n	102	TUBG1/2	1,27	1,19	n	137	FYTTD1	-	1,97	n
33	CD44	2,95	2,89	c	68	TUBGCP3	2,07	2,12	c	103	SEP2	1,26	2,2	c	138	RBM22	-	3,59	n
34	TUFM	2,94	2,73	c	69	ZNF687	2,07	2,01	n	104	RRAGA/B	1,26	1,04	n	139	TTN	-	3,73	n
35	SNX9	2,93	2,86	c	70	PSMD13	2,02	1,98	n	105	DAP3	1,25	1,74	n	140	KAT6A	-	4,68	n

Table 22. Cellular component clustering for N-MYC interacting proteins identified in MS.
List of selected GO terms enriched by analyzing the mean extreme outliers obtained from the MS of HA-MYCN-WT (n = 58) and -P44L (n = 87) duplicates. Terms referring to nuclear proteins and chromatin remodeling are shown. FDR, false rate discovery; fold enr., fold enrichment.

GO term	HA-N-MYC-WT			HA-N-MYC-P44L		
	Hits (58)	Fold enr.	FDR	Hits (87)	Fold enr.	FDR
NuA4 histone acetyltransferase complex	8	> 100	6.36E-12	10	> 100	1.70E-14
H4/H2A histone acetyltransferase complex	8	> 100	1.27E-11	10	> 100	2.54E-14
H4 histone acetyltransferase complex	9	71.90	1.65E-11	12	63.91	1.47E-14
Histone acetyltransferase complex	9	37.62	2.50E-09	13	36.23	1.01E-13
Acetyltransferase complex	9	33.70	4.17E-09	13	32.45	2.46E-13
Protein acetyltransferase complex	9	33.70	5.01E-09	13	32.45	2.96E-13
Nucleoplasm	33	2.98	6.13E-08	42	2.53	1.69E-07
Swr1 complex	5	> 100	2.57E-07	5	92.18	1.07E-06
SWI/SNF superfamily-type complex	7	29.96	8.45E-07	8	22.83	6.02E-07
ATPase complex	7	28.60	1.07E-06	8	21.79	7.93E-07
Histone deacetylase complex	6	29.96	8.61E-06	6	19.97	6.52E-05
Piccolo NuA4 histone acetyltransferase complex	3	> 100	6.16E-05	3	> 100	1.66E-04
Nuclear chromatin	14	4.87	6.23E-05	16	3.71	3.82E-04
Chromatin	15	4.44	6.94E-05	16	3.16	1.99E-03
Nucleus	39	1.87	1.23E-04	55	1.76	3.35E-05
MLL1 complex	3	34.79	6.56E-03	4	30.92	7.00E-04
MLL1/2 complex	3	34.79	6.76E-03	4	30.92	7.19E-04
Methyltransferase complex	4	12.08	2.01E-02	5	10.07	6.28E-03
Histone methyltransferase complex				4	10.53	2.16E-02
STAGA complex				2	39.94	4.33E-02

There was only a small number of 21 proteins that appeared to be differentially bound by the two N-MYC variants. Among them, we picked those candidates with the highest enrichment in either the wild-type or mutant N-MYC complexes and known nuclear location, where N-MYC executes its transcriptional activities. To determine the cellular location, we used the online database GeneCards and selected those proteins with a confidence score of 4 or 5 for subcellular localization. Therefore, we decided to focus on PEG10, more enriched in the wild-type HA-N-MYC complexes, and BMP2K, DAB2 and YEATS2 in the mutant N-MYC complexes **[Figure 13B]**, none of them previously reported to bind N-MYC. We confirmed their interaction with N-MYC by co-immunoprecipitation (Co-IP), but at the same time, this experiment did not support the differential binding due to the presence of the mutation **[Figure 14]**. These results brought us to the conclusion that the P44L mutation does not have any impact in the interaction of N-MYC with those binding partners enriched in our N-MYC complexes.
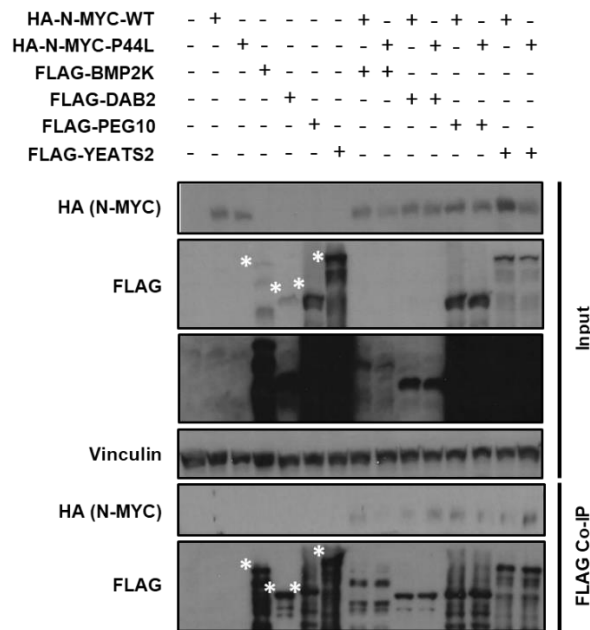
Figure 14. Validation of N-MYC protein interactors with altered binding due to P44L mutation. Immunoblots of HEK293 cells transiently transfected with expression vectors for HA-N-MYC and candidates for which binding to N-MYC is potentially affected by the P44L mutation. The white asterisks represent the specific bands of N-MYC interactors candidates in the input and FLAG co-IP. Vinculin input served as a loading control.

6.3.3. Identification of novel N-MYC protein interactors

Among the top 140 N-MYC interactors enriched during the MS analysis of native wild-type and P44L mutant N-MYC complexes, we also identified 45 other nuclear proteins which had not been previously reported to bind N-MYC. We decided to make a selection of potential novel N-MYC interactors and validate their binding via Co-IP. The selection criteria among the top 140 was based on: 1) only nuclear proteins; 2) proteins whose interaction with N-MYC was not previously reported in protein databases or in previous MS-based N-MYC interactome analysis; and 3) according to the literature we found regarding the physiological role of the candidates, the most promising and logical proteins to possibly interact with N-MYC were selected.

Using these criteria, we came up with six additional candidates to be validated by Co-IP [**Table 21**, proteins marked in blue]: DVL2, TROVE2 and the proto-oncogene proteins FOXK1, TLE1, CBLL1 and MCRS1. FOXK1 is a transcription factor that has been reported to positively regulate the Wnt pathway, by binding to DVL2 and translocating it to the nucleus: DVL2 is the central intracellular effector of the Wnt pathway, and it was also

enriched in our N-MYC complexes. FOXK1 has been suggested as a potential oncoprotein due to its high protein expression in several types of cancers (Gentzel and Schambony 2017, Wang et al. 2015). Furthermore, some members of the FOX transcription factors family, like FOXR1, FOXR2 and FOXK2, have been reported to interact with C-MYC (Kalkat et al. 2018, Li et al. 2015), making FOXK1 an even more promising candidate to validate. TLE1, another oncogenic candidate, belongs to a family of transcription factors which recruit cofactors to repress transcription, and inhibition of TLE1 in leukemias overexpressing N-MYC leads to more proliferating and aggressive tumors (Ramasamy et al. 2016). CBLL1 is an E3 ubiquitin ligase and plays a major role in tumorigenesis of several cancers (Castosa et al. 2018, Figueroa, Fujita and Gorospe 2009, Hui et al. 2019). Last but not least, MCRS1 is involved in several cellular processes, including growth, migration, senescence and transformation, and it is overexpressed in non-small cell lung cancer (NSCLC). Silencing of MCRS1 has been reported to downregulate C-MYC, although MCRS1 was not observed to directly bind to the promoter region of C-MYC (Liu et al. 2015). Therefore, further studies are required to elucidate the relation between both proteins. Lastly, TROVE2 is a ribonuclear protein which binds misfolded non-coding RNAs, pre-5S rRNA, and different small cytoplasmic RNA molecules known as Y RNAs, and it may stabilize these RNA molecules and protect them from degradation (Boccitto and Wolin 2019).

For the Co-IP validation, we used FLAG-tagged expression vectors of FOXK1, DVL2, TLE1, CBLL1, MCRS1 and TROVE2. We were able to confirm the interaction of N-MYC with FOXK1, MCRS1 and CBLL1 with variable strength **[Figure 15A]**. This suggests that their binding to N-MYC is more dynamic than the binding to MAX, its obligate dimerization partner for regulating transactivation, or limited to certain complexes.

We further characterized the stronger FOXK1/N-MYC interaction since the related FOXR2 has been shown before to bind C-MYC and to promote cell proliferation and oncogenic transformation (Li et al. 2016). Deletion analysis of RFP-FOXK1 fusions revealed a strong interaction of N-MYC with the forkhead-associated domain (FHA) of FOXK1, a phosphopeptide recognition domain that could provide readouts of N-MYC phosphorylation **[Figure 15B].**
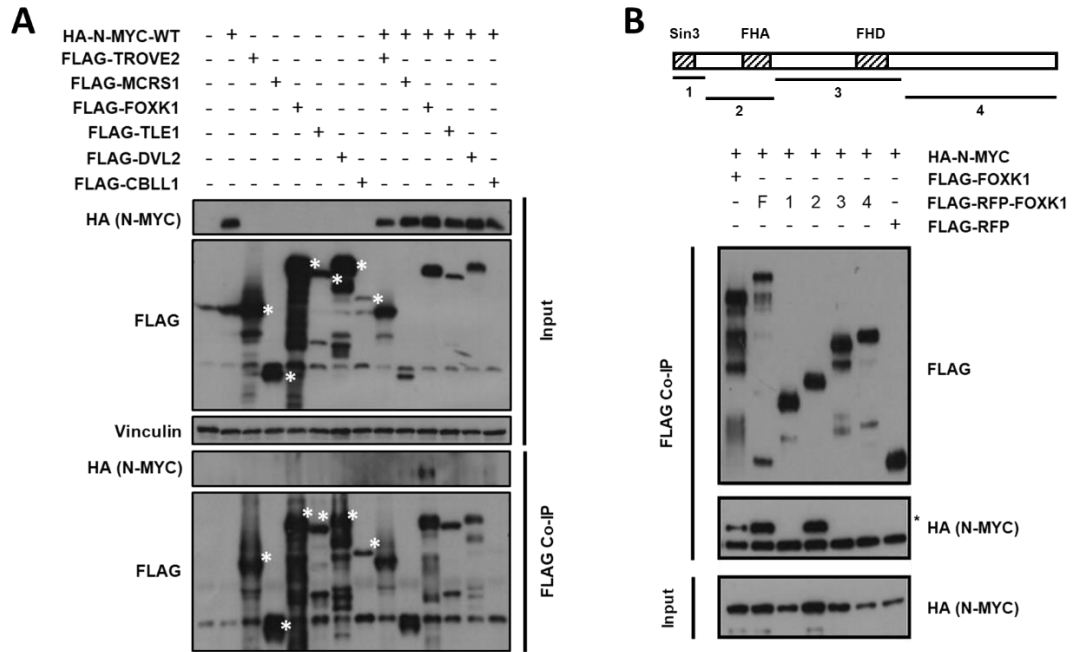
Figure 15. Characterization of novel N-MYC interactors.
(**A**) Immunoblots of HEK293 cells transiently transfected with expression vectors for HA-N-MYC and potential novel N- MYC interaction partners. White asterisks identify the specific bands for N-MYC interactors. (**B**) Scheme of FOXK1 deletion mutants and co-IP of HA-N-MYC with flag-tagged FOXK1 deletion mutants in HEK293 cells. The asterisk in FLAG-IP blot marks the band corresponding to HA-N-MYC protein. F: full-length FOXK1; 1-4: FOXK1 deletion mutants.

6.3.4. Gene expression correlation of *MYCN* and novel interactors in WT and neuroblastoma

After confirming the interaction of N-MYC with BMP2K, DAB2, PEG10, YEATS2, FOXK1, MCRS1 and CBLL1, which had not been reported previously, we asked ourselves if there would be any association in their gene expression in WT. We used the largest microarray analysis datasets from publicly available WT patient cohort data in the R2: microarray analysis and visualization platform. Two WT datasets were selected: "Kool - 71 - MAS5.0 - u133p2", with mRNA levels of blastemal WT undergoing the SIOP protocol (Wegert et al. 2015), and "Perlman - 224 - MAS5.0 - u133a", consisting of 224 favorable histology WTs following the NWTS/COG protocol (Gadd et al. 2012). Additionally, since *MYCN* amplification is a very common event in neuroblastoma, present in approximately 25 % of cases and correlated with high-risk disease and poor prognosis (Huang and Weiss 2013), we decided to analyze the gene expression correlation in this malignancy using

the largest available dataset as well, "Kocak - 649 - custom - ag44kcwolf" (Kocak et al. 2013).

Using the dataset from WT patients undergoing the SIOP protocol, we could observe that the mRNA levels of all these new interactors were significantly correlated to *MYCN*s (p < 0.005): except for *BMP2K* and *DAB2*, whose expression was negatively correlated to *MYCN*s, there was a positive correlation in the expression of *MYCN* and all interactors **[Figure 16,** 1st column**]**. The same significant correlation was also observed when using a dataset from a cohort of neuroblastoma patients, except for *MCRS1*, where the significance of the correlation was a bit lower (p < 0.05); and for *PEG10*, which expression correlated negatively with *MYCN*s although it was significant **[Figure 16,** 2nd column**]**. In addition, when we tested the correlation using a dataset from a WT cohort belonging to a NWTS/COG study, *DAB2*, *YEATS2* and *CBLL1* showed again a significant positive correlation **[Figure 16,** 3rd column**]**.

Extended expression analysis in an independent cohort of 322 Wilms tumor cases by realtime-PCR confirmed the correlated expression of *PEG10* and *YEATS2* with *MYCN* **[Figure 17]**. Especially *MYCN* and *PEG10* also showed very similar patterns of expression in different subtypes of Wilms tumors, predominantly the high risk blastemal type **[Supplement 10.4]**, where *YEATS2* was also significantly overexpressed. This data set also confirmed the prior association of higher *MYCN* levels with fatal outcome and relapse (6.5 and 2.5-fold respectively, p <0.001), but this was not seen for its interacting partners **[Supplement 10.4]**.

Figure 16. Expression of *MYCN* and protein interactors in WT and neuroblastoma.
Scatter plots showing mRNA expression (log2) of *MYCN* (x axes) and interaction partners (y axes) in different WT and neuroblastoma patient cohorts. The data was obtained from microarray analysis datasets publicly available in R2 (http://r2.amc.nl). For WT, we used two different datasets, with patients undergoing the SIOP or NWTS/COG protocols. For each correlation, the coefficient of determination (R^2) and the p-value (p) are indicated.
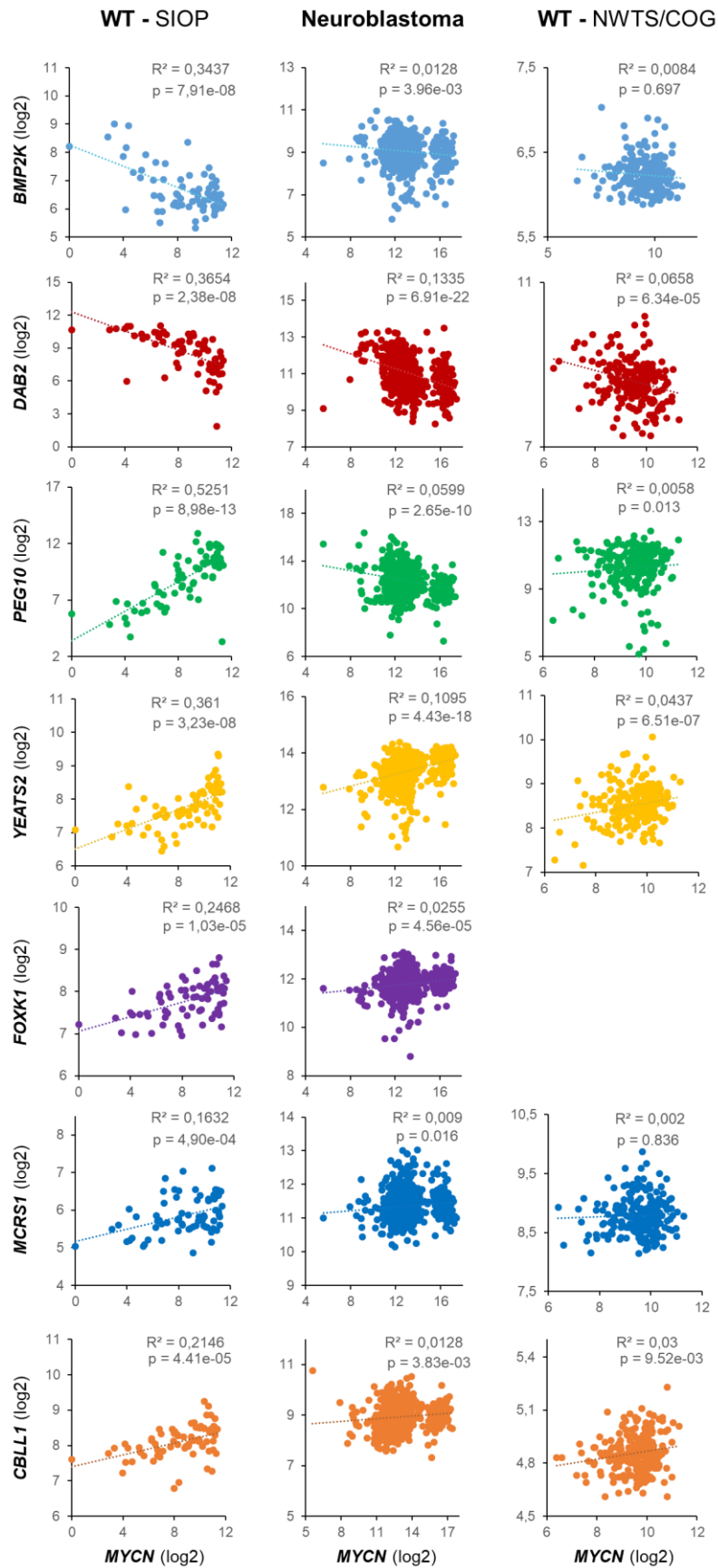*(See figure on next page)*

Figure 16. Expression of *MYCN* and protein interactors in WT and neuroblastoma.
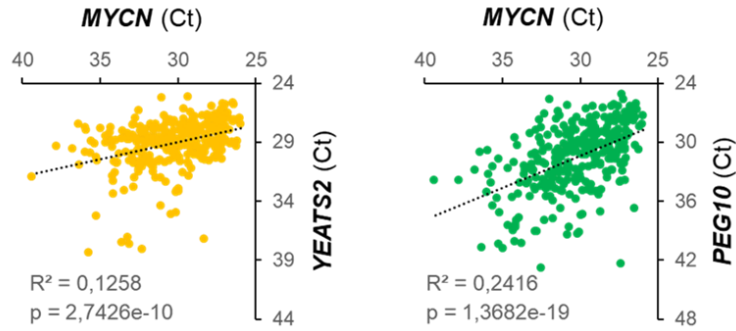*(See legend on previous page)*

Figure 17. Expression of *MYCN*, *YEATS2* and *PEG10* in WT.
Scatter plots with cycle threshold (Ct) values, representing the correlation between *MYCN* (x-axis) and *YEATS2*/*PEG10* expression (y-axes) in 299 WTs. Coefficients of determination (R^2) and p-values (p) are indicated.

6.3.5. *MYCN* P44L influence on N-MYC phosphorylation and stability

The P44 residue of N-MYC is located within a predicted phosphorylation motif for different kinases, such as the b-adrenergic receptor kinase, GSK-3, ERK1, ERK2 and CDK5 (Amanchy et al., 2007). This motif involves the residues D41-P45, where S42 and T43 have the potential to be phosphorylated. We decided to study the possible impact of the P44L mutation on the phosphorylation level of N-MYC at these positions and its stability. This analysis was also extended to the residues T58 and S62, components of the N-MYC phosphodegron and the most reported phosphorylated residues: previous studies suggested an impact of the P44L mutation in these phosphosites, having a potential role in protein stability (Kato et al. 2019).

We performed a phospho-assay using wild-type and mutant HA-N-MYC overexpressed in HEK293 cells and purified by IP, where the N-MYC peptides were analyzed for post-translational modifications (PTM) by MS. The quality of the IP elutions was assessed by Western blot analysis and Silver staining, where we confirmed the presence of N-MYC and MAX in the elutions, but also that the denaturing conditions applied during the purification of N-MYC resulted in less interactors being eluted together **[Figure 18B]**.

The MS analysis detected several peptides corresponding to the amino-terminus of our purified wild-type HA-N-MYC, which as expected presented partially phosphorylated T58 and S62 residues. But it also detected a novel, frequent phosphorylation at S42 and T43 **[Figure 18A]**: the phosphorylation of these two last residues could not be

distinguished due to their proximity. When we analyzed the peptides corresponding to the amino-terminus of the mutant HA-N-MYC, we observed that the peptides from HA-N-MYC-P44L harboring the T58 and S62 residues presented a similar ratio of phosphorylation compared to the wild-type scenario, so the mutation, contrary to previous suggestions, had no impact in the phosphorylation of these positions. We could validate this observation by Western blot analysis, where antibodies against T58- and S62-phosphorylated MYC gave same results for both wild-type and mutant HA-N-MYC **[Figure 18C]**. Interestingly, the peptides of the mutated HA-N-MYC showed a lack of phosphorylation at S42/T43 **[Figure 18A]**, probably due to the replacement of the proline amino acid by the larger leucine in the mutant, making it difficult for the adjacent phosphosites to be phosphorylated. The number of identified wild-type and mutant peptides containing the S42/T43 residues was relatively low in our MS, possibly due to their hydrophobicity or charge, which made them more difficult to be detected by MS. The extracted ion chromatographs obtained from these peptides could confirm the complete lack of phosphorylation at S42/T43 at HA-N-MYC-P44L **[Supplement 10.5]**.

We subsequently performed a protein stability assay, to assess if this lack of phosphorylation could have any consequences in N-MYC stability. Inhibition of *de novo* protein synthesis and proteasome degradation, by cycloheximide and MG-132 respectively, revealed that mutant N-MYC presented the same protein stability as its wild-type counterpart **[Figure 18D]**.

Putting these results together, we concluded that the P44L mutation had no influence on the T58/S62 phosphodegron of N-MYC, but it prevented the phosphorylation of the phosphosites S42/T43. However, the stability of N-MYC remains unaltered in presence of the mutation.

6.3.6. Effect of *MYCN* P44L and *MAX* R60Q on cell proliferation

Having observed the impact of the *MAX* R60Q and *MYCN* P44L mutations respectively on DNA-binding and protein phosphorylation, we decided to analyze if these mutations could subsequently have an impact on cell proliferation via MTT assays. We used biological triplicates of HEK293 cells stably transfected with wild-type or mutant HA-N-MYC and FLAG-MAX inducible expression vectors, and induced them in a manner so all
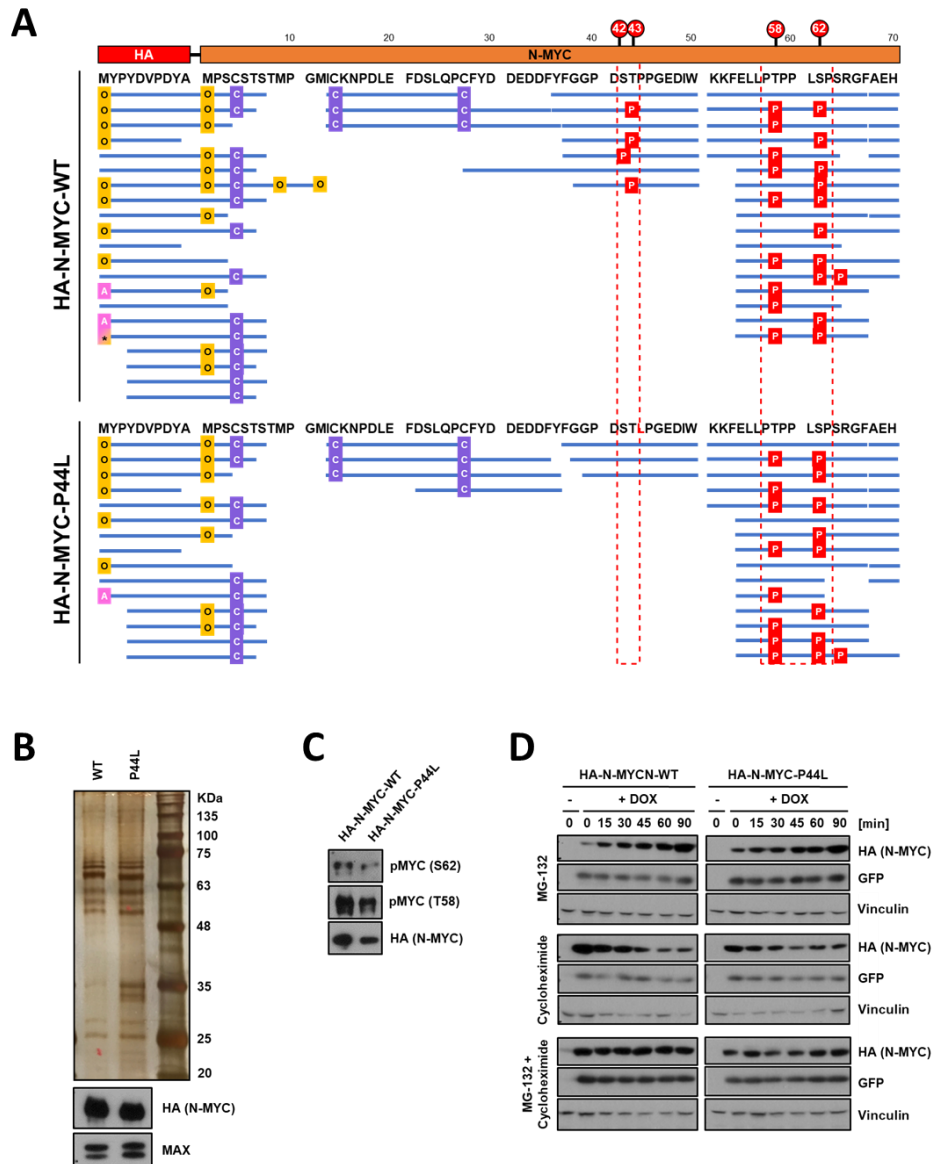
Figure 18. Impact of *MYCN* P44L mutation on protein stability and phosphorylation.
(A) Graphical summary of the results of MS peptide analyses. The amino-termini of wild-type and P44L mutant HA-N-MYC are depicted with the corresponding amino acid residues and positions in the top. Blue lines represent peptides identified by MS after digestion with chymotrypsin. Identified protein modifications included phosphorylation (P, in red), oxidation of methionine (O, in yellow), protein N-terminal acetylation (A, in pink) and carbamidomethylation (C, in violet). Dashed boxes indicate the phosphorylated residues identified by MS, corresponding to the positions S42, T43, T58 and S62. **(B)** IP elutions of HA-N-MYC complexes from HEK293 pSB-ETiE-HA-MYCN-WT or -P44L (WT and P44L) cells under denaturing conditions, separated in an acrylamide gel using SDS-PAGE and revealed with a silver staining. At the bottom, the corresponding immunoblots confirming the overexpression and purification of wild-type and P44L mutant N-MYC, as well as MAX. **(C)** Western blot analysis showing phosphorylation status of T58 and S62 in HA-N-MYC. **(D)** Immunoblots from protein stability assays of wild-type and mutant HA-N-MYC in stably transfected HEK293 cells. Inhibitor treatment with MG-132 and / or cycloheximide was performed for 0 - 90 minutes as indicated. GFP expression is coupled to MYCN via an IRES sequence **[Figure 8]**.

of them would have a comparable expression, also as minimal as possible, to imitate cellular physiological conditions. This protein expression was assessed before performing the MTT assay, by doxycycline-titrating cell clones and selecting those with similar expression with low doxycycline concentrations.

We analyzed the proliferation level of each cell line for 4 days, including untransfected HEK293 cells as well as doxycycline-induced and uninduced cells as control samples. At the 4th day we additionally harvested cells representing the same cell lines and treatments, which had been cultured in parallel to the cells used for the MTT assay, to verify their protein expression. We found out that the HEK293 cells overexpressing the MAX-R60Q mutant proliferated with the same speed as those cells expressing the wild-type vector, so this mutation had no effect on cell proliferation. Our analysis of cell proliferation did not reveal neither an influence of the P44L mutation in HEK293 cells **[Figure 19A]**, but these data have to be viewed with caution, since these cells appear quite sensitive to N-MYC overexpression. Induction of the wild-type or mutant transgene led to a compensatory reduction in the levels of endogenous C-MYC (MYC) expression and growth arrest and apoptosis, irrespective of the mutation status **[Figure 19B]**. It has been reported that overexpression of C-MYC sensitizes cells to apoptosis by a variety of stimuli (Hoffman and Liebermann 2008), meaning that with our expression system we could have exceeded the maximal amount of MYC which HEK293 cells can cope with, and activated apoptosis.
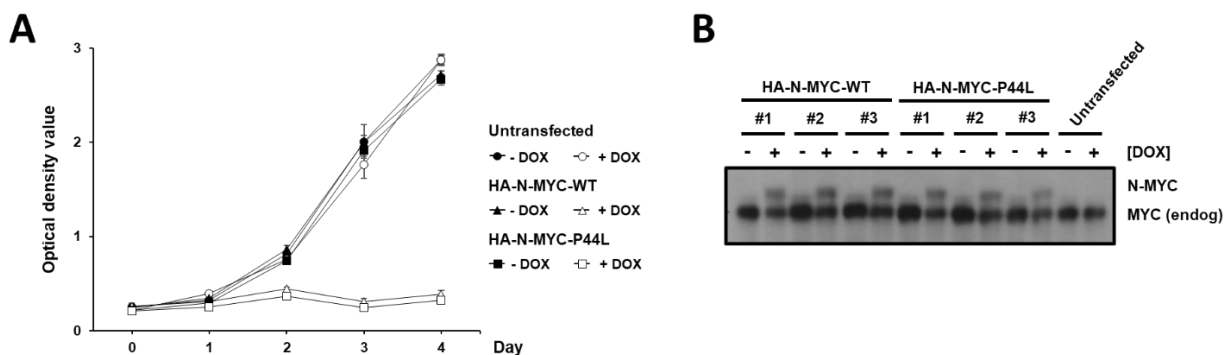

Figure 19. Effects of *MYCN* P44L on cell proliferation.
(A) Growth curves (MTT assay) of HEK293 clones expressing wild-type or mutant HA-N-MYC. The results represent the mean values obtained from biological triplicates. **(B)** Western blot analysis of HA-N-MYC-expressing HEK293 clones used in (A), showing their endogenous C-MYC and induced N-MYC expression at day 4.

7. Discussion

MYC proteins are a family of transcription factors which regulate a large diversity of cellular processes, by inducing the expression of the genes involved in these processes. Therefore, it is no wonder that dysregulation of MYC proteins has a large impact in development of cancer, as proven by the identification of different types of *MYC* and *MYCN* alterations in a large variety of cancers, WT included, and their recurrent correlation with poor prognosis and reduced disease-free survival (Carabet et al. 2018, Rickman et al. 2018). This makes the *MYCN* oncogene not only a significant target to be studied for novel therapeutic approaches in cancer, but also because *MYCN* aberrations have the potential to become relevant biomarkers for early risk-stratification of patients, which in some types of cancers like WT there is an urgent need of.

7.1. *MYCN/MAX* alterations as risk factors

In WT it was mostly copy number gain of *MYCN* (Williams et al. 2015) and elevated expression (Wittmann et al. 2008) that were linked to reduced survival. Exome sequencing recently revealed point mutations of *MYCN* (P44L) and its heterodimer partner *MAX* (R60Q) in WT (Wegert et al. 2015, Williams et al. 2015, Gadd et al. 2017). We have now performed the largest screening for *MYCN* P44L and *MAX* R60Q using 810 and 782 WT patients respectively. *MYCN* P44L was identified in 3 % of cases, similar to previous studies. The *MAX* R60Q mutation had a frequency of 0.9 %, slightly lower than reported before (1.7 %) (Gadd et al. 2017) and it was the only relevant alteration to be found in the *MAX* CDS, unlike in pheochromocytoma (Comino-Mendez et al. 2011). *MAX* R60Q mutations appear to be late clonal events suggested by their variable presence in multiply sampled tumors. Both, *MYCN* and *MAX* mutations were significantly associated with relapse and metastasis, which may make them valuable additions to biomarkers for the prediction of clinical course.

Although diffuse anaplasia is the strongest clinical predictor of poor outcome in WT, we did not find neither *MYCN* nor *MAX* mutations in 34 diffuse and 15 focal anaplastic tumors from our collection. In the American COG cohort *MYCN* mutations were 3 times less frequent in diffuse anaplastic tumors and there were no *MAX* mutations (Gadd et

al. 2017). Even if this skewing did not reach statistical significance, it is likely that *MYCN*/*MAX* mutations bear prognostic value, independent of histologically defined risk from diffuse anaplasia.

In a previous study, our group showed that, like copy number gains, high *MYCN* expression is correlated with relapse and fatal outcome in a cohort of 102 WT (Wittmann et al. 2008). This could be corroborated in the present study in a larger series of 293 patients, further strengthening the possible role of *MYCN* expression as a biomarker in WT stratification. It is conceivable that all three alterations detected for *MYCN*, P44L point mutations, copy number gain, or elevated mRNA expression, which together affect a greater share of WTs, may act in a similar manner and independently contribute to higher risk of relapse and poor outcome.

7.2. Functional role of *MYCN* P44L and *MAX* R60Q

The *MAX* R60Q mutation was proposed to alter DNA binding strength and perhaps dimerization due to its location in the helix-loop-helix domain (Wegert et al. 2015, Gadd et al. 2017). It has been found in several other tumor types (Tate et al. 2019) and *in vitro* binding assays have indeed confirmed a strongly reduced affinity of the mutant protein for cognate E-box binding sites (Wang et al. 2017). In PC12 cells a related R60W mutation and several other MAX mutants were shown to have reduced regulatory capacity, observed as repression in that system (Comino-Mendez et al. 2015). This fits to our observation of a reduced transcriptional activation potential of MAX-R60Q compared to the wild-type protein. This likely disturbs the balance of other N-MYC containing transcriptional complexes of the MYC/MAX/MXD1 network. Surprisingly, expression of wild-type or mutant MAX protein in HEK293 cells did not change in proliferation in our hands, but the effects may be more subtle or cell type dependent. In line with this, such *MAX* mutations have been described as oncogenic drivers in multiple myeloma, but the mutant tumors showed lower MYC levels and a better prognosis (Wang et al. 2017).

The *MYCN* P44L mutation remains enigmatic in its functional effects. The mutation is located N-terminal to the conserved MBI, an area that is poorly represented in 3D structures of N-MYC proteins. *In silico* prediction by Netphos 2.0 (Blom et al. 1999) highlighted a potential loss of phosphorylation sites S42 and especially T43 in the mutant

protein. Our detailed MS analyses of tryptic fragments revealed strong phosphorylation at one of the sites, which could not be distinguished based on peptide masses, in the wild-type protein. The mutant protein completely lacked phosphorylation at these positions, while the well-known T58 and S62 sites were phosphorylated equally efficient. Thus, the T58/S62 phosphodegron appears not to be affected. Analyses of protein stability and cell tolerance to overexpression did not reveal substantial differences between both N-MYC versions, accordingly. The lack of conservation of S42/T43 in other MYC paralogues rather calls for a N-MYC specific role of this phosphorylation site and not a general mechanism for all MYC proteins.

The highly stereotypic proline to leucine mutation together with the concomitant difference in phosphorylation hinted at possibly different binding partners for N-MYC-P44L. Comparative MS analysis of N-MYC containing complexes revealed very similar sets of co-purified proteins, but when we analyzed the top candidates for differential binding, none of them could unequivocally be reproduced as binding more poorly or better to one of the N-MYC proteins. Thus, at the resolution used in our study in HEK293 cells, there seems to be no clear candidate that would differentially bind the wild-type or mutant N-MYC. Regarding the impact of the mutant on cell proliferation, as well as its binding to uncharacterized interacting partners and their association to dephosphorylated N-MYC at S42/T43, further functional studies for this mutant would be required, to get a complete understanding of this marker and how to fully exploit it in future molecular treatments.

7.3. N-MYC novel interactors

The enrichment of N-MYC native complexes and their analysis via MS allowed us to identify in the range of 40-50 novel N-MYC interactors, and for some of them, the interaction could be validated via co-IP experiments. The recognition of new protein partners is of great value, as they can reveal N-MYC protein functions which were previously unknown, and also broaden the number of potential therapeutic targets which can be exploited in tumors with high N-MYC protein levels.

Seven novel N-MYC interactors were confirmed via MS and IP: BMP2K, DAB2, PEG10, YEATS2, FOXK1, MCRS1 and CBLL1, all of them previously reported as potential

oncogenes. Furthermore, their expression levels were correlated with *MYCN* in two cohorts of WT patients and a neuroblastoma data set. For *PEG10* and *YEATS2*, we could validate these correlations using qRT-PCR on a larger cohort. These genes may thus represent additional candidates for prognostic biomarkers or targets in WT.

The connection of some of these proteins to MYC proteins, or even the information regarding their own functions or interactome, is quite limited, like for BMP2K and DAB2. BMP2K is a kinase belonging to the NAK family, and there is only little information available regarding its role in tumor formation: it has a presumed regulatory role in attenuating the program of osteoblast differentiation (Kearns et al. 2001), and it has been proven that it also contributes to IRS2-dependent invasion in breast carcinoma cells (Mercado-Matos et al. 2018). DAB2 is a candidate tumor suppressor which is downregulated in many tumors (Anupam et al. 2006, Huang et al. 2001, Kleeff et al. 2002, Mok et al. 1994), and serves as an adaptor protein in many cellular processes (Morris et al. 2002, Rosenbauer et al. 2002, Tseng et al. 2001, Zhou and Hsieh 2001). However, there is still limited information about its interactome, as well as how DAB2 connects its diverse cellular functions to its tumor suppressor activity. The identification of the N-MYC interaction with BMP2K and DAB2 could help to elucidate the mechanisms in which these two proteins contribute to tumor formation in different cancers.

The same situation applies to CBLL1, an E3 ubiquitin ligase which, as mentioned before, has been reported to be overexpressed in several cancers and to play a major role in their tumorigenesis (Hui et al. 2019, Figueroa et al. 2009). Although there are a few E3 ligases directly involved in the targeted proteasomal degradation of MYC proteins, the identification of the N-MYC-CBLL1 interaction could lead to further studies aiming to analyze the functional connection between CBLL1 and N-MYC, and to identify a possible contribution of CBLL1 in MYC proteins oncogenic roles and vice versa.

For PEG10 and MCRS1, there are some previous studies establishing an association with MYC proteins. Both proteins are involved in several cellular processes, including cell proliferation and migration. On one hand, *PEG10* is a paternally expressed imprinted oncogene which contributes to cell invasion in different types of cancer (Deng et al. 2014, Ip et al. 2007, Zang et al. 2015). It has been reported to be a direct downstream

target of C-MYC, by binding E-box sequences in the first *PEG10* intron and activating its transcription (Li et al. 2006). Therefore, further studies will be required to understand the functional connection between PEG10 and N-MYC. On the other hand, MCRS1 is directly involved with transcriptional regulation: it has been reported to be a putative regulatory component of the INO80 chromatin remodeling complex (Hargreaves and Crabtree 2011), whose components TIP48, TIP49 and ACTL6A were also significantly enriched in our IP/MS. This could point to a possible connection of MYC proteins to the INO80 complexes, and provide an additional MYC-mediated mechanism of transcriptional activation. Additionally, *MCRS1* is overexpressed in NSCLC, just like *YEATS2*, and C-MYC has been reported to be a downstream target of MCRS1, although MCRS1 was not observed to directly bind the C-MYC promoter region (Liu et al. 2015).

By contrast, there are previous reports about the interaction of MYC with FOX proteins or YEATS2. FOXK1 belongs to the evolutionarily conserved superfamily of FOX transcription factors, and the small subfamily *FOXK* is ubiquitously expressed in various tissues and organs. FOXK1 binds to DNA sequence to regulate several biological processes in which MYC is also involved (Fujii and Nakamura 2010, Shi et al. 2012, Sukonina et al. 2019), all of them closely related to cancer initiation, development, metastasis, angiogenesis and drug resistance. This explains the role of deregulated *FOXK1* in various types of cancers, and it has been even presented as an unfavorable prognostic biomarker for some of them (Liu et al. 2019), but the regulatory mechanism of FOXK proteins still need to be completely understood. L-MYC has been reported to interact with FOXK1, but so far C-MYC has been identified as FOXK2 and FOXR2 interactors (Li et al., 2016, Kalkat et al. 2018). This C-MYC-FOXR2 interaction has been characterized more in detail, where the MBII and III are required to form a ternary FOXR2-MYC/MAX complex independent of MAX-MAD1 association. Using quantitative proteomics, FOXK1 was reported to also bind MAX (Hein et al. 2015), so the formation of ternary N-MYC/MAX/FOXK1 complexes could be possible too. With our study, we provide evidence for FOXK1 binding to N-MYC via its FHA domain, emphasizing the possible connection between these two major transcriptional regulators and oncogenes, and presenting a further potential actor in how FOXK1 perform its regulatory mechanisms.

YEATS2 is a scaffolding subunit of the ATAC complex, a conserved metazoan complex that is involved in transcriptional activation thanks to it histone acetyltransferase activity (Wang et al. 2008). Other components of this complex, like the histone acetyltransferase GCN5, have already been reported to bind MYC proteins (McMahon, Wood and Cole 2000), and the direct interaction of YEATS2 with C-MYC was recently identified using a high throughput screen (Kalkat et al. 2018), although the interaction with its homologue N-MYC was not identified up to this study. We now show a similar association of YEATS2 with N-MYC. This may contribute to oncogenesis since knockdown of *YEATS2* in lung cancer cells led to growth suppression, survival reduction and downregulation of a large number of ribosomal proteins genes (Mi et al. 2017), being all of them key MYC functions (van Riggelen, Yetil and Felsher 2010).

In conclusion, we identified a set of novel N-MYC interactors which dysregulation had been previously reported to contribute in many different cancers. Further studies elucidating their exact functional relationship with N-MYC in tumor development will be required, which could provide new molecular strategies for the treatment of amplified N-MYC tumors, recurrently associated with poor prognosis, and for some of these novel proteins, it could contribute to understand their tumorigenic mechanisms in other types of cancers.

8. References

Adhikary, S. & M. Eilers (2005) Transcriptional regulation and transformation by Myc proteins. *Nat Rev Mol Cell Biol,* 6**,** 635-45.

Adhikary, S., F. Marinoni, A. Hock, E. Hulleman, N. Popov, R. Beier, S. Bernard, M. Quarto, M. Capra, S. Goettig, U. Kogel, M. Scheffner, K. Helin & M. Eilers (2005) The ubiquitin ligase HectH9 regulates transcriptional activation by Myc and is essential for tumor cell proliferation. *Cell,* 123**,** 409-21.

Adzhubei, I., D. M. Jordan & S. R. Sunyaev (2013) Predicting functional effect of human missense mutations using PolyPhen-2. *Curr Protoc Hum Genet,* Chapter 7**,** Unit7.20.

Akamatsu, S., A. W. Wyatt, D. Lin, S. Lysakowski, F. Zhang, S. Kim, C. Tse, K. Wang, F. Mo, A. Haegert, S. Brahmbhatt, R. Bell, H. Adomat, Y. Kawai, H. Xue, X. Dong, L. Fazli, H. Tsai, T. L. Lotan, M. Kossai, J. M. Mosquera, M. A. Rubin, H. Beltran, A. Zoubeidi, Y. Wang, M. E. Gleave & C. C. Collins (2015) The Placental Gene PEG10 Promotes Progression of Neuroendocrine Prostate Cancer. *Cell Rep,* 12**,** 922-36.

Alami, J., B. R. Williams & H. Yeger (2003) Derivation and characterization of a Wilms' tumour cell line, WiT 49. *Int J Cancer,* 107**,** 365-74.

Althoff, K., A. Beckers, E. Bell, M. Nortmeyer, T. Thor, A. Sprussel, S. Lindner, K. De Preter, A. Florin, L. C. Heukamp, L. Klein-Hitpass, K. Astrahantseff, C. Kumps, F. Speleman, A. Eggert, F. Westermann, A. Schramm & J. H. Schulte (2015) A Cre-conditional MYCN-driven neuroblastoma mouse model as an improved tool for preclinical studies. *Oncogene,* 34**,** 3357-68.

Amanchy, R., Periaswamy, B., Mathivanan, S., Reddy, R., Tattikota, S. G., & Pandey, A. (2007). A curated compendium of phosphorylation motifs. Nature biotechnology, 25(3), 285–286.

Amente, S., A. Bertoni, A. Morano, L. Lania, E. V. Avvedimento & B. Majello (2010) LSD1-mediated demethylation of histone H3 lysine 4 triggers Myc-induced transcription. *Oncogene,* 29**,** 3691-702.

Amente, S., G. Milazzo, M. C. Sorrentino, S. Ambrosio, G. Di Palo, L. Lania, G. Perini & B. Majello (2015) Lysine-specific demethylase (LSD1/KDM1A) and MYCN cooperatively repress tumor suppressor genes in neuroblastoma. *Oncotarget,* 6**,** 14572-83.

Anupam, K., C. Tusharkant, S. D. Gupta & R. Ranju (2006) Loss of disabled-2 expression is an early event in esophageal squamous tumorigenesis. *World J Gastroenterol,* 12**,** 6041-5.

Babyn, P., C. Owens, M. Gyepes & G. J. D'Angio (1995) Imaging patients with Wilms tumor. *Hematol Oncol Clin North Am,* 9**,** 1217-52.

Baluapuri, A., J. Hofstetter, N. Dudvarski Stankovic, T. Endres, P. Bhandare, S. M. Vos, B. Adhikari, J. D. Schwarz, A. Narain, M. Vogt, S. Y. Wang, R. Duster, L. A. Jung, J. T. Vanselow, A. Wiegering, M. Geyer, H. M. Maric, P. Gallant, S. Walz, A. Schlosser, P. Cramer, M. Eilers & E. Wolf (2019) MYC Recruits SPT5 to RNA Polymerase II to Promote Processive Transcription Elongation. *Mol Cell,* 74**,** 674-687.e11.

Baluapuri, A., E. Wolf & M. Eilers (2020) Target gene-independent functions of MYC oncoproteins. *Nat Rev Mol Cell Biol,* 21**,** 255-267.

Bao, J. & A. S. Zervos (1996) Isolation and characterization of Nmi, a novel partner of Myc proteins. *Oncogene,* 12**,** 2171-6.

Bedard, M., L. Maltais, M. Montagne & P. Lavigne (2017) Miz-1 and Max compete to engage c-Myc: implication for the mechanism of inhibition of c-Myc transcriptional activity by Miz-1. *Proteins,* 85**,** 199-206.

Beltran, H. (2014) The N-myc Oncogene: Maximizing its Targets, Regulation, and Therapeutic Potential. *Mol Cancer Res,* 12**,** 815-22.

Bhakta, N., Q. Liu, K. K. Ness, M. Baassiri, H. Eissa, F. Yeo, W. Chemaitilly, M. J. Ehrhardt, J. Bass, M. W. Bishop, K. Shelton, L. Lu, S. Huang, Z. Li, E. Caron, J. Lanctot, C. Howell, T. Folse,

V. Joshi, D. M. Green, D. A. Mulrooney, G. T. Armstrong, K. R. Krull, T. M. Brinkman, R. B. Khan, D. K. Srivastava, M. M. Hudson, Y. Yasui & L. L. Robison (2017) The cumulative burden of surviving childhood cancer: an initial report from the St Jude Lifetime Cohort Study (SJLIFE). *Lancet,* 390**,** 2569-2582.

Blackwood, E. M. & R. N. Eisenman (1991) Max: a helix-loop-helix zipper protein that forms a sequence-specific DNA-binding complex with Myc. *Science,* 251**,** 1211-7.

Blom, N., S. Gammeltoft & S. Brunak (1999). Sequence and structure-based prediction of eukaryotic protein phosphorylation sites. *Journal of molecular biology, 294(5), 1351– 1362.*

Boccitto, M. & S. L. Wolin (2019) Ro60 and Y RNAs: structure, functions, and roles in autoimmunity. *Crit Rev Biochem Mol Biol,* 54**,** 133-152.

Brenner, C., R. Deplus, C. Didelot, A. Loriot, E. Vire, C. De Smet, A. Gutierrez, D. Danovi, D. Bernard, T. Boon, P. G. Pelicci, B. Amati, T. Kouzarides, Y. de Launoit, L. Di Croce & F. Fuks (2005) Myc represses transcription through recruitment of DNA methyltransferase corepressor. *Embo j,* 24**,** 336-46.

Breslow, N., A. Olshan, J. B. Beckwith & D. M. Green (1993) Epidemiology of Wilms tumor. *Med Pediatr Oncol,* 21**,** 172-81.

Brok, J., M. Lopez-Yurda, H. V. Tinteren, T. D. Treger, R. Furtwangler, N. Graf, C. Bergeron, M. M. van den Heuvel-Eibrink, K. Pritchard-Jones, O. E. Olsen, B. de Camargo, A. Verschuur & F. Spreafico (2018) Relapse of Wilms' tumour and detection methods: a retrospective analysis of the 2001 Renal Tumour Study Group-International Society of Paediatric Oncology Wilms' tumour protocol database. *Lancet Oncol,* 19**,** 1072-1081.

Buchel, G., A. Carstensen, K. Y. Mak, I. Roeschert, E. Leen, O. Sumara, J. Hofstetter, S. Herold, J. Kalb, A. Baluapuri, E. Poon, C. Kwok, L. Chesler, H. M. Maric, D. S. Rickman, E. Wolf, R. Bayliss, S. Walz & M. Eilers (2017) Association with Aurora-A Controls N-MYC-Dependent Promoter Escape and Pause Release of RNA Polymerase II during the Cell Cycle. *Cell Rep,* 21**,** 3483-3497.

Burnichon, N., A. Cascon, F. Schiavi, N. P. Morales, I. Comino-Mendez, N. Abermil, L. Inglada-Perez, A. A. de Cubas, L. Amar, M. Barontini, S. B. de Quiros, J. Bertherat, Y. J. Bignon, M. J. Blok, S. Bobisse, S. Borrego, M. Castellano, P. Chanson, M. D. Chiara, E. P. Corssmit, M. Giacche, R. R. de Krijger, T. Ercolino, X. Girerd, E. B. Gomez-Garcia, A. Gomez-Grana, I. Guilhem, F. J. Hes, E. Honrado, E. Korpershoek, J. W. Lenders, R. Leton, A. R. Mensenkamp, A. Merlo, L. Mori, A. Murat, P. Pierre, P. F. Plouin, T. Prodanov, M. Quesada-Charneco, N. Qin, E. Rapizzi, V. Raymond, N. Reisch, G. Roncador, M. Ruiz-Ferrer, F. Schillo, A. P. Stegmann, C. Suarez, E. Taschin, H. J. Timmers, C. M. Tops, M. Urioste, F. Beuschlein, K. Pacak, M. Mannelli, P. L. Dahia, G. Opocher, G. Eisenhofer, A. P. Gimenez-Roqueplo & M. Robledo (2012) MAX mutations cause hereditary and sporadic pheochromocytoma and paraganglioma. *Clin Cancer Res,* 18**,** 2828-37.

Carabet, L. A., P. S. Rennie & A. Cherkasov (2018) Therapeutic Inhibition of Myc in Cancer. Structural Bases and Computer-Aided Drug Discovery Approaches. *Int J Mol Sci,* 20.

Carroll, P. A., B. W. Freie, H. Mathsyaraja & R. N. Eisenman (2018) The MYC transcription factor network: balancing metabolism, proliferation and oncogenesis. *Front Med,* 12**,** 412-425.

Cascon, A. & M. Robledo (2012) MAX and MYC: a heritable breakup. *Cancer Res,* 72**,** 3119-24.

Castosa, R., O. Martinez-Iglesias, D. Roca-Lema, A. Casas-Pais, A. Díaz-Díaz, P. Iglesias, I. Santamarina, B. Graña, L. Calvo, M. Valladares-Ayerbes, Á. Concha & A. Figueroa (2018) Hakai overexpression effectively induces tumour progression and metastasis in vivo. *Sci Rep,* 8**,** 3466.

Chagtai, T., C. Zill, L. Dainese, J. Wegert, S. Savola, S. Popov, W. Mifsud, G. Vujanic, N. Sebire, Y. Le Bouc, P. F. Ambros, L. Kager, M. J. O'Sullivan, A. Blaise, C. Bergeron, L. H. Mengelbier, D. Gisselsson, M. Kool, G. A. Tytgat, M. M. van den Heuvel-Eibrink, N. Graf, H. van Tinteren, A. Coulomb, M. Gessler, R. D. Williams & K. Pritchard-Jones (2016) Gain of 1q As a Prognostic Biomarker in Wilms Tumors (WTs) Treated With Preoperative

Chemotherapy in the International Society of Paediatric Oncology (SIOP) WT 2001 Trial: A SIOP Renal Tumours Biology Consortium Study. *J Clin Oncol,* 34**,** 3195-203.

Chandramohan, V., N. D. Mineva, B. Burke, S. Jeay, M. Wu, J. Shen, W. Yang, S. R. Hann & G. E. Sonenshein (2008) c-Myc represses FOXO3a-mediated transcription of the gene encoding the p27(Kip1) cyclin dependent kinase inhibitor. *J Cell Biochem,* 104**,** 2091-106.

Chang, D. W., G. F. Claassen, S. R. Hann & M. D. Cole (2000) The c-Myc transactivation domain is a direct modulator of apoptotic versus proliferative signals. *Mol Cell Biol,* 20**,** 4309-19.

Chen, H., H. Liu & G. Qing (2018) Targeting oncogenic Myc as a strategy for cancer treatment. *Signal Transduct Target Ther,* 3**,** 5.

Cheng, S. W., K. P. Davies, E. Yung, R. J. Beltran, J. Yu & G. V. Kalpana (1999) c-MYC interacts with INI1/hSNF5 and requires the SWI/SNF complex for transactivation function. *Nat Genet,* 22**,** 102-5.

Choi, W. S., B. C. Jeong, Y. J. Joo, M. R. Lee, J. Kim, M. J. Eck & H. K. Song (2010) Structural basis for the recognition of N-end rule substrates by the UBR box of ubiquitin ligases. *Nat Struct Mol Biol,* 17**,** 1175-81.

Cloos, P. A., J. Christensen, K. Agger & K. Helin (2008) Erasing the methyl mark: histone demethylases at the center of cellular differentiation and disease. *Genes Dev,* 22**,** 1115-40.

Cohen, P. & S. Frame (2001) The renaissance of GSK3. *Nat Rev Mol Cell Biol,* 2**,** 769-76.

Cohn, S. L., H. Salwen, M. W. Quasney, N. Ikegaki, J. M. Cowan, C. V. Herst, R. H. Kennett, S. T. Rosen, J. A. DiGiuseppe & G. M. Brodeur (1990) Prolonged N-myc protein half-life in a neuroblastoma cell line lacking N-myc amplification. *Oncogene,* 5**,** 1821-7.

Comino-Mendez, I., F. J. Gracia-Aznarez, F. Schiavi, I. Landa, L. J. Leandro-Garcia, R. Leton, E. Honrado, R. Ramos-Medina, D. Caronia, G. Pita, A. Gomez-Grana, A. A. de Cubas, L. Inglada-Perez, A. Maliszewska, E. Taschin, S. Bobisse, G. Pica, P. Loli, R. Hernandez-Lavado, J. A. Diaz, M. Gomez-Morales, A. Gonzalez-Neira, G. Roncador, C. Rodriguez-Antona, J. Benitez, M. Mannelli, G. Opocher, M. Robledo & A. Cascon (2011) Exome sequencing identifies MAX mutations as a cause of hereditary pheochromocytoma. *Nat Genet,* 43**,** 663-7.

Comino-Mendez, I., L. J. Leandro-Garcia, G. Montoya, L. Inglada-Perez, A. A. de Cubas, M. Curras-Freixes, C. Tysoe, L. Izatt, R. Leton, A. Gomez-Grana, V. Mancikova, M. Apellaniz-Ruiz, M. Mannelli, F. Schiavi, J. Favier, A. P. Gimenez-Roqueplo, H. J. Timmers, G. Roncador, J. F. Garcia, C. Rodriguez-Antona, M. Robledo & A. Cascon (2015) Functional and in silico assessment of MAX variants of unknown significance. *J Mol Med (Berl),* 93**,** 1247-55.

Conacci-Sorrell, M., L. McFerrin & R. N. Eisenman (2014) An overview of MYC and its interactome. *Cold Spring Harb Perspect Med,* 4**,** a014357.

Coster, G. & M. Goldberg (2010) The cellular response to DNA damage: a focus on MDC1 and its interacting proteins. *Nucleus,* 1**,** 166-78.

Cox, J., M. Y. Hein, C. A. Luber, I. Paron, N. Nagaraj & M. Mann (2014) Accurate proteome-wide label-free quantification by delayed normalization and maximal peptide ratio extraction, termed MaxLFQ. *Mol Cell Proteomics,* 13**,** 2513-26.

Cox, J. & M. Mann (2008) MaxQuant enables high peptide identification rates, individualized p.p.b.-range mass accuracies and proteome-wide protein quantification. *Nat Biotechnol,* 26**,** 1367-72.

Dang, C. V. (2012) MYC on the path to cancer. *Cell,* 149**,** 22-35.

Dang, C. V. & W. M. Lee (1988) Identification of the human c-myc protein nuclear translocation signal. *Mol Cell Biol,* 8**,** 4048-54.

Dardenne, E., H. Beltran, M. Benelli, K. Gayvert, A. Berger, L. Puca, J. Cyrta, A. Sboner, Z. Noorzad, T. MacDonald, C. Cheung, K. S. Yuen, D. Gao, Y. Chen, M. Eilers, J. M. Mosquera, B. D. Robinson, O. Elemento, M. A. Rubin, F. Demichelis & D. S. Rickman (2016) N-Myc Induces an EZH2-Mediated Transcriptional Program Driving Neuroendocrine Prostate Cancer. *Cancer Cell,* 30**,** 563-577.

Davidoff, A. M. (2012) Wilms tumor. *Adv Pediatr,* 59**,** 247-67.

Dela Cruz, F. S., D. Diolaiti, A. T. Turk, A. R. Rainey, A. Ambesi-Impiombato, S. J. Andrews, M. M. Mansukhani, P. L. Nagy, M. J. Alvarez, A. Califano, F. Forouhar, B. Modzelewski, C. M. Mitchell, D. J. Yamashiro, L. J. Marks, J. L. Glade Bender & A. L. Kung (2016) A case study of an integrative genomic and experimental therapeutic approach for rare tumors: identification of vulnerabilities in a pediatric poorly differentiated carcinoma. *Genome Med,* 8**,** 116.

Deng, X., Y. Hu, Q. Ding, R. Han, Q. Guo, J. Qin, J. Li, R. Xiao, S. Tian, W. Hu, Q. Zhang & J. Xiong (2014) PEG10 plays a crucial role in human lung cancer proliferation, progression, prognosis and metastasis. *Oncol Rep,* 32**,** 2159-67.

Eberhardy, S. R. & P. J. Farnham (2001) c-Myc mediates activation of the cad promoter via a post-RNA polymerase II recruitment mechanism. *J Biol Chem,* 276**,** 48562-71.

Facchini, L. M., S. Chen, W. W. Marhin, J. N. Lear & L. Z. Penn (1997) The Myc negative autoregulation mechanism requires Myc-Max association and involves the c-myc P2 minimal promoter. *Mol Cell Biol,* 17**,** 100-14.

Fagnocchi, L., A. Cherubini, H. Hatsuda, A. Fasciani, S. Mazzoleni, V. Poli, V. Berno, R. L. Rossi, R. Reinbold, M. Endele, T. Schroeder, M. Rocchigiani, Z. Szkarlat, S. Oliviero, S. Dalton & A. Zippo (2016) A Myc-driven self-reinforcing regulatory network maintains mouse embryonic stem cell identity. *Nat Commun,* 7**,** 11903.

Farrell, A. S. & R. C. Sears (2014) MYC degradation. *Cold Spring Harb Perspect Med,* 4.

Faussillon, M., I. Murakami, M. Bichat, L. Telvi, C. Jeanpierre, C. Nezelof, F. Jaubert & J. Gogusev (2008) Molecular cytogenetic anomalies and phenotype alterations in a newly established cell line from Wilms tumor with diffuse anaplasia. *Cancer Genet Cytogenet,* 184**,** 22-30.

Feng, X. H., Y. Y. Liang, M. Liang, W. Zhai & X. Lin (2002) Direct interaction of c-Myc with Smad2 and Smad3 to inhibit TGF-beta-mediated induction of the CDK inhibitor p15(Ink4B). *Mol Cell,* 9**,** 133-43.

Ferrucci, F., R. Ciaccio, S. Monticelli, P. Pigini, S. di Giacomo, S. Purgato, D. Erriquez, R. Bernardoni, M. Norris, M. Haber, G. Milazzo & G. Perini (2018) MAX to MYCN intracellular ratio drives the aggressive phenotype and clinical outcome of high risk neuroblastoma. *Biochim Biophys Acta Gene Regul Mech,* 1861**,** 235-245.

Figueroa, A., Y. Fujita & M. Gorospe (2009) Hacking RNA: Hakai promotes tumorigenesis by enhancing the RNA-binding function of PSF. *Cell Cycle,* 8**,** 3648-51.

Fladvad, M., K. Zhou, A. Moshref, S. Pursglove, P. Safsten & M. Sunnerhagen (2005) N and C-terminal sub-regions in the c-Myc transactivation region and their joint role in creating versatility in folding and binding. *J Mol Biol,* 346**,** 175-89.

Fujii, Y. & M. Nakamura (2010) FOXK2 transcription factor is a novel G/T-mismatch DNA binding protein. *J Biochem,* 147**,** 705-9.

Furtwängler, R. 2008. *Das Nephroblastom und andere pädiatrische Nierentumoren*. Pädiatr Prax.

Furtwangler, R., N. Nourkami, M. Alkassar, D. von Schweinitz, J. P. Schenk, C. Rube, S. Siemer, I. Leuschner & N. Graf (2011) Update on relapses in unilateral nephroblastoma registered in 3 consecutive SIOP/GPOH studies - a report from the GPOH-nephroblastoma study group. *Klin Padiatr,* 223**,** 113-9.

Gabay, M., Y. Li & D. W. Felsher (2014) MYC activation is a hallmark of cancer initiation and maintenance. *Cold Spring Harb Perspect Med,* 4.

Gaczynska, M., & Osmulski, P. A. (2005). Small-molecule inhibitors of proteasome activity. Methods in molecular biology (Clifton, N.J.), 301, 3–22.

Gadd, S., V. Huff, C. C. Huang, E. C. Ruteshouser, J. S. Dome, P. E. Grundy, N. Breslow, L. Jennings, D. M. Green, J. B. Beckwith & E. J. Perlman (2012) Clinically relevant subsets identified by gene expression patterns support a revised ontogenic model of Wilms tumor: a Children's Oncology Group Study. *Neoplasia,* 14**,** 742-56.

Gadd, S., V. Huff, A. L. Walz, A. Ooms, A. E. Armstrong, D. S. Gerhard, M. A. Smith, J. M. G. Auvil, D. Meerzaman, Q. R. Chen, C. H. Hsu, C. Yan, C. Nguyen, Y. Hu, L. C. Hermida, T. Davidsen, P. Gesuwan, Y. Ma, Z. Zong, A. J. Mungall, R. A. Moore, M. A. Marra, J. S. Dome, C. G. Mullighan, J. Ma, D. A. Wheeler, O. A. Hampton, N. Ross, J. M. Gastier-Foster, S. T. Arold & E. J. Perlman (2017) A Children's Oncology Group and TARGET initiative exploring the genetic landscape of Wilms tumor. *Nat Genet,* 49**,** 1487-1494.

Gallant, P., Y. Shiio, P. F. Cheng, S. M. Parkhurst & R. N. Eisenman (1996) Myc and Max homologs in Drosophila. *Science,* 274**,** 1523-7.

Gartel, A. L., X. Ye, E. Goufman, P. Shianov, N. Hay, F. Najmabadi & A. L. Tyner (2001) Myc represses the p21(WAF1/CIP1) promoter and interacts with Sp1/Sp3. *Proc Natl Acad Sci U S A,* 98**,** 4510-5.

Garvin, A. J., J. L. Sullivan, D. D. Bennett, W. S. Stanley, T. Inabnett & D. A. Sens (1987) The in vitro growth, heterotransplantation, and immunohistochemical characterization of the blastemal component of Wilms' tumor. *Am J Pathol,* 129**,** 353-63.

Gentzel, M. & A. Schambony (2017) Dishevelled Paralogs in Vertebrate Development: Redundant or Distinct? *Front Cell Dev Biol,* 5**,** 59.

Grandori, C., S. M. Cowley, L. P. James & R. N. Eisenman (2000) The Myc/Max/Mad network and the transcriptional control of cell behavior. *Annu Rev Cell Dev Biol,* 16**,** 653-99.

Gratias, E. J., J. S. Dome, L. J. Jennings, Y. Y. Chi, J. Tian, J. Anderson, P. Grundy, E. A. Mullen, J. I. Geller, C. V. Fernandez & E. J. Perlman (2016) Association of Chromosome 1q Gain With Inferior Survival in Favorable-Histology Wilms Tumor: A Report From the Children's Oncology Group. *J Clin Oncol,* 34**,** 3189-94.

Green, D. M., C. A. Cotton, M. Malogolowkin, N. E. Breslow, E. Perlman, J. Miser, M. L. Ritchey, P. R. Thomas, P. E. Grundy, G. J. D'Angio, J. B. Beckwith, R. C. Shamberger, G. M. Haase, M. Donaldson, R. Weetman, M. J. Coppes, P. Shearer, P. Coccia, M. Kletzel, R. Macklis, G. Tomlinson, V. Huff, R. Newbury & D. Weeks (2007) Treatment of Wilms tumor relapsing after initial treatment with vincristine and actinomycin D: a report from the National Wilms Tumor Study Group. *Pediatr Blood Cancer,* 48**,** 493-9.

Gregory, M. A. & S. R. Hann (2000) c-Myc proteolysis by the ubiquitin-proteasome pathway: stabilization of c-Myc in Burkitt's lymphoma cells. *Mol Cell Biol,* 20**,** 2423-35.

Gregory, M. A., Y. Qi & S. R. Hann (2003) Phosphorylation by glycogen synthase kinase-3 controls c-myc proteolysis and subnuclear localization. *J Biol Chem,* 278**,** 51606-12.

Gutjahr, P., M. Schwenger, H. J. Spaar, J. Michaelis, D. Niethammer, H. Jurgens, J. Kuhl, R. Ludwig, J. Kutzner, D. Schmidt & et al. (1990) [The importance of preoperative chemotherapy and radiotherapy in 373 children with Wilms' tumor]. *Dtsch Med Wochenschr,* 115**,** 248-53.

Ha, T. C., F. Spreafico, N. Graf, S. Dallorso, J. S. Dome, M. Malogolowkin, R. Furtwangler, J. P. Hale, V. Moroz, D. Machin & K. Pritchard-Jones (2013) An international strategy to determine the role of high dose therapy in recurrent Wilms' tumour. *Eur J Cancer,* 49**,** 194-210.

Hargreaves, D. C. & G. R. Crabtree (2011) ATP-dependent chromatin remodeling: genetics, genomics and mechanisms. *Cell Res,* 21**,** 396-420.

Hatton, K. S., K. Mahon, L. Chin, F. C. Chiu, H. W. Lee, D. Peng, S. D. Morgenbesser, J. Horner & R. A. DePinho (1996) Expression and activity of L-Myc in normal mouse development. *Mol Cell Biol,* 16**,** 1794-804.

Hein, M. Y., N. C. Hubner, I. Poser, J. Cox, N. Nagaraj, Y. Toyoda, I. A. Gak, I. Weisswange, J. Mansfeld, F. Buchholz, A. A. Hyman & M. Mann (2015) A human interactome in three quantitative dimensions organized by stoichiometries and abundances. *Cell,* 163**,** 712-23.

Herbst, A., S. E. Salghetti, S. Y. Kim & W. P. Tansey (2004) Multiple cell-type-specific elements regulate Myc protein stability. *Oncogene,* 23**,** 3863-71.

Herold, S., J. Kalb, G. Buchel, C. P. Ade, A. Baluapuri, J. Xu, J. Koster, D. Solvie, A. Carstensen, C. Klotz, S. Rodewald, C. Schulein-Volk, M. Dobbelstein, E. Wolf, J. Molenaar, R. Versteeg, S. Walz & M. Eilers (2019) Recruitment of BRCA1 limits MYCN-driven accumulation of stalled RNA polymerase. *Nature,* 567**,** 545-549.

Hoffman, B. & D. A. Liebermann (2008) Apoptotic signaling by c-MYC. *Oncogene*, *27*(50), 6462–6472.

Hopewell, R. & E. B. Ziff (1995) The nerve growth factor-responsive PC12 cell line does not express the Myc dimerization partner Max. *Mol Cell Biol,* 15**,** 3470-8.

Horner, M. J., L. A. G. Ries, M. Krapcho, N. Neyman, R. Aminou, N. Howlander, S. F. Altekruse, E. J. Feuer, L. Huang, A. Mariotto, B. A. Miller, D. R. Lewis, M. P. Eisner, D. G. Stinchcomb & B. K. Edwards. 2009. SEER Cancer Statistics Review, 1975-2006. Based on November 2008 SEER data submission, posted to the SEER web site, 2009. In. National Cancer Institute. Bethesda, MD.

Houghton, P. J., C. L. Morton, C. Tucker, D. Payne, E. Favours, C. Cole, R. Gorlick, E. A. Kolb, W. Zhang, R. Lock, H. Carol, M. Tajbakhsh, C. P. Reynolds, J. M. Maris, J. Courtright, S. T. Keir, H. S. Friedman, C. Stopford, J. Zeidner, J. Wu, T. Liu, C. A. Billups, J. Khan, S. Ansher, J. Zhang & M. A. Smith (2007) The pediatric preclinical testing program: description of models and early testing results. *Pediatr Blood Cancer,* 49**,** 928-40.

Hu, Q., F. Gao, W. Tian, E. C. Ruteshouser, Y. Wang, A. Lazar, J. Stewart, L. C. Strong, R. R. Behringer & V. Huff (2011) Wt1 ablation and Igf2 upregulation in mice result in Wilms tumors with elevated ERK1/2 phosphorylation. *J Clin Invest,* 121**,** 174-83.

Huang, M. & W. A. Weiss (2013) Neuroblastoma and MYCN. *Cold Spring Harb Perspect Med,* 3**,** a014415.

Huang, Y., H. Friess, J. Kleeff, I. Esposito, Z. Zhu, S. Liu, S. C. Mok, A. Zimmermann & M. W. Buchler (2001) Doc-2/hDab2 expression is up-regulated in primary pancreatic cancer but reduced in metastasis. *Lab Invest,* 81**,** 863-73.

Huff, V. (1998) Wilms tumor genetics. *American Journal of Medical Genetics,* 79**,** 260-267.

Hui, L., S. Zhang, M. Wudu, H. Ren, Y. Xu, Q. Zhang & X. Qiu (2019) CBLL1 is highly expressed in non-small cell lung cancer and promotes cell proliferation and invasion. *Thorac Cancer,* 10**,** 1479-1488.

Humphrey, G. W., Y. H. Wang, T. Hirai, R. Padmanabhan, D. M. Panchision, L. F. Newell, R. D. McKay & B. H. Howard (2008) Complementary roles for histone deacetylases 1, 2, and 3 in differentiation of pluripotent stem cells. *Differentiation,* 76**,** 348-56.

Hunt, S. E., W. McLaren, L. Gil, A. Thormann, H. Schuilenburg, D. Sheppard, A. Parton, I. M. Armean, S. J. Trevanion, P. Flicek & F. Cunningham (2018) Ensembl variation resources. *Database (Oxford),* 2018.

Hwang, I. Y., J. S. Roe, J. H. Seol, H. R. Kim, E. J. Cho & H. D. Youn (2012) pVHL-mediated transcriptional repression of c-Myc by recruitment of histone deacetylases. *Mol Cells,* 33**,** 195-201.

Ip, W. K., P. B. Lai, N. L. Wong, S. M. Sy, B. Beheshti, J. A. Squire & N. Wong (2007) Identification of PEG10 as a progression related biomarker for hepatocellular carcinoma. *Cancer Lett,* 250**,** 284-91.

Izsvak, Z. & Z. Ivics (2004) Sleeping beauty transposition: biology and applications for molecular therapy. *Mol Ther,* 9**,** 147-56.

Izumi, H. & Y. Kaneko (2014) Trim32 facilitates degradation of MYCN on spindle poles and induces asymmetric cell division in human neuroblastoma cells. *Cancer Res,* 74**,** 5620-30.

Izumi, H., C. Molander, L. Z. Penn, A. Ishisaki, K. Kohno & K. Funa (2001) Mechanism for the transcriptional repression by c-Myc on PDGF beta-receptor. *J Cell Sci,* 114**,** 1533-44.

Jaenicke, L. A., B. von Eyss, A. Carstensen, E. Wolf, W. Xu, A. K. Greifenberg, M. Geyer, M. Eilers & N. Popov (2016) Ubiquitin-Dependent Turnover of MYC Antagonizes MYC/PAF1C Complex Accumulation to Drive Transcriptional Elongation. *Mol Cell,* 61**,** 54-67.

Kalkat, M., D. Resetca, C. Lourenco, P. K. Chan, Y. Wei, Y. J. Shiah, N. Vitkin, Y. Tong, M. Sunnerhagen, S. J. Done, P. C. Boutros, B. Raught & L. Z. Penn (2018) MYC Protein Interactome Profiling Reveals Functionally Distinct Regions that Cooperate to Drive Tumorigenesis. *Mol Cell,* 72**,** 836-848.e7.

Kato, G. J., J. Barrett, M. Villa-Garcia & C. V. Dang (1990) An amino-terminal c-myc domain required for neoplastic transformation activates transcription. *Mol Cell Biol,* 10**,** 5914-20.

Kato, G. J., D. S. Wechsler & C. V. Dang (1992) DNA binding by the Myc oncoproteins. *Cancer Treat Res,* 63**,** 313-25.

Kato, K., F. Miya, N. Hamada, Y. Negishi, Y. Narumi-Kishimoto, H. Ozawa, H. Ito, I. Hori, A. Hattori, N. Okamoto, M. Kato, T. Tsunoda, Y. Kanemura, K. Kosaki, Y. Takahashi, K. I. Nagata & S. Saitoh (2019) MYCN de novo gain-of-function mutation in a patient with a novel megalencephaly syndrome. *J Med Genet,* 56**,** 388-395.

Kearns, A. E., M. M. Donohue, B. Sanyal & M. B. Demay (2001) Cloning and characterization of a novel protein kinase that impairs osteoblast differentiation in vitro. *J Biol Chem,* 276**,** 42213-8.

Kleeff, J., Y. Huang, S. C. Mok, A. Zimmermann, H. Friess & M. W. Buchler (2002) Down-regulation of DOC-2 in colorectal cancer points to its role as a tumor suppressor in this malignancy. *Dis Colon Rectum,* 45**,** 1242-8.

Kocak, H., S. Ackermann, B. Hero, Y. Kahlert, A. Oberthuer, D. Juraeva, F. Roels, J. Theissen, F. Westermann, H. Deubzer, V. Ehemann, B. Brors, M. Odenthal, F. Berthold & M. Fischer (2013). Hox-C9 activates the intrinsic pathway of apoptosis and is associated with spontaneous regression in neuroblastoma. *Cell death & disease, 4(4), e586.*

Kohl, N. E., N. Kanda, R. R. Schreck, G. Bruns, S. A. Latt, F. Gilbert & F. W. Alt (1983) Transposition and amplification of oncogene-related sequences in human neuroblastomas. *Cell,* 35**,** 359-67.

Kouzine, F., D. Levens & L. Baranello (2014) DNA topology and transcription. *Nucleus,* 5**,** 195-202.

Kumar, G. (2018) Principle and Method of Silver Staining of Proteins Separated by Sodium Dodecyl Sulfate-Polyacrylamide Gel Electrophoresis. *Methods Mol Biol,* 1853**,** 231-236.

Kumar, P., S. Henikoff & P. C. Ng (2009) Predicting the effects of coding non-synonymous variants on protein function using the SIFT algorithm. *Nat Protoc,* 4**,** 1073-81.

Kurland, J. F. & W. P. Tansey (2008) Myc-mediated transcriptional repression by recruitment of histone deacetylase. *Cancer Res,* 68**,** 3624-9.

Lange, J., S. M. Peterson, J. R. Takashima, Y. Grigoriev, M. L. Ritchey, R. C. Shamberger, J. B. Beckwith, E. Perlman, D. M. Green & N. E. Breslow (2011) Risk factors for end stage renal disease in non-WT1-syndromic Wilms tumor. *J Urol,* 186**,** 378-86.

Laurenti, E., A. Wilson & A. Trumpp (2009) Myc's other life: stem cells and beyond. *Curr Opin Cell Biol,* 21**,** 844-54.

Lee, L. A., C. Dolde, J. Barrett, C. S. Wu & C. V. Dang (1996) A link between c-Myc-mediated transcriptional repression and neoplastic transformation. *J Clin Invest,* 97**,** 1687-95.

Li, C. M., A. A. Margolin, M. Salas, L. Memeo, M. Mansukhani, H. Hibshoosh, M. Szabolcs, A. Klinakis & B. Tycko (2006) PEG10 is a c-MYC target gene in cancer cells. *Cancer Res,* 66**,** 665-72.

Li, H., T. H. Lee & H. Avraham (2002) A novel tricomplex of BRCA1, Nmi, and c-Myc inhibits c-Myc-induced human telomerase reverse transcriptase gene (hTERT) promoter activity in breast cancer. *J Biol Chem,* 277**,** 20965-73.

Li, X., W. Wang, J. Wang, A. Malovannaya, Y. Xi, W. Li, R. Guerra, D. H. Hawke, J. Qin & J. Chen (2015) Proteomic analyses reveal distinct chromatin-associated and soluble transcription factor complexes. *Mol Syst Biol,* 11**,** 775.

Li, X., W. Wang, Y. Xi, M. Gao, M. Tran, K. E. Aziz, J. Qin, W. Li & J. Chen (2016) FOXR2 Interacts with MYC to Promote Its Transcriptional Activities and Tumorigenesis. *Cell Rep,* 16**,** 487-497.

Liu, M., K. Zhou, Y. Huang & Y. Cao (2015) The candidate oncogene (MCRS1) promotes the growth of human lung cancer cells via the miR-155-Rb1 pathway. *J Exp Clin Cancer Res,* 34**,** 121.

Liu, P. Y., D. Erriquez, G. M. Marshall, A. E. Tee, P. Polly, M. Wong, B. Liu, J. L. Bell, X. D. Zhang, G. Milazzo, B. B. Cheung, A. Fox, A. Swarbrick, S. Huttelmaier, M. Kavallaris, G. Perini, J. S. Mattick, M. E. Dinger & T. Liu (2014) Effects of a novel long noncoding RNA, lncUSMycN, on N-Myc expression and neuroblastoma progression. *J Natl Cancer Inst,* 106.

Liu, T., A. E. Tee, A. Porro, S. A. Smith, T. Dwarte, P. Y. Liu, N. Iraci, E. Sekyere, M. Haber, M. D. Norris, D. Diolaiti, G. Della Valle, G. Perini & G. M. Marshall (2007) Activation of tissue transglutaminase transcription by histone deacetylase inhibition as a therapeutic approach for Myc oncogenesis. *Proc Natl Acad Sci U S A,* 104**,** 18682-7.

Liu, X., J. Tesfai, Y. A. Evrard, S. Y. Dent & E. Martinez (2003) c-Myc transformation domain recruits the human STAGA complex and requires TRRAP and GCN5 acetylase activity for transcription activation. *J Biol Chem,* 278**,** 20405-12.

Liu, X., M. Vorontchikhina, Y. L. Wang, F. Faiola & E. Martinez (2008) STAGA recruits Mediator to the MYC oncoprotein to stimulate transcription and cell proliferation. *Mol Cell Biol,* 28**,** 108-21.

Liu, Y., W. Ding, H. Ge, M. Ponnusamy, Q. Wang, X. Hao, W. Wu, Y. Zhang, W. Yu, X. Ao & J. Wang (2019) FOXK transcription factors: Regulation and critical role in cancer. *Cancer Letters,* 458**,** 1-12.

Malogolowkin, M., C. A. Cotton, D. M. Green, N. E. Breslow, E. Perlman, J. Miser, M. L. Ritchey, P. R. Thomas, P. E. Grundy, G. J. D'Angio, J. B. Beckwith, R. C. Shamberger, G. M. Haase, M. Donaldson, R. Weetman, M. J. Coppes, P. Shearer, P. Coccia, M. Kletzel, R. Macklis, G. Tomlinson, V. Huff, R. Newbury & D. Weeks (2008) Treatment of Wilms tumor relapsing after initial treatment with vincristine, actinomycin D, and doxorubicin. A report from the National Wilms Tumor Study Group. *Pediatr Blood Cancer,* 50**,** 236-41.

Malynn, B. A., I. M. de Alboran, R. C. O'Hagan, R. Bronson, L. Davidson, R. A. DePinho & F. W. Alt (2000) N-myc can functionally replace c-myc in murine development, cellular growth, and differentiation. *Genes Dev,* 14**,** 1390-9.

Marshall, G. M., S. Gherardi, N. Xu, Z. Neiron, T. Trahair, C. J. Scarlett, D. K. Chang, P. Y. Liu, K. Jankowski, N. Iraci, M. Haber, M. D. Norris, J. Keating, E. Sekyere, G. Jonquieres, F. Stossi, B. S. Katzenellenbogen, A. V. Biankin, G. Perini & T. Liu (2010) Transcriptional upregulation of histone deacetylase 2 promotes Myc-induced oncogenic effects. *Oncogene,* 29**,** 5957-68.

Matsunaga, E. (1981) Genetics of Wilms' tumor. *Hum Genet,* 57**,** 231-46.

Matsushima, H. & E. Bogenmann (1993) Expression of trkA cDNA in neuroblastomas mediates differentiation in vitro and in vivo. *Mol Cell Biol,* 13**,** 7447-56.

McMahon, S. B., H. A. Van Buskirk, K. A. Dugan, T. D. Copeland & M. D. Cole (1998) The novel ATM-related protein TRRAP is an essential cofactor for the c-Myc and E2F oncoproteins. *Cell,* 94**,** 363-74.

McMahon, S. B., Wood, M. A., & Cole, M. D. (2000). The essential cofactor TRRAP recruits the histone acetyltransferase hGCN5 to c-Myc. *Molecular and cellular biology*, 20(2), 556–562.

McQuaid, S. & A. O'Meara (1990) N-myc oncogene amplification in paediatric tumours. *Ir J Med Sci,* 159**,** 172-4.

Mercado-Matos, J., J. Janusis, S. Zhu, S. S. Chen & L. M. Shaw (2018) Identification of a Novel Invasion-Promoting Region in Insulin Receptor Substrate 2. *Mol Cell Biol,* 38.

Metzger, M. L. & J. S. Dome (2005) Current therapy for Wilms' tumor. *Oncologist,* 10**,** 815-26.

Mi, W., H. Guan, J. Lyu, D. Zhao, Y. Xi, S. Jiang, F. H. Andrews, X. Wang, M. Gagea, H. Wen, L. Tora, S. Y. R. Dent, T. G. Kutateladze, W. Li, H. Li & X. Shi (2017) YEATS2 links histone acetylation to tumorigenesis of non-small cell lung cancer. *Nat Commun,* 8**,** 1088.

Mok, S. C., K. K. Wong, R. K. Chan, C. C. Lau, S. W. Tsao, R. C. Knapp & R. S. Berkowitz (1994) Molecular cloning of differentially expressed genes in human epithelial ovarian cancer. *Gynecol Oncol,* 52**,** 247-52.

Morris, S. M., S. D. Arden, R. C. Roberts, J. Kendrick-Jones, J. A. Cooper, J. P. Luzio & F. Buss (2002) Myosin VI binds to and localises with Dab2, potentially linking receptor-mediated endocytosis and the actin cytoskeleton. *Traffic,* 3**,** 331-41.

Mugrauer, G., F. W. Alt & P. Ekblom (1988) N-myc proto-oncogene expression during organogenesis in the developing mouse as revealed by in situ hybridization. *J Cell Biol,* 107**,** 1325-35.

Mugrauer, G. & P. Ekblom (1991) Contrasting expression patterns of three members of the myc family of protooncogenes in the developing and adult mouse kidney. *J Cell Biol,* 112**,** 13-25.

Nakata, K., Y. Ito, W. Magadi, A. Bonaventure, C. A. Stiller, K. Katanoda, T. Matsuda, I. Miyashiro, K. Pritchard-Jones & B. Rachet (2018) Childhood cancer incidence and survival in Japan and England: A population-based study (1993-2010). *Cancer Sci,* 109**,** 422-434.

Nau, M. M., B. J. Brooks, J. Battey, E. Sausville, A. F. Gazdar, I. R. Kirsch, O. W. McBride, V. Bertness, G. F. Hollis & J. D. Minna (1985) L-myc, a new myc-related gene amplified and expressed in human small cell lung cancer. *Nature,* 318**,** 69-73.

Norris, M. D., M. J. Brian, M. R. Vowels & B. W. Stewart (1988) N-myc amplification in Wilms' tumor. *Cancer Genet Cytogenet,* 30**,** 187-9.

Orphanides, G., T. Lagrange & D. Reinberg (1996) The general transcription factors of RNA polymerase II. *Genes Dev,* 10**,** 2657-83.

Otto, T., S. Horn, M. Brockmann, U. Eilers, L. Schuttrumpf, N. Popov, A. M. Kenney, J. H. Schulte, R. Beijersbergen, H. Christiansen, B. Berwanger & M. Eilers (2009) Stabilization of N-Myc is a critical function of Aurora A in human neuroblastoma. *Cancer Cell,* 15**,** 67-78.

Oughtred, R., C. Stark, B. J. Breitkreutz, J. Rust, L. Boucher, C. Chang, N. Kolas, L. O'Donnell, G. Leung, R. McAdam, F. Zhang, S. Dolma, A. Willems, J. Coulombe-Huntington, A. Chatr-Aryamontri, K. Dolinski & M. Tyers (2019) The BioGRID interaction database: 2019 update. *Nucleic Acids Res,* 47**,** D529-d541.

Parisi, F., S. Riccardo, M. Daniel, M. Saqcena, N. Kundu, A. Pession, D. Grifoni, H. Stocker, E. Tabak & P. Bellosta (2011) Drosophila insulin and target of rapamycin (TOR) pathways regulate GSK3 beta activity to control Myc stability and determine Myc expression in vivo. *BMC Biol,* 9**,** 65.

Perez-Riverol, Y., Csordas, A., Bai, J., Bernal-Llinares, M., Hewapathirana, S., Kundu, D. J., Inuganti, A., Griss, J., Mayer, G., Eisenacher, M., Pérez, E., Uszkoreit, J., Pfeuffer, J., Sachsenberg, T., Yilmaz, S., Tiwary, S., Cox, J., Audain, E., Walzer, M., Jarnuczak, A. F., … Vizcaíno, J. A. (2019). The PRIDE database and related tools and resources in 2019: improving support for quantification data. *Nucleic acids research, 47(D1), D442–D450.*

Perini, G., D. Diolaiti, A. Porro, & G. Della Valle (2005) In vivo transcriptional regulation of N-Myc target genes is controlled by E-box methylation. Proceedings of the National Academy of Sciences of the United States of America, 102(34), 12117–12122.

Perotti, D., F. Spreafico, F. Torri, B. Gamba, P. D'Adamo, S. Pizzamiglio, M. Terenziani, S. Catania, P. Collini, M. Nantron, A. Pession, M. Bianchi, P. Indolfi, P. D'Angelo, F. Fossati-Bellani, P. Verderio, F. Macciardi & P. Radice (2012) Genomic profiling by whole-genome single nucleotide polymorphism arrays in Wilms tumor and association with relapse. *Genes Chromosomes Cancer,* 51**,** 644-53.

Peter, S., J. Bultinck, K. Myant, L. A. Jaenicke, S. Walz, J. Muller, M. Gmachl, M. Treu, G. Boehmelt, C. P. Ade, W. Schmitz, A. Wiegering, C. Otto, N. Popov, O. Sansom, N. Kraut & M. Eilers

(2014) Tumor cell-specific inhibition of MYC function using small molecule inhibitors of the HUWE1 ubiquitin ligase. *EMBO Mol Med, 6***,** 1525-41.

Peukert, K., P. Staller, A. Schneider, G. Carmichael, F. Hanel & M. Eilers (1997) An alternative pathway for gene regulation by Myc. *Embo j,* 16**,** 5672-86.

Phillips, S. E. (1994) Built by association: structure and function of helix-loop-helix DNA-binding proteins. *Structure,* 2**,** 1-4.

Pode-Shakked, N., R. Shukrun, M. Mark-Danieli, P. Tsvetkov, S. Bahar, S. Pri-Chen, R. S. Goldstein, E. Rom-Gross, Y. Mor, E. Fridman, K. Meir, A. Simon, M. Magister, N. Kaminski, V. S. Goldmacher, O. Harari-Steinberg & B. Dekel (2013) The isolation and characterization of renal cancer initiating cells from human Wilms' tumour xenografts unveils new therapeutic targets. *EMBO Mol Med,* 5**,** 18-37.

Poole, C. J. & J. van Riggelen (2017) MYC-Master Regulator of the Cancer Epigenome and Transcriptome. *Genes (Basel),* 8.

Popov, N., C. Schulein, L. A. Jaenicke & M. Eilers (2010) Ubiquitylation of the amino terminus of Myc by SCF(beta-TrCP) antagonizes SCF(Fbw7)-mediated turnover. *Nat Cell Biol,* 12**,** 973-81.

Popov, N., M. Wanzel, M. Madiredjo, D. Zhang, R. Beijersbergen, R. Bernards, R. Moll, S. J. Elledge & M. Eilers (2007) The ubiquitin-specific protease USP28 is required for MYC stability. *Nat Cell Biol,* 9**,** 765-74.

Rakheja, D., K. S. Chen, Y. Liu, A. A. Shukla, V. Schmid, T. C. Chang, S. Khokhar, J. E. Wickiser, N. J. Karandikar, J. S. Malter, J. T. Mendell & J. F. Amatruda (2014) Somatic mutations in DROSHA and DICER1 impair microRNA biogenesis through distinct mechanisms in Wilms tumours. *Nat Commun,* 2**,** 4802.

Ramasamy, S., B. Saez, S. Mukhopadhyay, D. Ding, A. M. Ahmed, X. Chen, F. Pucci, R. Yamin, J. Wang, M. J. Pittet, C. M. Kelleher, D. T. Scadden & D. A. Sweetser (2016) Tle1 tumor suppressor negatively regulates inflammation in vivo and modulates NF-κB inflammatory pathway. *Proc Natl Acad Sci U S A,* 113**,** 1871-6.

Rao, R. A., N. Dhele, S. Cheemadan, A. Ketkar, G. R. Jayandharan, D. Palakodeti & S. Rampalli (2015) Ezh2 mediated H3K27me3 activity facilitates somatic transition during human pluripotent reprogramming. *Sci Rep,* 5**,** 8229.

Richards, M. W., S. G. Burgess, E. Poon, A. Carstensen, M. Eilers, L. Chesler & R. Bayliss (2016) Structural basis of N-Myc binding by Aurora-A and its destabilization by kinase inhibitors. *Proc Natl Acad Sci U S A,* 113**,** 13726-13731.

Richart, L., E. Carrillo-de Santa Pau, A. Rio-Machin, M. P. de Andres, J. C. Cigudosa, V. J. S. Lobo & F. X. Real (2016) BPTF is required for c-MYC transcriptional activity and in vivo tumorigenesis. *Nat Commun,* 7**,** 10153.

Rickman, D. S., J. H. Schulte & M. Eilers (2018) The Expanding World of N-MYC-Driven Tumors. *Cancer Discov,* 8**,** 150-163.

Romero, O. A., M. Torres-Diz, E. Pros, S. Savola, A. Gomez, S. Moran, C. Saez, R. Iwakawa, A. Villanueva, L. M. Montuenga, T. Kohno, J. Yokota & M. Sanchez-Cespedes (2014) MAX inactivation in small cell lung cancer disrupts MYC-SWI/SNF programs and is synthetic lethal with BRG1. *Cancer Discov,* 4**,** 292-303.

Rosenbauer, F., A. Kallies, M. Scheller, K. P. Knobeloch, C. O. Rock, M. Schwieger, C. Stocking & I. Horak (2002) Disabled-2 is transcriptionally regulated by ICSBP and augments macrophage spreading and adhesion. *Embo j,* 21**,** 211-20.

Royer-Pokora, B., M. Busch, M. Beier, C. Duhme, C. de Torres, J. Mora, A. Brandt & H. D. Royer (2010) Wilms tumor cells with WT1 mutations have characteristic features of mesenchymal stem cells and express molecular markers of paraxial mesoderm. *Hum Mol Genet,* 19**,** 1651-68.

Ruteshouser, E. C., S. M. Robinson & V. Huff (2008) Wilms tumor genetics: mutations in WT1, WTX, and CTNNB1 account for only about one-third of tumors. *Genes Chromosomes Cancer,* 47**,** 461-70.

Sadak, K. T., M. L. Ritchey & J. S. Dome (2013) Paediatric genitourinary cancers and late effects of treatment. *Nat Rev Urol,* 10**,** 15-25.

Sakamuro, D. & G. C. Prendergast (1999) New Myc-interacting proteins: a second Myc network emerges. *Oncogene,* 18**,** 2942-54.

Satou, A., T. Taira, S. M. Iguchi-Ariga & H. Ariga (2001) A novel transrepression pathway of c-Myc. Recruitment of a transcriptional corepressor complex to c-Myc by MM-1, a c-Myc-binding protein. *J Biol Chem,* 276**,** 46562-7.

Schaub, R., A. Burger, D. Bausch, F. K. Niggli, B. W. Schafer & D. R. Betts (2007) Array comparative genomic hybridization reveals unbalanced gain of the MYCN region in Wilms tumors. *Cancer Genet Cytogenet,* 172**,** 61-5.

Schmid, P., W. A. Schulz & H. Hameister (1989) Dynamic expression pattern of the myc protooncogene in midgestation mouse embryos. *Science,* 243**,** 226-9.

Schneider-Poetsch, T., Ju, J., Eyler, D. E., Dang, Y., Bhat, S., Merrick, W. C., Green, R., Shen, B., & Liu, J. O. (2010). Inhibition of eukaryotic translation elongation by cycloheximide and lactimidomycin. *Nature chemical biology*, *6*(3), 209–217.

Scott, R. H., Murray, A., Baskcomb, L., Turnbull, C., Loveday, C., Al-Saadi, R., Williams, R., Breatnach, F., Gerrard, M., Hale, J., Kohler, J., Lapunzina, P., Levitt, G. A., Picton, S., Pizer, B., Ronghe, M. D., Traunecker, H., Williams, D., Kelsey, A., Vujanic, G. M., … Rahman, N. (2012). Stratification of Wilms tumor by genetic and epigenetic analysis. Oncotarget, 3(3), 327–335.

Segers, H., M. M. van den Heuvel-Eibrink, R. D. Williams, H. van Tinteren, G. Vujanic, R. Pieters, K. Pritchard-Jones & N. Bown (2013) Gain of 1q is a marker of poor prognosis in Wilms' tumors. *Genes Chromosomes Cancer,* 52**,** 1065-74.

Shams, R., H. Asadzadeh Aghdaei, A. Behmanesh, A. Sadeghi, M. Zali, S. Salari & J. M. Padron (2020) MicroRNAs Targeting MYC Expression: Trace of Hope for Pancreatic Cancer Therapy. A Systematic Review. *Cancer Manag Res,* 12**,** 2393-2404.

Shandilya, J. & S. G. Roberts (2012) The transcription cycle in eukaryotes: from productive initiation to RNA polymerase II recycling. *Biochim Biophys Acta,* 1819**,** 391-400.

Sheiness, D. & J. M. Bishop (1979) DNA and RNA from uninfected vertebrate cells contain nucleotide sequences related to the putative transforming gene of avian myelocytomatosis virus. *J Virol,* 31**,** 514-21.

Shi, X., A. M. Wallis, R. D. Gerard, K. A. Voelker, R. W. Grange, R. A. DePinho, M. G. Garry & D. J. Garry (2012) Foxk1 promotes cell proliferation and represses myogenic differentiation by regulating Foxo4 and Mef2. *J Cell Sci,* 125**,** 5329-37.

Shi, Y. J., C. Matson, F. Lan, S. Iwase, T. Baba & Y. Shi (2005) Regulation of LSD1 histone demethylase activity by its associated factors. *Mol Cell,* 19**,** 857-64.

Shihab, H. A., J. Gough, D. N. Cooper, P. D. Stenson, G. L. Barker, K. J. Edwards, I. N. Day & T. R. Gaunt (2013) Predicting the functional, molecular, and phenotypic consequences of amino acid substitutions using hidden Markov models. *Hum Mutat,* 34**,** 57-65.

Shrivastava, A., J. Yu, S. Artandi & K. Calame (1996) YY1 and c-Myc associate in vivo in a manner that depends on c-Myc levels. *Proc Natl Acad Sci U S A,* 93**,** 10638-41.

Sjostrom, S. K., G. Finn, W. C. Hahn, D. H. Rowitch & A. M. Kenney (2005) The Cdk1 complex plays a prime role in regulating N-myc phosphorylation and turnover in neural precursors. *Dev Cell,* 9**,** 327-38.

Soucek, L., M. Helmer-Citterich, A. Sacco, R. Jucker, G. Cesareni & S. Nasi (1998) Design and properties of a Myc derivative that efficiently homodimerizes. *Oncogene,* 17**,** 2463-72.

Spreafico, F., K. Pritchard Jones, M. H. Malogolowkin, C. Bergeron, J. Hale, J. de Kraker, S. Dallorso, T. Acha, B. de Camargo, J. S. Dome & N. Graf (2009) Treatment of relapsed Wilms tumors: lessons learned. *Expert Rev Anticancer Ther,* 9**,** 1807-15.

Staller, P., K. Peukert, A. Kiermaier, J. Seoane, J. Lukas, H. Karsunky, T. Moroy, J. Bartek, J. Massague, F. Hanel & M. Eilers (2001) Repression of p15INK4b expression by Myc through association with Miz-1. *Nat Cell Biol,* 3**,** 392-9.

Stelzer, G., N. Rosen, I. Plaschkes, S. Zimmerman, M. Twik, S. Fishilevich, T. I. Stein, R. Nudel, I. Lieder, Y. Mazor, S. Kaplan, D. Dahary, D. Warshawsky, Y. Guan-Golan, A. Kohn, N. Rappaport, M. Safran & D. Lancet (2016) The GeneCards Suite: From Gene Data Mining to Disease Genome Sequence Analyses. *Curr Protoc Bioinformatics,* 54**,** 1.30.1-1.30.33.

Strieder, V. & W. Lutz (2003) E2F proteins regulate MYCN expression in neuroblastomas. *J Biol Chem,* 278**,** 2983-9.

Sukonina, V., H. Ma, W. Zhang, S. Bartesaghi, S. Subhash, M. Heglind, H. Foyn, M. J. Betz, D. Nilsson, M. E. Lidell, J. Naumann, S. Haufs-Brusberg, H. Palmgren, T. Mondal, M. Beg, M. P. Jedrychowski, K. Tasken, A. Pfeifer, X. R. Peng, C. Kanduri & S. Enerback (2019) FOXK1 and FOXK2 regulate aerobic glycolysis. *Nature,* 566**,** 279-283.

Tansey, W. P. (2014) Mammalian MYC Proteins and Cancer. *New Journal of Science,* 2014**,** 27.

Tate, J. G., Bamford, S., Jubb, H. C., Sondka, Z., Beare, D. M., Bindal, N., Boutselakis, H., Cole, C. G., Creatore, C., Dawson, E., Fish, P., Harsha, B., Hathaway, C., Jupe, S. C., Kok, C. Y., Noble, K., Ponting, L., Ramshaw, C. C., Rye, C. E., Speedy, H. E., … Forbes, S. A. (2019). COSMIC: the Catalogue Of Somatic Mutations In Cancer. *Nucleic acids research*, 47(D1), D941–D947.

Tavana, O., D. Li, C. Dai, G. Lopez, D. Banerjee, N. Kon, C. Chen, A. Califano, D. J. Yamashiro, H. Sun & W. Gu (2016) HAUSP deubiquitinates and stabilizes N-Myc in neuroblastoma. *Nat Med,* 22**,** 1180-1186.

Torrezan, G. T., E. N. Ferreira, A. M. Nakahata, B. D. Barros, M. T. Castro, B. R. Correa, A. C. Krepischi, E. H. Olivieri, I. W. Cunha, U. Tabori, P. E. Grundy, C. M. Costa, B. de Camargo, P. A. Galante & D. M. Carraro (2014) Recurrent somatic mutation in DROSHA induces microRNA profile changes in Wilms tumour. *Nat Commun,* 5**,** 4039.

Treger, T. D., T. Chowdhury, K. Pritchard-Jones & S. Behjati (2019) The genetic changes of Wilms tumour. *Nat Rev Nephrol,* 15**,** 240-251.

Tseng, C. P., C. H. Huang, C. C. Tseng, M. H. Lin, J. T. Hsieh & C. H. Tseng (2001) Induction of disabled-2 gene during megakaryocyte differentiation of k562 cells. *Biochem Biophys Res Commun,* 285**,** 129-35.

Tu, W. B., S. Helander, R. Pilstal, K. A. Hickman, C. Lourenco, I. Jurisica, B. Raught, B. Wallner, M. Sunnerhagen & L. Z. Penn (2015) Myc and its interactors take shape. *Biochim Biophys Acta,* 1849**,** 469-83.

Urbach, A., A. Yermalovich, J. Zhang, C. S. Spina, H. Zhu, A. R. Perez-Atayde, R. Shukrun, J. Charlton, N. Sebire, W. Mifsud, B. Dekel, K. Pritchard-Jones & G. Q. Daley (2014) Lin28 sustains early renal progenitors and induces Wilms tumor. *Genes Dev,* 28**,** 971-82.

van de Wetering, M., E. Sancho, C. Verweij, W. de Lau, I. Oving, A. Hurlstone, K. van der Horn, E. Batlle, D. Coudreuse, A. P. Haramis, M. Tjon-Pon-Fong, P. Moerer, M. van den Born, G. Soete, S. Pals, M. Eilers, R. Medema & H. Clevers (2002) The beta-catenin/TCF-4 complex imposes a crypt progenitor phenotype on colorectal cancer cells. *Cell,* 111**,** 241-50.

van den Heuvel-Eibrink, M. M., J. A. Hol, K. Pritchard-Jones, H. van Tinteren, R. Furtwangler, A. C. Verschuur, G. M. Vujanic, I. Leuschner, J. Brok, C. Rube, A. M. Smets, G. O. Janssens, J. Godzinski, G. L. Ramirez-Villar, B. de Camargo, H. Segers, P. Collini, M. Gessler, C. Bergeron, F. Spreafico & N. Graf (2017) Position paper: Rationale for the treatment of Wilms tumour in the UMBRELLA SIOP-RTSG 2016 protocol. *Nat Rev Urol,* 14**,** 743-752.

van Riggelen, J., A. Yetil & D. W. Felsher (2010) MYC as a regulator of ribosome biogenesis and protein synthesis. *Nat Rev Cancer,* 10**,** 301-9.

Varan, A. (2008) Wilms' tumor in children: an overview. *Nephron Clin Pract,* 108**,** c83-90.

Vennstrom, B., D. Sheiness, J. Zabielski & J. M. Bishop (1982) Isolation and characterization of c-myc, a cellular homolog of the oncogene (v-myc) of avian myelocytomatosis virus strain 29. *J Virol,* 42**,** 773-9.

Vujanic, G. M., M. Gessler, A. Ooms, P. Collini, A. Coulomb-l'Hermine, E. D'Hooghe, R. R. de Krijger, D. Perotti, K. Pritchard-Jones, C. Vokuhl, M. M. van den Heuvel-Eibrink & N. Graf

(2018) The UMBRELLA SIOP-RTSG 2016 Wilms tumour pathology and molecular biology protocol. *Nat Rev Urol,* 15**,** 693-701.

Vujanic, G. M., B. Sandstedt, D. Harms, A. Kelsey, I. Leuschner & J. de Kraker (2002) Revised International Society of Paediatric Oncology (SIOP) working classification of renal tumors of childhood. *Med Pediatr Oncol,* 38**,** 79-82.

Walker, C. J., C. M. Rush, P. Dama, M. J. O'Hern, C. M. Cosgrove, J. L. Gillespie, R. A. Zingarelli, B. Smith, M. E. Stein, D. G. Mutch, R. Shakya, C. W. Chang, K. Selvendiran, J. W. Song, D. E. Cohn & P. J. Goodfellow (2018) MAX Mutations in Endometrial Cancer: Clinicopathologic Associations and Recurrent MAX p.His28Arg Functional Characterization. *J Natl Cancer Inst,* 110**,** 517-526.

Walz, A. L., A. Ooms, S. Gadd, D. S. Gerhard, M. A. Smith, J. M. Guidry Auvil, D. Meerzaman, Q. R. Chen, C. H. Hsu, C. Yan, C. Nguyen, Y. Hu, R. Bowlby, D. Brooks, Y. Ma, A. J. Mungall, R. A. Moore, J. Schein, M. A. Marra, V. Huff, J. S. Dome, Y. Y. Chi, C. G. Mullighan, J. Ma, D. A. Wheeler, O. A. Hampton, N. Jafari, N. Ross, J. M. Gastier-Foster & E. J. Perlman (2015) Recurrent DGCR8, DROSHA, and SIX homeodomain mutations in favorable histology Wilms tumors. *Cancer Cell,* 27**,** 286-97.

Walz, S., F. Lorenzin, J. Morton, K. E. Wiese, B. von Eyss, S. Herold, L. Rycak, H. Dumay-Odelot, S. Karim, M. Bartkuhn, F. Roels, T. Wustefeld, M. Fischer, M. Teichmann, L. Zender, C. L. Wei, O. Sansom, E. Wolf & M. Eilers (2014) Activation and repression by oncogenic MYC shape tumour-specific gene expression profiles. *Nature,* 511**,** 483-7.

Wang, D., H. Hashimoto, X. Zhang, B. G. Barwick, S. Lonial, L. H. Boise, P. M. Vertino & X. Cheng (2017) MAX is an epigenetic sensor of 5-carboxylcytosine and is altered in multiple myeloma. *Nucleic Acids Res,* 45**,** 2396-2407.

Wang, Q., H. Zhang, K. Kajino & M. I. Greene (1998) BRCA1 binds c-Myc and inhibits its transcriptional and transforming activity in cells. *Oncogene,* 17**,** 1939-48.

Wang, W., X. Li, M. Lee, S. Jun, K. E. Aziz, L. Feng, M. K. Tran, N. Li, P. D. McCrea, J. I. Park & J. Chen (2015) FOXKs promote Wnt/β-catenin signaling by translocating DVL into the nucleus. *Dev Cell,* 32**,** 707-18.

Wang, Y. L., F. Faiola, M. Xu, S. Pan & E. Martinez (2008) Human ATAC Is a GCN5/PCAF-containing acetylase complex with a novel NC2-like histone fold module that interacts with the TATA-binding protein. *J Biol Chem,* 283**,** 33808-15.

Wanzel, M., S. Herold & M. Eilers (2003) Transcriptional repression by Myc. *Trends Cell Biol,* 13**,** 146-50.

Wegert, J., S. Bausenwein, S. Roth, N. Graf, E. Geissinger & M. Gessler (2012) Characterization of primary Wilms tumor cultures as an in vitro model. *Genes Chromosomes Cancer,* 51**,** 92-104.

Wegert, J., N. Ishaque, R. Vardapour, C. Georg, Z. Gu, M. Bieg, B. Ziegler, S. Bausenwein, N. Nourkami, N. Ludwig, A. Keller, C. Grimm, S. Kneitz, R. D. Williams, T. Chagtai, K. Pritchard-Jones, P. van Sluis, R. Volckmann, J. Koster, R. Versteeg, T. Acha, M. J. O'Sullivan, P. K. Bode, F. Niggli, G. A. Tytgat, H. van Tinteren, M. M. van den Heuvel-Eibrink, E. Meese, C. Vokuhl, I. Leuschner, N. Graf, R. Eils, S. M. Pfister, M. Kool & M. Gessler (2015) Mutations in the SIX1/2 pathway and the DROSHA/DGCR8 miRNA microprocessor complex underlie high-risk blastemal type Wilms tumors. *Cancer Cell,* 27**,** 298-311.

Wegert, J., L. Zauter, S. Appenzeller, C. Otto, S. Bausenwein, C. Vokuhl, K. Ernestus, R. Furtwangler, N. Graf & M. Gessler (2020) High-risk blastemal Wilms tumor can be modeled by 3D spheroid cultures in vitro. *Oncogene,* 39**,** 849-861.

Weirich, A., I. Leuschner, D. Harms, G. M. Vujanic, J. Troger, U. Abel, N. Graf, D. Schmidt, R. Ludwig & P. A. Voute (2001) Clinical impact of histologic subtypes in localized non-anaplastic nephroblastoma treated according to the trial and study SIOP-9/GPOH. *Ann Oncol,* 12**,** 311-9.

Weirich, A., R. Ludwig, N. Graf, U. Abel, I. Leuschner, G. M. Vujanic, O. Mehls, J. Boos, J. Beck, B. Royer-Pokora & P. A. Voute (2004) Survival in nephroblastoma treated according to the trial and study SIOP-9/GPOH with respect to relapse and morbidity. *Ann Oncol,* 15**,** 808-20.

Weiss, W. A., K. Aldape, G. Mohapatra, B. G. Feuerstein & J. M. Bishop (1997) Targeted expression of MYCN causes neuroblastoma in transgenic mice. *Embo j,* 16**,** 2985-95.

Williams, R. D., R. Al-Saadi, T. Chagtai, S. Popov, B. Messahel, N. Sebire, M. Gessler, J. Wegert, N. Graf, I. Leuschner, M. Hubank, C. Jones, G. Vujanic & K. Pritchard-Jones (2010) Subtype-specific FBXW7 mutation and MYCN copy number gain in Wilms' tumor. *Clin Cancer Res,* 16**,** 2036-45.

Williams, R. D., R. Al-Saadi, R. Natrajan, A. Mackay, T. Chagtai, S. Little, S. N. Hing, K. Fenwick, A. Ashworth, P. Grundy, J. R. Anderson, J. S. Dome, E. J. Perlman, C. Jones & K. Pritchard-Jones (2011) Molecular profiling reveals frequent gain of MYCN and anaplasia-specific loss of 4q and 14q in Wilms tumor. *Genes Chromosomes Cancer,* 50**,** 982-95.

Williams, R. D., T. Chagtai, M. Alcaide-German, J. Apps, J. Wegert, S. Popov, G. Vujanic, H. van Tinteren, M. M. van den Heuvel-Eibrink, M. Kool, J. de Kraker, D. Gisselsson, N. Graf, M. Gessler & K. Pritchard-Jones (2015) Multiple mechanisms of MYCN dysregulation in Wilms tumour. *Oncotarget,* 6**,** 7232-43.

Wittmann, S., C. Wunder, B. Zirn, R. Furtwängler, J. Wegert, N. Graf & M. Gessler (2008) New prognostic markers revealed by evaluation of genes correlated with clinical parameters in Wilms tumors. *Genes, chromosomes & cancer, 47(5), 386–395.*

Wong, M., A. E. L. Tee, G. Milazzo, J. L. Bell, R. C. Poulos, B. Atmadibrata, Y. Sun, D. Jing, N. Ho, D. Ling, P. Y. Liu, X. D. Zhang, S. Huttelmaier, J. W. H. Wong, J. Wang, P. Polly, G. Perini, C. J. Scarlett & T. Liu (2017) The Histone Methyltransferase DOT1L Promotes Neuroblastoma by Regulating Gene Transcription. *Cancer Res,* 77**,** 2522-2533.

Wong, P. P., F. Miranda, K. V. Chan, C. Berlato, H. C. Hurst & A. G. Scibetta (2012) Histone demethylase KDM5B collaborates with TFAP2C and Myc to repress the cell cycle inhibitor p21(cip) (CDKN1A). *Mol Cell Biol,* 32**,** 1633-44.

Wood, M. A., S. B. McMahon & M. D. Cole (2000) An ATPase/helicase complex is an essential cofactor for oncogenic transformation by c-Myc. *Mol Cell,* 5**,** 321-30.

Wu, S., C. Cetinkaya, M. J. Munoz-Alonso, N. von der Lehr, F. Bahram, V. Beuger, M. Eilers, J. Leon & L. G. Larsson (2003) Myc represses differentiation-induced p21CIP1 expression via Miz-1-dependent interaction with the p21 core promoter. *Oncogene,* 22**,** 351-60.

Xu, J., E. Y. Wong, C. Cheng, J. Li, M. T. Sharkar, C. Y. Xu, B. Chen, J. Sun, D. Jing & P. X. Xu (2014) Eya1 interacts with Six2 and Myc to regulate expansion of the nephron progenitor pool during nephrogenesis. *Dev Cell,* 31**,** 434-47.

Yang, J., A. M. AlTahan, D. Hu, Y. Wang, P. H. Cheng, C. L. Morton, C. Qu, A. C. Nathwani, J. M. Shohet, T. Fotsis, J. Koster, R. Versteeg, H. Okada, A. L. Harris & A. M. Davidoff (2015) The role of histone demethylase KDM4B in Myc signaling in neuroblastoma. *J Natl Cancer Inst,* 107**,** djv080.

Zang, W., T. Wang, J. Huang, M. Li, Y. Wang, Y. Du, X. Chen & G. Zhao (2015) Long noncoding RNA PEG10 regulates proliferation and invasion of esophageal cancer cells. *Cancer Gene Ther,* 22**,** 138-44.

Zhang, X., X. Chen, J. Lin, T. Lwin, G. Wright, L. C. Moscinski, W. S. Dalton, E. Seto, K. Wright, E. Sotomayor & J. Tao (2012) Myc represses miR-15a/miR-16-1 expression through recruitment of HDAC3 in mantle cell and other non-Hodgkin B-cell lymphomas. *Oncogene,* 31**,** 3002-3008.

Zhao, X., J. I. Heng, D. Guardavaccaro, R. Jiang, M. Pagano, F. Guillemot, A. Iavarone & A. Lasorella (2008) The HECT-domain ubiquitin ligase Huwe1 controls neural differentiation and proliferation by destabilizing the N-Myc oncoprotein. *Nat Cell Biol,* 10**,** 643-53.

Zhou, J. & J. T. Hsieh (2001) The inhibitory role of DOC-2/DAB2 in growth factor receptor-mediated signal cascade. DOC-2/DAB2-mediated inhibition of ERK phosphorylation via binding to Grb2. *J Biol Chem,* 276**,** 27793-8.

Zimmerman, K. A., G. D. Yancopoulos, R. G. Collum, R. K. Smith, N. E. Kohl, K. A. Denis, M. M. Nau, O. N. Witte, D. Toran-Allerand, C. E. Gee & et al. (1986) Differential expression of myc family genes during murine development. *Nature,* 319**,** 780-3.

Zippo, A., A. De Robertis, R. Serafini & S. Oliviero (2007) PIM1-dependent phosphorylation of histone H3 at serine 10 is required for MYC-dependent transcriptional activation and oncogenic transformation. *Nat Cell Biol,* 9**,** 932-44.

9. Abbreviations and acronyms

A
ASP   allele-specific PCR

B
bHLH   basic helix-loop-helix
bp   basepair(s)
BSA   bovine serum albumin

C
CDS   coding sequence
Ct   cycle threshold

D
DNA   deoxyribonucleic acid
dNTP   deoxynucleoside-triphosphate
DTT   1,4-dithiothreitol
DUB   deubiquitinating enzyme

E
EDTA   ethylenediaminetetraacetic acid
EGTA   ethylene glycol bis(beta-aminoethyl ether)-N,N,N',N'-tetraacetic acid

F
FDR   False Discovery rate

G
gDNA   genomic DNA
GFP   green fluorescent protein
GO   gene ontology
GOI   gene of interest

H
HAT   histone acetyltransferase
HDAC   histone deacetylase
HDM   histone demethylase
HMT   histone methyltransferase
HRP   horseradish peroxidase

I
IP   immunoprecipitation
IQR   interquartile range
IRES   internal ribosome entry site

K
kDa   kilodalton(s)

L

LFQ	label-free quantification
Log2FC	Log2 fold change
LOH	loss of heterozygosity
Luc	luciferase
LZ	leucine-zipper

M

MB	MYC-boxes
mRNA	messenger RNA
MS	mass spectrometry

N

NLS	nuclear localization signal
NSCLC	non-small cell lung cancer
NWTS/COG	National Wilms Tumor Study/Children´s Oncology Group

P

PAGE	poly acrylamide gel electrophoresis
PBS	phosphate buffered saline
PCC	pheochromocytoma
PCR	polymerase chain reaction
PEI	polyethylenimine
POD	peroxidase
POL II	RNA polymerase II

R

RFP	red fluorescent protein
RNA	ribonucleic acid
rRNA	ribosomal RNA
RT	room temperature

S

SCLC	small cell lung cancer
SDS	sodium dodecyl sulfate
sec	second(s)
SIOP	*Societé Internationale d'Oncologie Pédiatrique* - Renal Tumors Study Group

T

TAD	transactivation domain
TSS	transcription start site

U

U	enzyme unit(s)
UTR	untranslated region

W

WT	Wilms tumor

10. Supplement

10.1. Oligonucleotides list

When required, ethylene glycol (*), Q5 High GC Enhancer (**) or Betain (***) are indicated.

Table 23. Oligonucleotides for *MYCN* P44L and *MAX* R60Q mutation screenings.

Oligonucleotides for DNA templates integrity control				
Gene name	**Oligo sequence (5'-3')** **Forward**	**Oligo sequence (5'-3')** **Reverse**	**Oligo** **annealing (°C)**	
XIST	Xist-1b TCCAGACCAATGAGAAG AATTAGACA	Xist-2 CGGCCACTACTATGAGCAGG	60°C	
Oligonucleotides for allele-specific PCR of genomic DNA				
Gene name **and mutation**	**Oligo sequence (5'-3')** **Forward**	**Oligo sequence (5'-3')** **Reverse**	**Oligo** **annealing (°C)**	
MYCN P44L	hMYCN-44-ASP-1 GGCGGCCCCGACTCGAC ACT	hMYCN-44-ASP-2 CAAGCAGCATCTCCGTGACCC AG	63,0 *	
MAX R60Q	MAX-ASP1 GCTTTTTCTCATATTGCC ACAGGCATCCTA	MAX-ASP3 GCCAAAGCCTGACCTGGCTGG	67,0	
SIX1 Q177R	hSix1-ASP-G CAGCAACTGGTTTAAGA ACCGGAGTCG	hSix1-ex1-rev3 gaggagaaaggacggcttcc	62,0 *	
DGCR8 E518K	hPasha-ASP-A GAAATCCGAGGTCTGCA TCCTGCATA	hPasha-ASP-rev CTCCCCAGCCCTGACCAAAGTT ACA	66,0	
DROSHA E1147K	hDrosha-1147ASP-A TCTTTTTCCAGAGGCCAC AATCAGAGAATTA	hDrosha-1147-ASP-rev ATGTGCTTTGTATACAATTTGC ACAATGAAATGA	57,0	
SIX2 Q177R	hSix2-ASP-G AACTGGTTCAAGAACCG GCGTCG	hSix2-ASP-rev GCAGAAGCCCTGCGAACCCC	66,0 *	
Oligonucleotides for sequence verification of mutations in genomic DNA and cDNA				
Gene name **and mutation**	**Oligo sequence (5'-3')** **Forward**	**Oligo sequence (5'-3')** **Reverse**	**Oligo** **annealing (°C)**	**Sequencing oligo** **sequence (5'-3')**
MYCN P44L (gDNA and cDNA)	hMYCN-for1 agtttgactcgctacagccc	hMYCN-rev1 agctcgttctcaagcagcat	60,0 *	hMYCN-rev1 agctcgttctcaagcagcat
MAX R60Q (gDNA)	MAX-for1 ctcactgcctggattgggtt	MAX-ASP3 GCCAAAGCCTGACCTGGCTGG	56,0	MAX-for1 ctcactgcctggattgggtt
MAX R60Q (cDNA)	MAX-exon3-for ttcacagtttgcgggactca	MAX-exon5-rev-neu cttgacctcgccttctccag	58,0	MAX-exon5-rev-neu cttgacctcgccttctccag
Oligonucleotides for *MAX* R60Q restriction analysis with ApaI				
Template used for **amplification**	**Oligo sequence (5'-3')** **Forward**	**Oligo sequence (5'-3')** **Reverse**	**Oligo** **annealing (°C)**	**Sequencing oligo** **sequence (5'-3')**
WT patient tumor material	MAX-for1 ctcactgcctggattgggtt	MAX-ASP3 GCCAAAGCCTGACCTGGCTGG	56,0	
MAX WT/R60Q plasmids	TYMV-for agatcgcctggagcaattcc	MAX-Exon5-rev-neu cttgacctcgccttctccag	58,0	TYMV-for agatcgcctggagcaattcc

Table 24. Oligonucleotides for screening of other *MAX* CDS variants.

Purpose of oligo combination	Oligo sequence (5'-3') Forward	Oligo sequence (5'-3') Reverse	Oligo annealing (°C)	Sequencing oligo sequence (5'-3')
MAX CDS amplification and sequencing	MAX-5'UTR-PCR-for gccgtaggaaatgagcgata	MAX-3'UTR-PCR-rev gggctctaccaacgaactga	60,0	MAX-3'UTR-seq-rev-neu tgaaaggaggatgagacg

Table 25. Oligonucleotides for cloning: amplification of GOI.

Oligonucleotides for cloning (amplification from plasmid)			
Gene name (and origin vector)	Oligo sequence (5'-3') Forward	Oligo sequence (5'-3') Reverse	Oligo ann. (°C)
FLAG-*MAX* R60Q (pBJ3-Max2)	NheI-Flag-MaxExon1-neu gcgGCTAGCaccATGgactacaaagacgatgacg ataaaATGAGCGATAACGATGACAT	MAX-R60Q-rev-neu AGGATTTGGGCCTGGGATGCCTTCT	60,0
FLAG-*MAX* R60Q (pBJ3-Max2)	MAX-R60Q-for-neu AGAAGGCATCCCAGGCCCAAATCCT	MAXExon5-AfeI ggtaccagcgctATCGATGAATTCCCGAG TGGCTTAGCTGGCCTCCATCCGGAG	60,0
FLAG-*MAX* WT/R60Q (pBJ3-Max2)	NheI-Flag-MaxExon1-neu gcgGCTAGCaccATGgactacaaagacgatgacg ataaaATGAGCGATAACGATGACAT	MAXExon5-AfeI ggtaccagcgctATCGATGAATTCCCGAG TGGCTTAGCTGGCCTCCATCCGGAG	60,0
HA-*MYCN* WT/P44L (pSB-ETiE-MYCN-WT/P44L)	NheI-HA-MYCN gcgGCTAGCaccATGtacccatacgatgttccaga ttacgctATGCCGAGCTGCTCCACGTC	MYCN-rev ggactgggcggtggaacc	60,0
FOXK1 (mutant #1) (pcDNA3.1-FLAG-FOXK1)	Foxk1-Age1 gcgACCGGTATGGCCGAAGTCGGCGAG	Foxk1-Xba1 gcgTCTAGActaGGAGTCCCCGGATACCCC	60,0
FOXK1 (mutant #2) (pcDNA3.1-FLAG-FOXK1)	Foxk1-Age2 gcgACCGGTGGGGTATCCGGGGACTCC	Foxk1-Xba2 gcgTCTAGActaTTCAGAGGGGAGATCTGGGG	60,0
Oligonucleotides for cloning (amplification from cDNA)			
Gene name (and origin vector)	Oligo sequence (5'-3') Forward	Oligo sequence (5'-3') Reverse	Oligo ann. (°C)
BMP2K (Oligo-dT ws603T)	Acc65I-BMP2K aaaggtaccATGAAGAAGTTCTCTCGGAT	BMP2K-XbaI ccctctagaCTACTGTTTAGAAGGAAATG	50,0 **
DAB2 (Oligo-dT ws429TA1)	NheI-FLAG-DAB2 agaGCTAGCcatggattacaaggatgacgacgata aggcctctaacgaagtagaaacaag	DAB2-NheI catgctagcTTAGGCAAAAGGATTTCCAA	58,0
FOXK1 (RHP HEK293)	Acc65I-FOXK1 cccggtaccATGGCCGAAGTCGGCGAGGA	FOXK1-XbaI ccctctagaTCACTCCCCGGTGCCTGGCC	72,0 **
MCRS1 (RHP HEK293)	Acc65I-MCRS1 cccggtaccATGGCATCAGGCACTGCCAG	MCRS1-XbaI ccctctagaTGTCCACTAGCACCTGCCAC	60,0
CBLL1 (Oligo-dT HEK293)	Acc65I-CBLL1 cccggtaccATGGATCACACTGACAATGA	CBLL1-XbaI ccctctagaTCATTGGTAATACGGTCTAT	60,0
TROVE2 (RHP HEK293)	EagI-TROVE2 gaacggccgatATGGAGGAATCTGTAAACCA	TROVE2-SalI gtcgacgggTTAAATCATATCTAATGTGA	58,0 *
DVL2 (Oligo-dT HEK293)	Acc65I-DVL2 cccggtaccATGGCGGGTAGCAGCACTGG	DVL2-XbaI ccctctagaCTACATAACATCCACAAAGA	60,0

Table 26. Oligonucleotides for real-time PCR.

Oligonucleotides for gene expression in WT patients			
Gene name	**Oligo sequence (5'-3') Forward**	**Oligo sequence (5'-3') Reverse**	**Oligo ann. (°C)**
HPRT	hHPRT-5'real-neu2 AAGATGGTCAAGGTCGCAAG	hHPRT-3'real-neu2 GTCAAGGGCATATCCTACAACAA	60,0 *
Exogenous *MYCN*	act2forw CCATACGATGTTCCAGATTACGC	LSL-MYCN-flox2 GTCATCTTCGTCCGGGTAGA	60,0 *
Endogenous *MYC*	c-Myc_5real TCCTCGGATTCTCTGCTCTC	c-Myc_3'real actctgaccttttgccagga	60,0 *
Oligonucleotides for gene expression in WT patients			
Gene name	**Oligo sequence (5'-3') Forward**	**Oligo sequence (5'-3') Reverse**	**Oligo ann. (°C)**
HPRT	hu-HPRT1 TGACACTGGCAAAACAATGCA	hu-HPRT2 GGTCCTTTTCACCAGCAAGCT	58
PEG10	PEG10-1 CCTTCCTGTCTTCGCAGAGG	PEG10-2 AGCTTCACTTCTGTGGGGATG	61,0 ***
YEATS2	YEATS2-1 ACCCTGAGAGCCTGAGGAAT	YEATS2-2 TGGAACTGTTGCAGGTCCTC	60
MYCN	hMYCN-real1 CACAAGGCCCTCAGTACCTC	hMYCN-real2 TTCTCCACAGTGACCACGTC	58,0 *

Table 27. Oligonucleotides for cloning: selection of positive clones and sequence verification.

Gene name (backbone vector)	Oligo sequence (5'-3') Forward	Oligo sequence (5'-3') Reverse	Oligo annealing (°C)	Seq. oligo sequence (5'-3') Forward 1	Seq. oligo sequence (5'-3') Reverse 1	Seq. oligo sequence (5'-3') Forward 2	Seq. oligo sequence (5'-3') Reverse 2
FLAG-*MAX* WT/R60Q (pSB-ETiE)	cmv-prom GCTCGTTTAGTGAACCGTCAG	MAX-R60Q-rev AGGATTTGGGCCCGGGATGCCTTCT	60,0	cmv-prom GCTCGTTTAGTGAACCGTCAG			
HA-*MYCN* WT/P44L (pSB-ETiE)	cmv-prom GCTCGTTTAGTGAACCGTCAG	hMYCN-rev1 agctcgttctcaagcagcat	58,0	cmv-prom GCTCGTTTAGTGAACCGTCAG			
BMP2K (pCDNA3.1-FLAG)	*DNA plasmid preparations of positive clones analyzed via single digest, to confirm BMP2K CDS insertion by plasmid size*			CMV-F CGCAAATGGGCGGTAGGCGTG	pTER-rev GATGGCTGGCAACTAGAAGG	BMP2K-for GTCCAGTCTCCAACATCAAT	BMP2K-rev GGGAGGTTCTTTTCATTCTT
DAB2 (pCDH)	pCMV1 TAGGCGTGTACGGTGGGAG	FLAG-NheI atgGCTAGcttatcgtcgtcatccttgtaat	52,0	CMV-F CGCAAATGGGCGGTAGGCGTG	DAB2-NheI catgctagcTTAGGCAAAAGGATTTCCAA		DAB2-rev ACACCACCTAGACCCACCAG
PEG10 (p3FL)	pCMV1 TAGGCGTGTACGGTGGGAG	hPEG10-rev CTCCGACTGCTTCATGACCT	57,0	CMV-F CGCAAATGGGCGGTAGGCGTG			
FOXK1 (pCDNA3.1-FLAG)	Acc65I-FOXK1 cccggtaccATGGCCGAAGTCGGCGAGGA	FOXK1-rev GCGCATGAGGAACTCGAAC	55,0	CMV-F CGCAAATGGGCGGTAGGCGTG	pcDNA3.1-RP_1 CAAACAACAGATGGCTGGC		
MCRS1 (pCDNA3.1-FLAG)	Acc65I-MCRS1 cccggtaccATGGCATCAGGCACTGCCAG	MCRS1-rev TTTGCCCGGGTAGAAGAT	55,0	CMV-F CGCAAATGGGCGGTAGGCGTG	pcDNA3.1-RP_1 CAAACAACAGATGGCTGGC		
CBLL1 (pCDNA3.1-FLAG)	Acc65I-CBLL1 cccggtaccATGGATCACACTGACAATGA	CBLL1-rev ACAGCTCACCCCCTTTACA	55,0	CMV-F CGCAAATGGGCGGTAGGCGTG	pcDNA3.1-RP_1 CAAACAACAGATGGCTGGC		
TROVE2 (p3FL)	EagI-TROVE2 gaacggccgatATGGAGGAATCTGTAAACCA	TROVE2-rev CCACCTTCAGAACCGAAAC	55,0	CMV-F CGCAAATGGGCGGTAGGCGTG	hGH-polyA-rev GGAGTGGCAACTTCCAG		
DVL2 (pCDNA3.1-FLAG)	Acc65I-DVL2 cccggtaccATGGCGGGTAGCAGCACTGG	DVL2-rev CGAGGCTCATGGACTGGAG	58,0	CMV-F CGCAAATGGGCGGTAGGCGTG	pcDNA3.1-RP_1 CAAACAACAGATGGCTGGC		

10.2. Summary of mutation screening results

ID	Sex	Age (month)	Localization	Histology	Clinical stage	Late Metastasis	All Metastasis	Relapse	Death	Therapy	Mutation	Tumor DNA allele	Tumor cDNA allele	Other genomic alterations
ws02	m	85	le	m	1	n	n	n	n	ct	MYCN c.C13T:p.P44L	0,5	n.d.	
ws22	m	97	le	r	2	n	n	n	n	ct	MYCN c.C13T:p.P44L	0,2	n.d.	
ws34	m	50	ri	r	2	n	n	n	n	ct	MYCN c.C13T:p.P44L	0,2	0,2	
ws35	m	62	le	r	2	n	y	n	n	ct	MYCN c.C13T:p.P44L	0,2	0,0	
ws122	f	45	le	b*	1	-	-	n	y	ps	MYCN c.C13T:p.P44L	0,5	0,2	
ws145re	f	43	ri	e	2	n	y	y	n	ct	MYCN c.C13T:p.P44L	0,1	0,1	DROSHA-E1147K, SIX1-Q177R
ws215	m	75	le	r	3	y	y	y	n	ct	MYCN c.C13T:p.P44L	0,5	0,2	
ws261	f	178	-	m	3	n	n	n	n	ct	MYCN c.C13T:p.P44L	0,5	0,5	
ws378	f	81	ri	m	1	n	n	n	n	ct	MYCN c.C13T:p.P44L	0,5	0,5	
ws434	f	116	ri	r	2	n	n	n	n	ct	MYCN c.C13T:p.P44L	0,5	0,3	
ws465	f	66	le	e	3	n	y	n	n	ct	MYCN c.C13T:p.P44L	0,2	0,2	WT1-P66L
ws520	f	102	ri	st	1	n	n	n	y	ct	MYCN c.C13T:p.P44L	0,5	0,5	CTNNB1 del S45
ws558ii	m	55	le	r	1	y	y	y	y	ct	MYCN c.C13T:p.P44L	0,5	0,5	
ws628	m	88	ri	m	2	y	y	y	n	ct	MYCN c.C13T:p.P44L	0,5	0,5	
ws632	m	116	le	e	1	n	n	n	n	ct	MYCN c.C13T:p.P44L	0,5	0,5	
ws787	f	58	ri	r	2	n	n	n	n	ct	MYCN c.C13T:p.P44L	0,5	0,5	
ws792	m	52	le	m	1	n	n	n	n	ct	MYCN c.C13T:p.P44L	0,5	0,5	
ws811	f	23	ri	m	-	n	n	n	n	ct	MYCN c.C13T:p.P44L	0,2	0,5	DROSHA-E1147K
ws914	f	87	-	b	3	y	y	y	y	ct	MYCN c.C13T:p.P44L	1,0	1,0	TP53-R248W
ws969	f	58	le	r	1	n	n	n	n	ct	MYCN c.C13T:p.P44L	0,2	n.d.	
ws970ii	f	49	le	b	1	n	n	n	n	ct	MYCN c.C13T:p.P44L	0,1	0,1	
ws988	m	116	-	r	2	n	n	n	n	ct	MYCN c.C13T:p.P44L	0,2	0,1	
ws1129	f	109	-	b	3	y	y	y	n	ct	MYCN c.C13T:p.P44L	0,5	0,5	
ws1210	f	-	-	b	2	-	-	-	n	-	MYCN c.C13T:p.P44L	0,1	0,1	DROSHA-E1147K
ws243	m	85	le	r	1	n	n	n	n	ct	MAX c.G179A:p.R60Q	0,2	0,0	
ws299	m	54	ri	r	3	-	y	y	y	ct	MAX c.G179A:p.R60Q	0,1; 0,2; 0,3	0,3	
ws672	f	50	ri	r	3	n	y	y	n	ct	MAX c.G179A:p.R60Q	0,05; 0,1	n.d.	
ws692	m	21	ri	r	1	n	n	n	n	ct	MAX c.G179A:p.R60Q	0; 0,2	0,2	
ws806	f	26	ri	m	-	-	-	-	n	ct	MAX c.G179A:p.R60Q	0; 0,2	0,0	
ws931	f	38	ri	m	1	y	y	y	n	ct	MAX c.G179A:p.R60Q	0; 0,05; 0,2	n.d.	SIX1-Q177R
ws1106	m	12	-	b	2	y	y	n	n	ct	MAX c.G179A:p.R60Q	0; 0,2	n.d.	

f = female
m = male

le = left
ri = right

e = epithelial
m = mixed
n = necrotic
r = regressive
st = stromal
b = blastemal
b* = blastemal, primary surgery

ct = chemotherapy
ps = primary surgery

n = no relapse/metastasis after 2 years
- = no follow-up data after 2 years
"All metastasis" includes metastasis reported at WT diagnosis time

n.d. = not disponible

10.3. Statistics of mutation screenings

Numbers represent: incidence of mutation (first subgroup); incidence of mutation (second subgroup); p: p-value (two-tailed Fisher's exact test); N: number of analyzed cases for each parameter. 825 (*MYCN* P44L) and 797 (*MAX* R60Q) tumors were analyzed from 810 and 782 cases respectively, 15 of them being bilateral WT. *Late metastasis* represents patients where metastasis was reported within two years after WT diagnosis, and *All metastasis* includes also those cases with metastasis at diagnosis time. Gray shading highlights significant difference with $p < 0{,}05$.

Mutation	Histology								
	Low-risk	*Intermediate-risk*						*High-risk*	
	Compl. Necrotic No - Yes	Epithelial No - Yes	Stromal No - Yes	Mixed No - Yes	Regressive No - Yes	Focal Anaplastic No - Yes	Blastemal before CT No - Yes	Blastemal No - Yes	Diffuse Anaplastic No - Yes
MYCN P44L	24/794 0/31 p=1,000 N=825	21/744 3/81 p=0,723 N=825	23/745 1/80 p=0,721 N=825	18/594 6/231 p=0,822 N=825	15/558 9/267 p=0,659 N=825	24/810 0/15 p=1,000 N=825	23/800 1/25 p=0,527 N=825	20/764 4/61 p=0,094 N=825	24/791 0/34 p=0,619 N=825
MAX R60Q	7/767 0/30 p=1,000 N=797	7/717 0/80 p=1,000 N=797	7/720 0/77 p=1,000 N=797	5/572 2/225 p=1,000 N=797	3/542 4/255 p=0,219 N=797	7/782 0/15 p=1,000 N=797	7/773 0/24 p=1,000 N=797	6/740 1/57 p=0,406 N=797	7/763 0/34 p=1,000 N=797

| Mutation	Clinical data				
	Sex Male - Female	Late Metastasis No - Yes	All Metastasis No - Yes	Relapse No - Yes	Death No - Yes
MYCN P44L	10/359 14/448 p=0,837 N=807	18/659 4/83 p=0,295 N=742	15/557 7/194 p=0,470 N=751	18/681 5/53 p=0,020 N=734	21/766 3/44 p=0,137 N=810
MAX R60Q	4/346 3/433 p=0,706 N=779	3/637 2/75 p=0,088 N=712	2/536 4/187 p=0,042 N=723	4/658 2/49 p=0,059 N=707	6/742 1/40 p=0,309 N=782

10.4. Statistics of *MYCN*/*YEATS2*/*PEG10* expression in Wilms tumor

Numbers represent qRT-PCR data: Median Ct-value – IQR (first subgroup); Median Ct-value – IQR (second subgroup); p: p-value (Mann-Whitney-U test); N: number of cases each subgroup (299 tumors from 293 cases, 6 being bilateral). Gray shading highlights significant difference with p < 0,05. IQR = Interquartile range.

Clinical data				
		MYCN	**YEATS2**	**PEG10**
Sex Male / Female		29,86 - 4,24 30,29 - 3,85 p = 0,527 N = 125 / 168	28,93 - 2,43 28,78 - 2,09 p = 0,115 N = 125 / 168	31,38 - 4,74 30,90 - 4,30 p = 0,265 N = 125 / 168
Late Metastasis No / Yes		30,22 - 3,90 29,86 - 4,42 p = 0,288 N = 235 / 36	28,91 - 2,24 28,43 - 1,71 p = 0,189 N = 235 / 36	31,21 - 4,58 30,76 - 4,63 p = 0,545 N = 235 / 36
All Metastasis No / Yes		29,94 - 3,74 30,87 - 4,45 p = 0,291 N = 209 / 67	28,89 - 2,16 28,56 - 2,13 p = 0,606 N = 209 / 67	31,01 - 4,11 31,23 - 5,01 p = 0,249 N = 209 / 67
Relapse No / Yes		30,29 - 3,99 28,97 - 3,45 p = 0,015 N = 239 / 37	28,89 - 2,26 28,64 - 1,94 p = 0,270 N = 239 / 37	31,03 - 4,69 31,01 - 3,83 p = 0,888 N = 239 / 37
Death No / Yes		30,29 - 3,83 27,59 - 1,84 p = 0,000233 N = 273 / 20	28,83 - 2,27 28,54 - 1,17 p = 0,139 N = 273 / 20	31,03 - 4,59 30,03 - 3,89 p = 0,364 N = 273 / 20
Histology				
Histotype		**MYCN**	**YEATS2**	**PEG10**
Low risk	**Nephroblastomatosis** No / Yes	30,12 - 3,98 29,69 - 1,45 p = 0,662 N = 283 / 16	28,82 - 2,13 28,06 - 3,86 p = 0,831 N = 283 / 16	30,95 - 4,50 33,85 - 5,89 p = 0,016 N = 283 / 16
Low risk	**Completely Necrotic** No / Yes	29,94 - 3,70 33,64 - 2,41 p = 0,000169 N = 289 / 10	28,80 - 2,17 30,19 - 2,58 p = 0,093 N = 289 / 10	30,94 - 4,51 34,03 - 5,53 p = 0,00587 N = 289 / 10
Intermediate risk	**Epithelial** No / Yes	30,17 - 4,13 29,52 - 2,23 p = 0,581 N = 269 / 30	28,74 - 2,07 30,03 - 1,71 p = 0,00087 N = 269 / 30	30,97 - 4,64 31,24 - 3,96 p = 0,297 N = 269 / 30
Intermediate risk	**Stromal** No / Yes	29,86 - 3,86 31,10 - 2,48 p = 0,020 N = 271 / 28	28,78 - 2,31 28,92 - 1,28 p = 0,918 N = 271 / 28	31,20 - 4,62 29,04 - 3,80 p = 0,002 N = 271 / 28
Intermediate risk	**Mixed** No / Yes	30,29 - 4,05 29,65 - 3,28 p = 0,043 N = 222 / 77	28,81 - 2,37 28,79 - 1,85 p = 0,148 N = 222 / 77	31,22 - 4,64 30,59 - 3,92 p = 0,163 N = 222 / 77
Intermediate risk	**Regressive** No / Yes	29,57 - 3,39 31,92 - 3,03 p = 7,6116E-8 N = 227 / 72	28,81 - 2,10 28,76 - 2,42 p = 0,766 N = 227 / 72	30,57 - 4,10 32,77 - 3,91 p = 0,000137 N = 227 / 72
Intermediate risk	**Focal Anaplastic** No / Yes	30,07 - 3,83 28,38 - 5,22 p = 0,499 N = 295 / 4	28,80 - 2,14 28,27 - 3,88 p = 0,641 N = 295 / 4	31,02 - 4,70 30,06 - 1,98 p = 0,367 N = 295 / 4
Intermediate risk	**Blastemal, primary surgery** No / Yes	30,20 - 3,82 28,01 - 1,99 p = 0,007 N = 288 / 11	28,79 - 2,17 29,30 - 1,87 p = 0,428 N = 288 / 11	31,03 - 4,72 30,57 - 3,57 p = 0,352 N = 288 / 11
High risk	**Blastemal** No / Yes	30,30 - 3,76 27,68 - 2,10 p = 0,000001 N = 266 / 33	28,89 - 2,23 28,09 - 1,34 p = 0,010 N = 266 / 33	31,24 - 4,72 29,86 - 2,94 p = 0,001 N = 266 / 33
High risk	**Diffuse Anaplastic** No / Yes	30,11 - 3,81 28,34 - 3,53 p = 0,099 N = 281 / 18	28,81 - 2,16 28,69 - 2,75 p = 0,795 N = 281 / 18	31,10 - 4,51 29,85 - 6,60 p = 0,213 N = 281 / 18

10.5. Extracted ion chromatographs of phospho-assays

Extracted ion chromatographs from the phospho-assay, showing the abundance of detected peptides corresponding to the residues F37-W50 of the wild-type (WT) and P44L mutant N-MYC, either unphosphorylated or phosphorylated. The y-axis represents the relative abundance, and the x-axis indicates the elution time. The double peak in the phosphorylated N-MYC-P44L is due to an interruption of the electrospray, leading to a small gap with no signal during the MS.
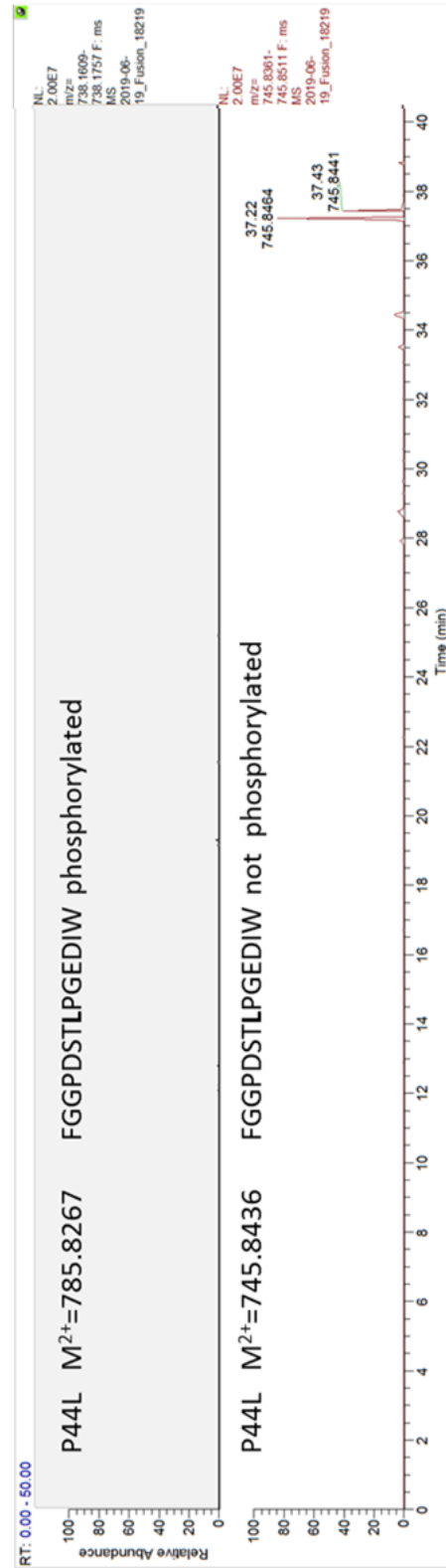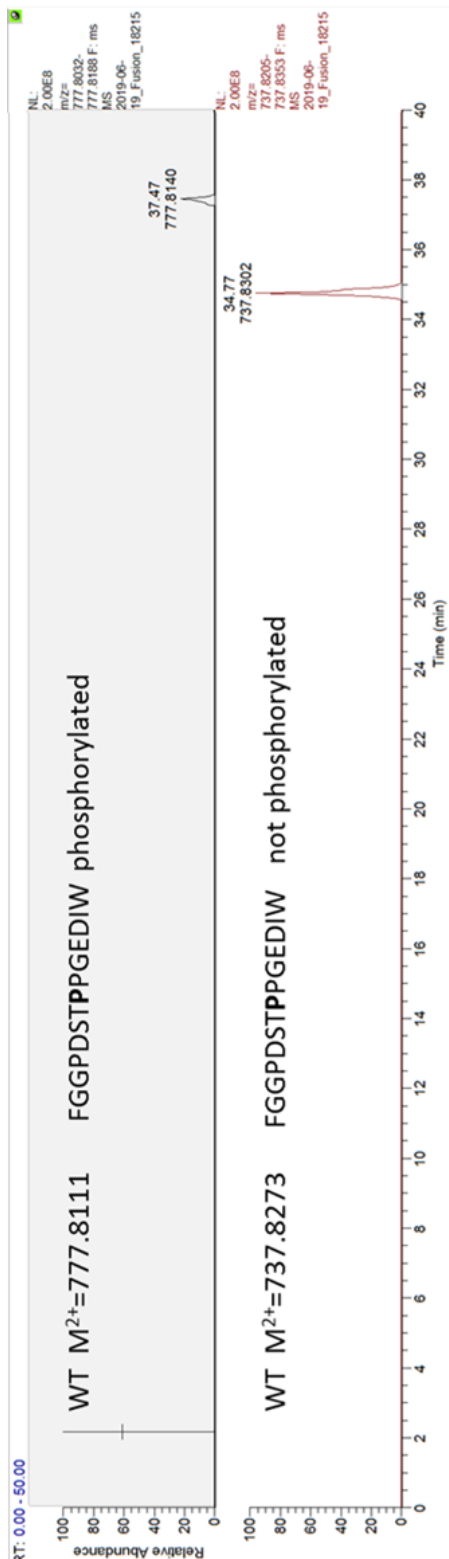
10.6. Oral presentations and posters

10/2019   EUREKA! 14th International GSLS Students symposium

Poster: *Analysis of MYCN and MAX alterations in Wilms Tumor*

10/2017   EUREKA! 12th International GSLS Students symposium

Poster: *Analysis of MYCN and MAX alterations in Wilms Tumor*

03/2017   19th International AEK Cancer Congress

Poster: *Analysis of MYCN and MAX alterations in Wilms Tumor*

10/2016   EUREKA! 11th International GSLS Students symposium

Poster: *Analysis of MYCN and MAX alterations in Wilms Tumor*

06/2016   6th International Tübingen-Symposium on Pediatric Solid Tumors

Oral presentation: *Analysis of MYCN and MAX alterations in Wilms Tumor*

10.7. Curriculum vitae

10.8. Affidavit

I hereby confirm that my thesis entitled "Analysis of *MYCN* and *MAX* alterations in Wilms Tumor" is the result of my own work. I did not receive any help or support from commercial consultants. All sources and / or materials applied are listed and specified in the thesis.

Furthermore, I confirm that this thesis has not yet been submitted as part of another examination process neither in identical nor in similar form.

Place, Date   Signature

Eidesstattliche Erklärung

Hiermit erkläre ich an Eides statt, die Dissertation „Analyse von *MYCN*- und *MAX*-Veränderungen im Wilms Tumor" eigenständig, d.h. insbesondere selbständig und ohne Hilfe eines kommerziellen Promotionsberaters, angefertigt und keine anderen als die von mir angegebenen Quellen und Hilfsmittel verwendet zu haben.

Ich erkläre außerdem, dass die Dissertation weder in gleicher noch in ähnlicher Form bereits in einem anderen Prüfungsverfahren vorgelegen hat.

Ort, Datum   Unterschrift

10.9. Acknowledgements